2015

Investigating Mechanisms of Telomere End-Protection

Shaheen Kabir

INVESTIGATING MECHANISMS OF TELOMERE END-PROTECTION

A Thesis Presented to the Faculty of

The Rockefeller University

in Partial Fulfillment of the Requirements for

the degree of Doctor of Philosophy

by

Shaheen Kabir

June 2015

INVESTIGATING MECHANISMS OF TELOMERE END-PROTECTION

Shaheen Kabir, Ph.D.

The Rockefeller University 2015

Shelterin is an essential telomeric protein complex that prevents DNA damage signaling and DNA repair in a compartmentalized manner. We assessed contributions of the conserved shelterin component, Rap1, to telomere end-protection. Rap1 was first discovered in budding yeast as a transcription factor and was later shown to bind directly to telomeres. Two important functions of Rap1 in yeast are: the negative regulation of telomere length, and the inhibition of the *d*ouble-*s*trand *b*reak (DSB) repair pathway *n*on *h*omologous *e*nd-*j*oining (NHEJ). Mammalian Rap1 interacts with shelterin factor TRF2, to localize to telomeres, and human Rap1 is implicated in repressing NHEJ.

Surprisingly, removal of Rap1 from telomeres revealed that mouse Rap1 was not required to inhibit NHEJ, but instead was critical for the repression of the DSB repair pathway *h*omology *d*irected *r*epair (HDR). We showed that complex formation of Rap1 and TRF2 was most likely necessary to repress HDR, although the mechanism of how it does so remains to be determined.

Two discrepancies exist between mouse and human Rap1 regarding repression of NHEJ and regulation of telomere length. Human Rap1 was proposed to inhibit NHEJ, but we observed no evidence of telomere fusions in

the mouse Rap1 knockout. Similarly, telomere elongation was observed upon knockdown of human Rap1, but no telomere length phenotypes were observed in Rap1-deficient mice. With the advent of new genome-editing technologies that facilitate targeting in human cells, we constructed TALEN-mediated knockouts of human Rap1 in numerous cell lines. Loss of human Rap1 did not lead to an induction of NHEJ, or show consistent changes in telomere length, indicating that similar to mouse Rap1, human Rap1 does not have an important function in protection or length regulation of human telomeres. Instead, we found that mammalian Rap1, like its unicellular orthologs, affects gene expression. Therefore, perhaps the conservation of Rap1 reflects its role in transcriptional regulation rather than a function at telomeres.

Organismal discrepancies regarding the function of shelterin components, other than Rap1, also exist. Targeting of human shelterin component POT1 (POT1a/b in the mouse) with shRNAs shows a reduction in 3' telomere overhangs and a mild induction of DNA damage signaling. However, deletion of mouse POT1a and –b results in extended 3' overhangs and a massive induction of the DNA damage response. To understand the role of human POT1 in telomere protection, we used TALENs to generate human knockout cell lines lacking POT1. We found that similar to mouse POT1, deletion of human POT1 elicited significant DNA damage signaling. Strikingly, the amount of 3' single-stranded DNA remained unchanged upon loss of POT1, highlighting a potential difference in overhang regulation between mice and humans.

In memory of –

My father

ACKNOWLEDGEMENTS

I extend my gratitude to my advisor, Titia de Lange, who devoted an extraordinary amount of time and energy into mentoring me, from which I have benefitted immensely. I thank my committee members Hironori Funabiki and Michael Young for their guidance over the years. I also thank Julie Cooper for agreeing to be the external examiner at my thesis defense. I thank Cris, Kristin, Marta, Stephanie, Emily and Sid at the Deans office for helping students navigate their graduate careers without any bureaucratic hassles.

I extend my appreciation to members of the de Lange lab, past and present, for their scientific support and for the collegial atmosphere at work. I thank Megan van Overbeek for showing me the ropes during my rotation, Hiro Takai for discussions on POT1, and John Maciejowski for reading parts of my thesis. The lab would not run without the support of Devon White, Adriana Garzon, Rosaura Mejia and Stew Barnes, and for that, I am grateful. I especially thank Ylli Doksani for our morning coffees, and Francisca Lottersberger for our afternoon coffees, which I will miss dearly. I'm thankful for my New York 'family', Agnel Sfeir, Isabelle Schmutz and Nazario Bosco for their constant support and our limitless adventures.

I thank my dear friends Courtney Klein, Chelsa Crowley, Mari Sheibley, Mieun Lee, Erika Brunet, Payaal Patel, Estee Perlmutter for keeping me sane in the best possible ways. I'm grateful to Anna Kruyer for being a fantastic

roommate and friend. I would also like to acknowledge Daria Zamolodchikov who introduced me to Styles in Microsoft Word, which greatly facilitated the formatting of this thesis.

Importantly, I thank my family, Khalid Kabir, Aparna Sarma and Zayed for bringing joy into my life. My parents, Hasina Kabir and Kabir Hyderally deserve the most thanks of all. I am inspired by my mother's strength, intelligence, and infinite capacity to love. I owe my work ethic to my father, who epitomized humility and perseverance, and took on every task with an unmatched rigor, asking for nothing in return. He will be remembered as a selfless man, passionate about his work and his family, traits I can only hope to embody. Lastly, I acknowledge Alexandre Bolze, whose admiration I strive to live up to. His scientific curiosity engages me and his passion for pushing limits motivates me.

TABLE OF CONTENTS

LIST OF FIGURES

LIST OF TABLES

LIST OF ABBREVIATIONS

53BP1	Tumor suppressor p53 binding protein 1
ALT	Alternative lengthening of telomeres
ATM	Ataxia telangiectasia mutated
ATR	ATM and Rad3 related
BrdU	Bromo-deoxyuridine
Chk2	Checkpoint kinase 2
CO-FISH	Chromosome orientation-fluorescence in situ hybridization
CST	Cdc13/CTC1, Stn1, Ten1
DDR	DNA damage response
DSB	Double-stranded break
G-quartet	Hoogsteen base-pairing of guanine residues resulting in a four-stranded DNA structure
HJ	Holliday Junction
dHJ	Double HJ
HDR	Homology-directed repair
KO	Knockout
MEF	Mouse embryonic fibroblast
MRN	Mre11, Rad50, Nbs1
NHEJ	Non homologous end-joining
C-NHEJ	Classical NHEJ
Alt-NHEJ	Alternative NHEJ

OB fold	Oligonucleotide/oligosaccharide binding fold
PD	Population doubling
POT1	Protection of telomeres 1
POT1-FL	Full-length human POT1
POT1-55	Isoform of human POT1 that lacks first N-term OB fold
POT1ΔOB	Dominant-negative allele of POT1, lacks first N-term OB fold
Rap1	Repressor/activator protein 1
ss	Single-stranded
SV40-LT	Simian virus 40-large T antigen
TALEN	Transcription activator-like effector nuclease
TERC	Telomerase RNA component
TERT	Telomerase reverse transcriptase
T-circle	Extrachromosomal circles containing telomeric DNA
T-loop	Invasion of the single-stranded 3' telomere terminus into duplex telomeric DNA
TRF1	Telomere repeat binding factor 1
TRF2	Telomere repeat binding factor 2
T-SCE	Telomere-sister chromatid exchange

Chapter 1: Introduction

1.1 The structure and function of telomeres

Telomeres are conserved nucleoprotein structures comprised of short tandem repetitive sequences and highly specific binding proteins that allow linear DNA to evade recognition as double-stranded breaks (DSBs). Telomeres derive their name from telos (end) and meros (part) after Hermann Muller irradiated *Drosophila melanogaster* and noted that he never found mutants with deletions or inversions that involved the natural ends of chromosomes [1]. Independently, Barbara McClintock observed from her expansive work in *Zea mays* that unlike the natural ends of chromosomes, the ends of broken chromosomes were prone to cycles of fusion and breakage, which were only halted in zygotes where broken ends were able to 'heal' [2]. These early observations illuminated special features of chromosome termini that preserve genomic integrity.

Telomere repeats vary in sequence and length, with a unifying feature being the G-rich nature of the strand that runs from 5' to 3' to the telomere terminus. In general the telomere ends in a 3' single-stranded (ss) overhang. Budding and fission yeasts have short telomeres of several hundred base pairs [3], while mammals have much longer telomeres ranging from 10-15 kb in humans [4] and from 20-50 kb in mice (Figure 1.1) [5,6].

Mammalian telomeric TTAGGG repeats [7-9] are bound by a six (seven in mouse) subunit protein complex termed shelterin (reviewed in [10]). Shelterin consists of two double-strand (ds) DNA binding proteins, TRF1 and TRF2 [11-14]. TRF1 and TRF2 have similar homodimerization (TRFH) domains and both form

homodimers that bind two copies of the half site 5'-YTAGGTTR-3' using their C-terminal Myb/SANT domains [15-17]. The two proteins differ in their N-terminus where TRF1 has an acidic domain while TRF2 has a basic domain [16]. A central region comprised minimally of 41 amino acids, present in TRF2 [18,19], but not TRF1, recruits Rap1 to the telomere [20]. Rap1 forms a 1:1 complex with TRF2 [21,22] using its C-terminus [23], and requires this interaction not only for its localization to the telomere [24]. TRF1 and TRF2 both bind to TIN2 [21,25-27], which serves as a bridge between the telomeric double-strand and single-strand binding proteins. TIN2 binds to TPP1 [26,28,29], which forms a heterodimer with the ssDNA binding protein POT1 [30] (POT1a and POT1b in the mouse) [31,32]. POT1 binds to the telomeric 3' overhang via its oligonucleotide/oligosaccharide binding (OB) domains with the minimal binding site 5'-TTAGGGTTAG-3' [33,34].

The telomeric protein complex of the fission yeast *Schizosaccharomyces pombe* (sp) resembles mammalian shelterin in that it contains Taz1 [35], a TRF ortholog that binds to duplex DNA and recruits spRap1 [36]. Bridging proteins Poz1 and Tpz1, proposed to be functional analogs of TIN2 and TPP1, serve to link Taz1/Rap1 to the ssDNA binding protein POT1 [30,37]. The highly diverged protozoa *Trypanosoma brucei* (tb) also has a TRF homolog (tbTRF) that binds telomeres and recruits tbRap1 [38,39]. Budding yeast however does not have a TRF/Taz-like protein at telomeres or a POT1 ortholog. Instead, Rap1 is the de facto telomere dsDNA binding protein in *Saccharomyces cerevisiae* (sc) [40-42]. The single-stranded 3' overhang in *S. cerevisiae* is bound by the CST (*C*dc13,

*S*tn1, *T*en1) complex [43], which modulates telomere length, recruits telomerase and protects the telomere terminus [44-47]. *S. pombe* contains Stn1 and Ten1 that bind to ssDNA and are required for telomere protection [48]. A similar CST complex, originally identified as an accessory factor of DNA polymerase α-primase [49,50], also exists in mammalian cells where its subunits are referred to as CTC1, Stn1 and Ten1. Mammalian CST participates in overhang maintenance [51] [52,53], but its function is different from budding yeast and its recruitment to telomeres is mediated by TPP1 and POT1 [52,54]. Despite the divergent nature of these complexes, they all perform the same function – the maintenance and protection of telomeres.

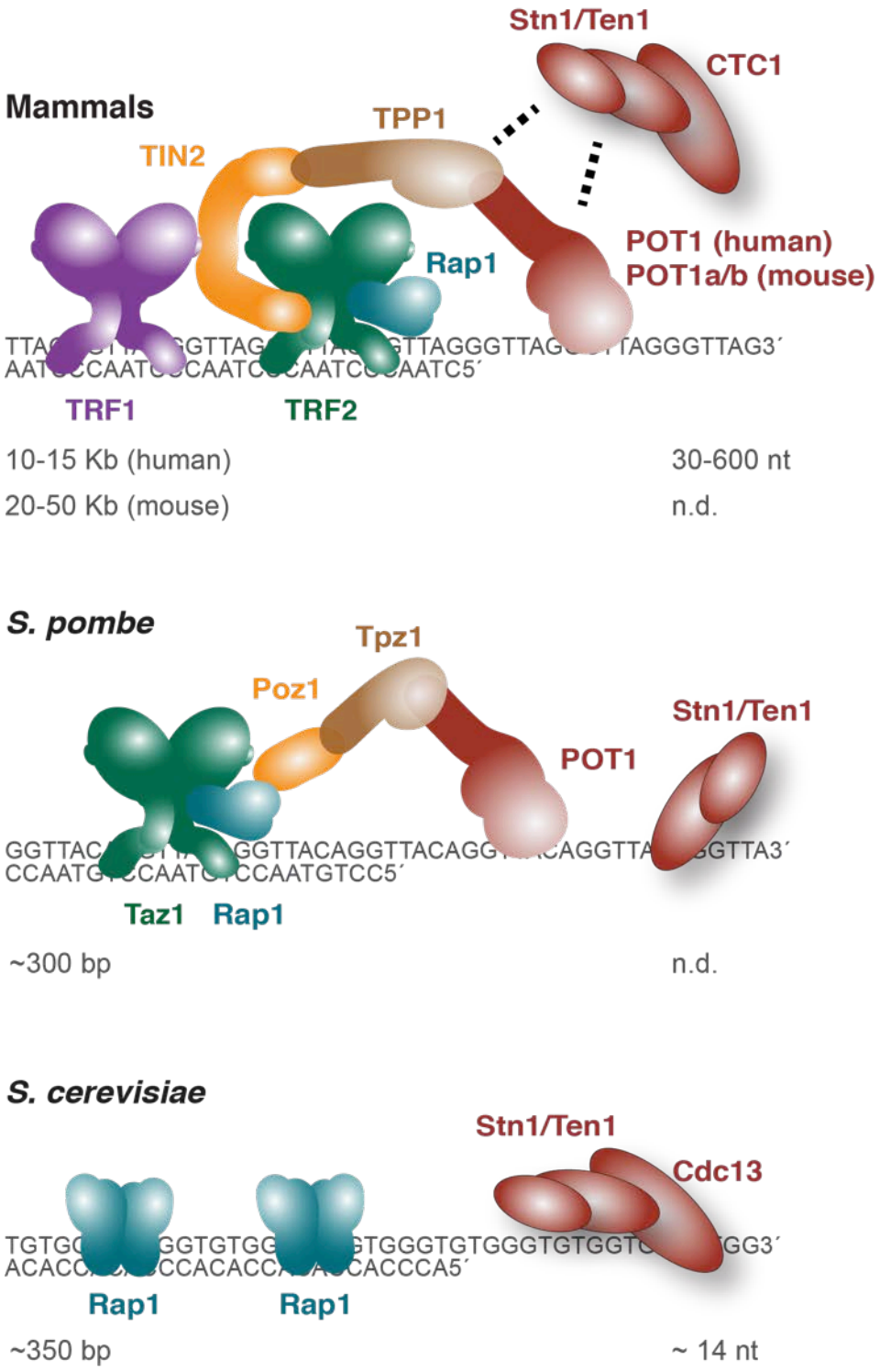

Figure 1.1 Telomere binding complexes in mammals and yeast. Telomere sequence repeats and associated binding complexes are depicted here. Approximate telomere lengths for duplex DNA and single-stranded overhang are indicated below.

1.2 Threats to chromosome termini

Chromosome ends face two ominous threats referred to as the end-replication problem and the end-protection problem. The end-replication problem originates from the inability of DNA replication to fully synthesize the 3' ends of linear DNA, which would result in shorter telomeres with every cell division thereby limiting the replicative potential of the cell [55-57]. The end-protection problem refers to the propensity of chromosome ends to be recognized as a DSB, which would result in disastrous consequences such as cell cycle arrest or apoptosis if DNA damage signaling and DSB repair were inappropriately activated (reviewed in [58]).

1.2.1 *Telomerase counteracts the end-replication problem*

Semi-conservative DNA replication involves two modes of DNA synthesis, leading- and lagging-strand synthesis. In leading-strand synthesis, the polymerase moves in the same direction as the replication fork allowing the molecule to be replicated to the very end, presumably resulting in a blunt end. In lagging-strand synthesis, DNA is synthesized in the opposite direction to the replication fork, necessitating RNA primers to initiate DNA synthesis in short stretches known as Okazaki fragments that are eventually ligated together once the RNA primers have been removed (reviewed in [59]). At a DNA end, lagging-strand synthesis could be incomplete due to lack of priming for the most distal

Okazaki fragment or due to removal of the most distal RNA primer, thus resulting in loss of the terminal sequence in the daughter cell [60].

In 1961 Leonard Hayflick noted that normal human fibroblasts are able to divide in culture for a limited number of (between 40-60) *p*opulation *d*oublings (PDs), after which they senesce [57]. This proliferative barrier was termed the Hayflick limit. Further work has illustrated that this phenotype was likely due to telomere shortening, and in order to bypass replicative senescence, cells with limiting telomere lengths require a mechanism by which telomere length can be maintained [61]. While fibroblasts tend to senesce with approximate telomere lengths of 5-7 kb, it is unclear what the minimal length requirement is for proper telomere function (reviewed in [62]).

One solution to the end-replication problem is provided by telomerase, a ribonucleoprotein enzyme. The *te*lomerase *R*NA *c*omponent, TERC or TR, serves as a template for synthesis of the G-rich telomeric strand by the catalytic subunit TERT (*te*lomerase *r*everse *t*ranscriptase). The prediction that a terminal transferase-like activity extended chromosome ends was based on the ability of yeast to maintain linearized plasmids containing ciliate telomeres, by addition of repetitive G-rich sequences [63]. The RNA component of telomerase was cloned from the ciliate *Tetrahymena* [64]. Genetic screens in *S. cerevisiae* for senescence mutants that displayed progressive telomere shortening [65,66], alongside biochemical fractionation of factors that co-purified with telomerase activity in *Euplotes aediculatus* [67] led to the discovery of the telomerase catalytic subunit

Est2 (*e*ver *s*horter *t*elomeres *2*). Following this discovery, mammalian components of telomerase were rapidly identified [68-70]. Indeed genetically engineered mice lacking TERC display shortening telomeres over several generations and exhibit chromosomal abnormalities by the fourth generation [71].

In human cells telomerase is expressed in the germline, but not in most somatic tissues [72]. However, telomerase activity is readily detectable in immortalized human cell lines that have either been transformed [73] or derived from tumors (reviewed in [62]). Approximately 90% of tumour biopsies tested were shown to express telomerase [74]. Lack of telomerase expression in somatic tissues suggests that limiting the replicative potential of a cell acts as a barrier to tumor development, and premalignant or malignant cells must reactivate telomerase or use an alternative method of telomere length maintenance to acquire their immortal properties.

Examination of other mammals such as elephants and whales indicated they have similar telomere lengths to humans and no telomerase activity in somatic cells. In contrast to these large long-lived mammals, mice and other short-lived mammals such as shrews and opossums have longer telomeres than humans and constitutive telomerase activity [6]. Gomes et al. noted that telomerase activity and telomere length generally correlated inversely with body size and lifespan, giving rise to the proposal that animals with a short lifespan accrue a lower mutational load and therefore may not require replicative aging as a tumor suppressor mechanism. It is clear that while telomerase is necessary to

counteract the end-replication problem, its expression and activity must be meticulously controlled.

1.2.2 *Telomere length regulation by telomere-binding proteins*

Initial insights into the mechanism of telomere length regulation were derived from studies in *S. cerevisiae* where increasing the number of scRap1 binding sites resulted in proportional shortening of the telomere [75]. Thus a cis-acting protein-counting mechanism was proposed where telomere-repeat addition by telomerase was inhibited based on the number of Rap1 molecules bound to the telomere. In agreement with these results, overexpression of TRF1 in a subclone of HT1080s (HTC75; a human fibrosarcoma telomerase-positivie cell line) led to telomere shortening, while expression of a dominant negative mutant of TRF1 ($TRF1^{66-385}$) that diminished TRF1 at telomeres resulted in telomere elongation [76]. Overexpression of TRF2 also led to telomere shortening and telomerase activity was not affected by TRF1 or TRF2 [76,77]. Thus the two dsDNA binding proteins negatively regulate telomere length through a similar 'protein-counting' mechanism as shown in yeast [75]. Similarly, when double-strand telomere binding protein Taz1 was deleted in *S. pombe*, negative regulation of telomere length was abolished. Interestingly, when spRap1 was deleted, telomeres also elongated [36], suggesting that recruitment to telomeres, as opposed to direct binding to telomeres, might be sufficient for telomere length control.

Surprisingly, overexpression of human Rap1 leads to telomere lengthening [20], but this elongation is observed even when a Rap1 mutant defective in localization to the telomere is overexpressed [23]. Considering the large nucleoplasmic pool of Rap1 that accumulated when exogenously expressed, it was hypothesized that the non-telomeric Rap1 titrates away a telomere-associated factor involved in length regulation, that otherwise along with Rap1 would inhibit telomere elongation. Mild extension of telomeres after partial knockdown of Rap1 in HTC75 cells provided further support for Rap1 as a negative regulator of telomere length [78].

Telomeres also elongated when POT1 binding to ssDNA was inhibited by expression of a POT1 mutant lacking its OB fold, POT1$^{\Delta OB}$ [79]. Furthermore, TIN2 and TPP1 levels reduced by shRNAs [80] [29] and expression of TIN2 mutants that could not bind TPP1 [25] resulted in telomere elongation, illustrating that recruitment of POT1 is required for negative regulation of telomere length. However, TPP1 and POT1 have also been implicated in the positive regulation of telomerase. The TPP1/POT1 heterodimer was shown to enhance telomerase processivity *in vitro* [81], with telomerase acting preferentially on substrates coated with POT1/TPP1 [82]. In addition, the OB fold of TPP1 can bind to and recruit TERT to telomeres [81,83-85]. Specifically, a group of surface-exposed amino acids in the OB fold of TPP1, referred to collectively as the TEL patch, is required for recruitment and activation of telomerase [86,87].

1.2.3 *The end-protection problem*

The integrity of the genome is constantly threatened by internal processes such as errors introduced during DNA replication and external sources such as genotoxic agents of radiation. Various mechanisms are in place to detect damaged DNA, collectively referred to as the DNA damage response (DDR), and to fix these lesions with DNA repair pathways. Mammalian DDR signaling occurs primarily through two kinases, the ATM (*a*taxia *t*elangiectasia *m*utated) kinase, activated by the MRN (*M*re11-*R*ad50-*N*bs1) complex that senses DSBs, and the ATR (*A*TM and *R*ad3 related) kinase that is activated by the binding of *R*eplication *P*rotein *A* (RPA) to ssDNA (reviewed in [88]). Chromosome ends are vulnerable to both of these pathways with the telomere terminus being recognized by ATM and the single-stranded overhang being a substrate for ATR activation.

Activation of ATM and/or ATR triggers cell-cycle checkpoints by phosphorylation of downstream effectors Chk2 [89-91] and Chk1 [92,93] respectively, that phosphorylate Cdc25 phosphatases [94], which in turn act to reduce the activity of cyclin-dependent kinases (CDKs), thereby leading to rapid cell-cycle arrest in intra-S or G2/M [95,96]. Phosphorylation of p53 [97-100] and downstream signaling also occurs to initiate a delayed response to DNA damage, leading to cell cycle arrest at the G1/S transition and senescence or apoptosis. These processes are thought to allow time for DNA repair to occur and prevent transmission of damaged DNA to daughter cells. Coupled with checkpoint

activation, signaling by ATM and ATR also promotes a localized response at the site of the lesion by recruitment and/or activation of DNA repair factors. Both ATM [101] and ATR [102] phosphorylate histone H2AX (γH2AX) in chromatin proximal to the damaged lesion. MDC1 (*M*ediator of DNA *d*amage *c*heckpoint *1*) binds to γH2AX and serves to amplify the DNA damage response [103-105]. Subsequent recruitment of E3 ubiquitin ligase RNF168 leads to ubiquitylation of lysine 15 on histone H2A or H2AX [106] resulting in recruitment of the DNA repair effector 53BP1 (tumor suppressor p*53 b*inding *p*rotein *1*) [107]. These DNA damage response proteins are not normally detected at the telomere; however, upon induction of telomere damage, H2AX becomes phosphorylated in the telomeric chromatin and DNA repair factors such as 53BP1 accumulate at the telomere. These indices of local DNA damage signaling are frequently used as readouts for telomere dysfunction [108,109].

DSB repair occurs through two major pathways, *n*on *h*omologous *e*nd-*j*oining (NHEJ) and *h*omology-*d*irected *r*epair (HDR). NHEJ is the main method of repairing breaks in the G1 phase of the cell cycle, while HDR predominates in S/G2 when the presence of a sister chromatid can provide a template for error-free repair. Two forms of NHEJ have been described: classical- and alternative-NHEJ (c-NHEJ and alt-NHEJ [110,111]). Essential components of c-NHEJ [112] consist of the Ku70/80 heterodimer which binds to DSBs [113,114], and DNA Ligase IV (Lig4) which is responsible for ligating the ends [115]. Alt-NHEJ on the other hand is promoted by PARP1 (*p*oly *a*denosine diphosphate *r*ibose *p*olymerase *1*) [116],

requires resection of the DNA end, and then makes use of small microhomologies and DNA Ligase 3 (Lig3) [117] to ligate the ends. Ku70/80 has been shown to inhibit alt-NHEJ, potentially by competing with PARP1 for DSBs [118]. Both types of NHEJ have been shown to be active at dysfunctional telomeres [24,119-121]. Inappropriate repair of chromosome ends by NHEJ results in fused dicentric chromosomes that are unstable in mitosis and can initiate breakage-fusion-bridge (BFB) cycles thereby leading to genomic instability [2].

The central tenets of HDR are resection of a 5' end to generate a 3' ssDNA overhang, formation of the Rad51 (*rad*iation sensitive *51*) filament to conduct a homology search, followed by strand invasion into a homologous region to initiate DNA repair (Figure 1.2). Termination of the telomere in a 3' single-stranded overhang makes it primed for HDR.

The MRN complex has been implicated in promoting DSB resection in cooperation with CtIP [122], as well as BRCA1 (*br*east *ca*ncer *1*) [123]. In addition, Exo1, a 5' to 3' exonuclease, in concert with Bloom (BLM), a member of the RecQ helicase family, have also been shown to mediate resection at DSBs [124,125]. Following resection, the current model derived from studies in yeast is that RPA initially coats the available ssDNA to facilitate assembly of the presynaptic filament and remove secondary structures within the ssDNA [126-128]. Mediator protein BRCA2 (*b*reast *c*ancer *2*) subsequently assists in displacement of RPA and loading of Rad51 to form the pre-synaptic filament [129-131]. Following strand invasion into the region of homology and DNA synthesis, 'second end capture'

can then occur where the strand not involved in initial invasion is captured to form a double Holliday junction (dHJ). If this dHJ is dissolved through the helicase action of BLM in conjunction with the topoisomerase TOP3α [132], the resulting product will be a non-crossover and innocuous to the cell (Figure 1.2A). However, if the dHJ is processed through resolvases such as the heterodimer Mus81-Eme or GEN1, the resulting outcome can be a crossover [133-135] (Figure 1.2B), which could have deleterious consequences at the telomere.

Due to the repetitive nature of telomeric DNA, strand invasion could take place at any point along the telomere and if the crossover results in an unequal exchange, the outcome is one lengthened telomere and one shortened telomere. This becomes problematic for the daughter cell that inherits the shorter telomere that can be dysfunctional or limit the replicative potential of the cell. These crossover events can be detected at dysfunctional telomeres by an assay called CO-FISH and are called *t*elomeric-*s*ister *c*hromatid *e*xchanges (T-SCEs) [136] (Figure 1.3). Unbridled HDR at the telomere is an alternative method (ALT, *Alt*ernative lengthening of telomeres) for telomere maintenance in the absence of telomerase (reviewed in [137]). ALT has been observed both in *in vitro* immortalized human cells and in a subset of human cancers [138,139], further illustrating the need for repression of HDR at the telomere. Alternatively, a process termed break induced replication (BIR) occurs when only one DSB is available for repair, for which the end of the telomere may be a likely substrate (Figure 1.2D). After strand invasion DNA synthesis may occur using the migrating D loop as a

template [140,141], recently referred to as bubble migration [142,143], with fill-in synthesis replicating the lagging strand. This process could potentially continue along for the length of the chromatid. In this case, while the danger of unequal T-SCEs is not preeminent, BIR could cause excessive lengthening of telomeres and affect the normal telomere-driven senescence program [144].

Another threat to telomeres includes their susceptibility to undergo excessive resection of their 5' end during the process of overhang generation. While telomeric overhangs naturally occur during lagging strand synthesis, leading ends would presumably require additional processing for overhang formation [145]. Telomeres require the 3' overhang both for protection from DNA repair and to create a substrate for telomerase, yet this process must be carefully controlled and inhibit excessive nucelolytic degradation.

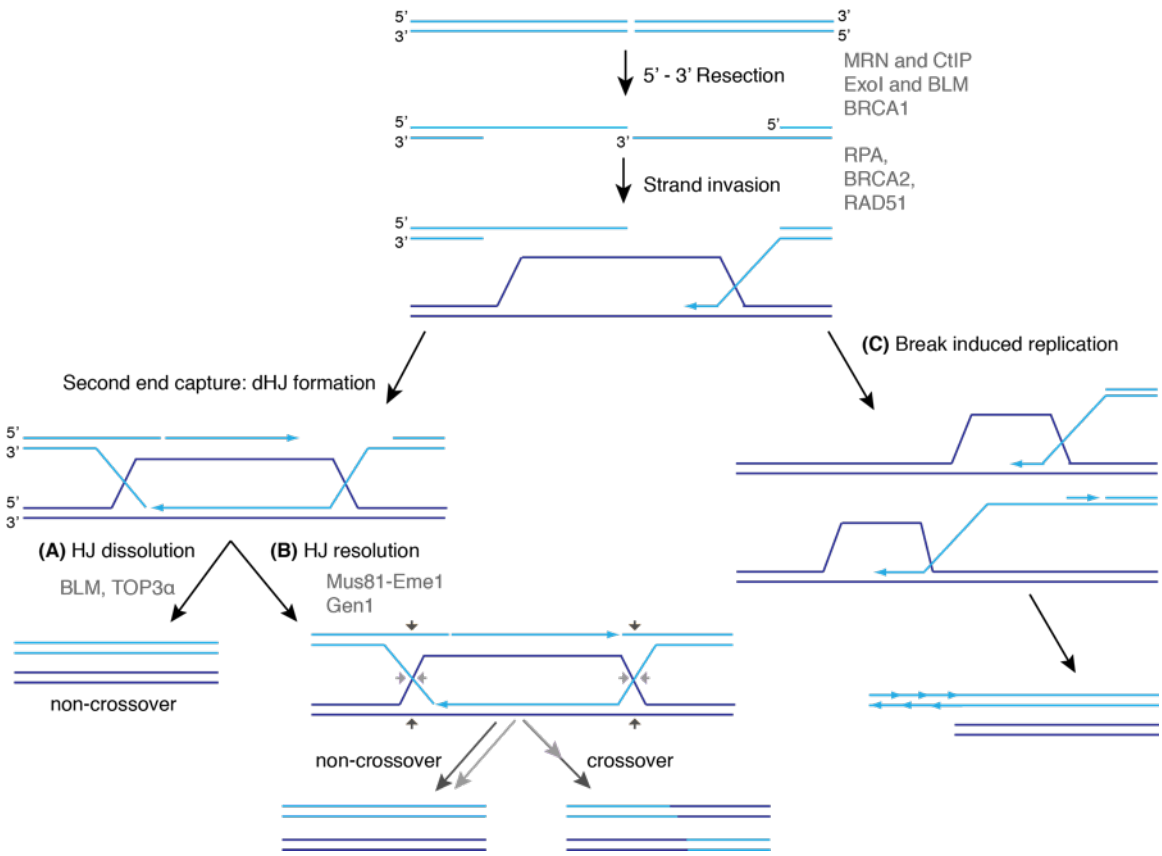

Figure 1.2 Homology-directed repair. Schematic illustrating processing steps in homology directed repair and potential outcomes. (A) Non-crossover products occur when *d*ouble *H*olliday *j*unctions (dHJ) are dissolved. (B) Both non-crossovers and crossovers can be the result dHJ resolution by nucleases. Non-crossovers can be detected by the CO-FISH assay (Figure 1.3A). (C) Break-induced replication is an alternate form of repair that can occur when only one DSB is available for repair, for example the telomere.

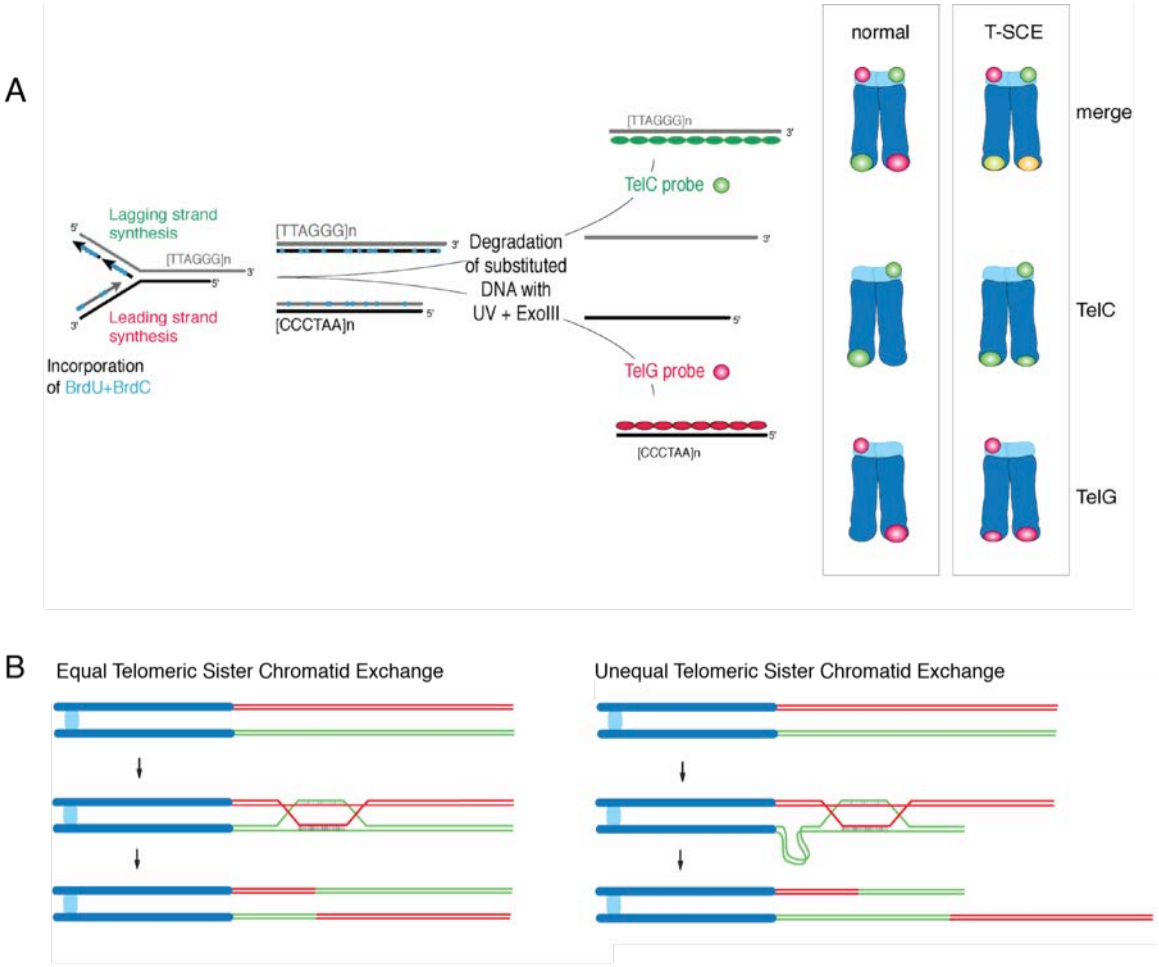

Figure 1.3 CO-FISH detects T-SCEs. Adapted from [154]. (A) *C*hromosome *o*rientation *f*luorescence *i*n *s*itu *h*ybridization (CO-FISH) is a method that can detect HDR events at the telomere that have been resolved as crossovers. Briefly, cells are incubated with BrdU and BrdC for one round of replication. Metaphases are then harvested and treated with UV to generate nicks in the newly synthesized strand due to BrdU/C sensitivity. This strand is then digested with Exonuclease III, leaving the parental DNA strands intact. Due to the G-rich and C-rich nature of complementary strands of telomeric DNA, exchange of sequence between sisters can be detected by hybridization and colocalization of fluorescent G-rich and C-rich probes. (B) Schematic showing telomere-sister chromatid exchanges (T-SCEs). An equal exchange would be innocuous, however an unequal exchange could be deleterious to the daughter cell that inherits the shortened telomere.

1.2.4 *Shelterin solves the end-protection problem*

Genetically engineered conditional mouse knockouts have revealed that shelterin components are essential (with an exception discussed in chapter 2) and disable threats to telomere integrity in a compartmentalized manner (Figure 1.4). TRF2 is responsible for inhibiting ATM activation and subsequent repair by NHEJ [24]. TRF2 is thought to repress ATM activation and NHEJ by facilitating formation of a t-loop, where the 3' overhang strand invades into the telomere duplex, thereby 'hiding' the end from the MRN complex and blocking the loading of Ku70/80 [146,147]. POT1 represses activation of the ATR kinase at telomeres [31,148]. Deletion of TIN2 and TPP1 in MEFs phenocopies the POT1a/b double knockout, thus revealing recruitment of POT1 to the telomere as the primary function of these two components [83,149-151]. POT1 is proposed to repress ATR activation by excluding RPA from binding to the single-stranded overhang [148,152,153]. TRF2 and POT1a/b also appear to prevent HDR since they repress the formation of T-SCEs when Ku70 is also absent [154,155]. However, the mechanism for shelterin-mediated repression of T-SCEs is unclear.

In contrast to the other shelterin components, TRF1 does not appear to play a critical role in protecting telomeres from DNA damage signaling and repair. Deletion of TRF1 resulted in activation of ATR signaling during progression of S-phase and in the appearance of fragile telomeres in metaphase spreads. These phenotypes were ascribed to the increase in replication fork-stalling when TRF1 was removed from telomeres [156,157]. DNA helicases BLM and RTEL1 also

facilitate replication of the telomere, presumably by removing G quartets that may form due to the G-rich sequence of telomeric DNA [156,158,159].

Removal of the entire shelterin complex from mouse telomeres resulting in shelterin-free telomeres revealed that chromosome ends are vulnerable to fusion even when canonical components of the c-NHEJ pathway, Ku80 and Lig4, are absent [120]. These fusions events are mediated by PARP1 and Lig3 dependent alt-NHEJ [120,121]. Detection of HDR in shelterin-free Ku80 deficient cells was not possible due to high levels of telomere fusions, however T-SCEs were observed in shelterin-free Lig4- and 53BP1- deficient cells. Additionally, when shelterin was deleted from 53BP1-deficient cells, telomeres underwent extensive nucleolytic degradation [120]. Thus, HDR, alt-NHEJ and 5' end resection are threats to telomeres that are thwarted redundantly by general repressors and multiple components of shelterin.

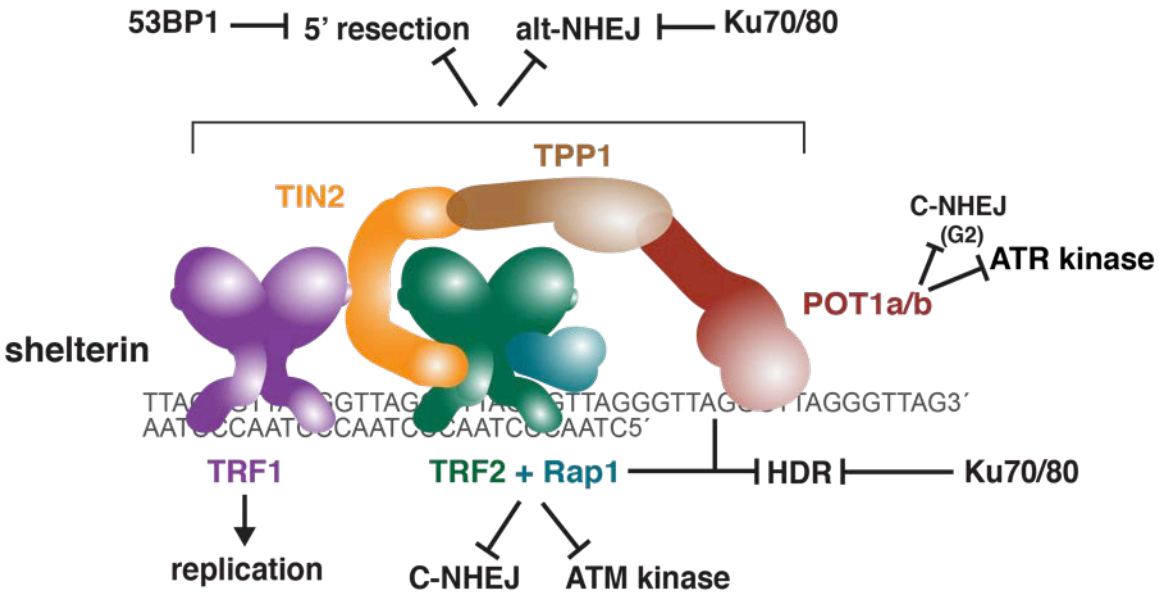

Figure 1.4 Shelterin solves the end-protection problem. Shelterin components are required to inhibit DNA damage signaling and repair at chromosome ends. Ku70/80 and 53BP1 acts as general repressors of HDR and resection respectively, but how they perform their dual function in telomere protection and promoting DNA repair is not yet understood.

1.2.5 *Phenotypes of TRF2 depletion*

Deletion of TRF2 from SV40-immortalized mouse embryonic fibroblasts (MEFs) led to the concomitant depletion of Rap1 protein from the telomere and the cell [24]. Removal of TRF2 using dominant negative alleles also results in diminished levels of Rap1 [160]. Consequently, analysis of phenotypes associated with loss of TRF2 could be due to either TRF2, or Rap1, or both. My aims (discussed in section 1.4) were to understand the contributions to and mechanisms of telomere protection endowed by Rap1.

Expression of dominant negative alleles of TRF2 in human cells or deletion of TRF2 in MEFs leads to activation specifically of the ATM kinase [24,148]. This signaling can be quantified by the appearance and localization of DNA repair factors and modifications such as 53BP1 and γH2AX, respectively, to majority of the telomeres, referred to as TIFs (*t*elomere dysfunction-*i*nduced *f*oci) [108]. Depletion of TRF2 also results in phosphorylation of Chk2, activation of p53 and apoptosis, consistent with ATM activation [161]. Massive induction of telomere-telomere fusions was also observed on metaphase spreads from cells lacking TRF2. These fusions primarily occurred in G1 [162] and were mediated by c-NHEJ as revealed by their dependency on the presence of Ku70 and Lig4 [24,154]. The fusion of dysfunctional telomeres is promoted by 53BP1-mediated mobility of telomeres [163,164] and inhibition of resection [165]. ATM deficiency abolishes both TIF formation and telomere fusions upon deletion of TRF2, establishing that DNA damage signaling is required for NHEJ-mediated DNA repair to occur [148]. In

addition, deletion of TRF2 in the context of Mre11 or Nbs1 deficiency also diminishes formation of TIFs and fusions indicating that MRN is required for ATM activation at dysfunctional telomeres, as it is at DSBs [166-168]. TRF2 protects telomeres from detection by ATM and repair by NHEJ by sequestering the overhang in a t-loop, visualized by electron microscopy and STORM imaging [147,169]. T-loop formation is thought to conceal the DNA end, thereby preventing binding of MRN or Ku70/80. In addition, ATM inhibition at linear telomeres not in the t-loop configuration may be mediated by the so-called iDDR, a 25 amino acid stretch (aa 407-431) in TRF2 that inhibits the E3 ubiquitin ligase RNF168, preventing accumulation of 53BP1 at telomeres [170].

Loss of TRF2 in Ku70-deficient MEFs leads to induction of HDR, visualized by the appearance of T-SCEs [154], indicating that TRF2 plays a role in repressing HDR. The Ku70/80 heterodimer, which is known to repress HDR at DSBs [171], represses HDR at telomeres independently of shelterin. The mechanism by which TRF2 represses HDR is not known.

A third function of TRF2 is the inhibition of t-loop cleavage where the t-loop is excised as an extrachromosomal circle and loss of telomeric DNA from chromosome ends is detectable on metaphase spreads and genomic blots [172]. The ability of TRF2 to prevent t-loop cleavage and its associated stochastic telomere losses is dependent on its N-terminal basic domain [172]. Biochemical experiments have shown that the basic domain of TRF2 can bind and stabilize Holliday Junctions (HJs), which would be expected to form at the base of the t-

loop when branch migration takes place [173,174]. Expression of a TRF2 mutant lacking the basic domain (TRF2$^{\Delta B}$) was able to repress NHEJ but stochastic events of t-loop cleavage were observed [172]. T-loop cleavage was diminished in TRF2$^{\Delta B}$-expressing cells when levels of HJ resolvases Mus81 and Gen1 were reduced by shRNAs [175], suggesting TRF2 restrains the action of these HDR-associated nucleases. Expression of TRF2$^{\Delta B}$ in TRF2 and Ku70 null cells does not however induce T-SCEs [154], revealing that TRF2 represses t-loop cleavage by HJ resolvases and HDR-mediated formation of T-SCEs through different mechanisms.

1.2.6 *Phenotypes of POT1 depletion*

ATR signaling at telomeres is repressed by the ssDNA binding protein POT1 [148]. Depletion of mouse POT1a results in a TIF response [31,32] that is exacerbated upon co-deletion of POT1b, however POT1b null MEFs alone exhibit no TIFs [31]. Deletion of POT1b, but not POT1a results in extended single-stranded overhangs [31] indicating that POT1a and POT1b have evolved to perform different functions of telomere protection. An RPA exclusion model has been proposed to explain POT1 inhibition of ATR activation [148,152], where POT1a prevents RPA from binding to the overhang [153]. RPA is substantially more abundant than the TPP1/POT1 heterodimer and binds single-stranded telomeric DNA with similar affinity, but the tethering of TPP1/POT1 to the rest of shelterin by TIN2 is proposed to give POT1 the ability to outcompete RPA [149,176].

The mechanism by which POT1b maintains telomere overhangs of correct length involves the recruitment of the CST complex to presumably perform fill-in synthesis of the C-rich strand. Leading- and lagging- strand overhangs are generated through different mechanisms, where leading-ends require initial processing by the Apollo/SNM1B nuclease [177,178] that is recruited by TRF2 [27,179,180]. POT1b is required to prevent hyper-resection of both leading and lagging ends by Apollo. Leading and lagging ends are however both extensively resected by Exo1 during S/G2 [181] in the presence of POT1b [52]. POT1b is then responsible for recruiting the CST complex that restores overhangs to their normal length [52].

Few chromosomal abnormalities are noted upon loss of POT1a/b, which include a low level of telomere fusions that occur in G2, and sister telomere 'associations', although the molecular basis of this phenotype is unclear [31,182]. The sustained DNA damage induced by POT1a/b deletion leads to endoreduplication and eventually growth arrest [31,183]. Deletion of both POT1a/b in Ku70 deficient cells leads to an induction of T-SCEs [155], indicating that either POT1a or POT1b is sufficient to inhibit HDR.

Human POT1 has two isoforms, POT1-FL (*f*ull-*l*ength) and POT1-55, which lacks the first of the two OB-folds [184]. No function has been reported for POT1-55. Depletion of human POT1 with shRNAs results in transient DDR activation [184], a slight reduction in overhang signals and growth arrest in primary cells [185] but not transformed cells [184]. Another feature of POT1 depletion from

human cells is loss of specificity of the 5' end. Greater than 80% of normal telomere ends have been reported to end in ATC-5' on the C-rich strand, while there appears to be less selectivity for terminal nucleotides on the G-rich strand[186]. Depletion of human POT1 abrogated sequence precision of the 5' end [184]. It remains to be seen whether the telomere maintenance mechanisms of human POT1 resemble those of mouse POT1a and PO1b.

1.3 Proposed functions and mechanisms of action for Rap1

1.3.1 *Identification of Rap1*

Rap1 was first purified and cloned from *S. cerevisiae* as a transcriptional regulator and thus named *r*epressor/*a*ctivator binding *p*rotein *1* [187]. Transcriptional regulation by scRap1 arises from its ability to bind directly to specific DNA sequences located in several promoter regions including ribosomal genes, as well as at silencer elements. The activation and silencing domains of scRap1 have been mapped to the C-terminus of Rap1 [188]. The *s*ilent *i*nformation *r*egulators Sir3p and Sir4p bind to this C-terminal region of Rap1 and function in sub-telomeric silencing of genes adjacent to telomeres [189,190]. Gene disruption of Rap1 in *S. cerevisiae* results in lethality, which was proposed to be due to its function in activation of ribosomal gene loci [187]. Further investigation revealed that Rap1 binds directly to telomeric DNA [40-42] and the requirement of Rap1 for viability was attributed to its role in telomere protection [191].

Initially identified in a yeast two-hybrid screen with human TRF2, mammalian Rap1 was found to be a distant ortholog of scRap1 [20]. Although the sequence conservation is extremely low (too low for a simple BLAST search), the two Rap1 proteins have a similar domain structure featuring a single N-terminal BRCT domain, a central region with homology to the Myb DNA binding domain, and a *R*ap1-specific *C-t*erminal (RCT) protein-interaction domain (Figure 1.5). However, unlike budding yeast Rap1, which recognizes telomeric DNA directly through the cooperation of its Myb domain with a second motif that forms a Myb-like fold [41,192], mammalian Rap1 associates with telomeres solely through its interaction with TRF2 [20]. The Myb domain of mammalian Rap1 is not suited for DNA binding because its surface lacks positive charge and therefore is more likely to bind to a protein [193]. The targets of the single BRCT domain in the Rap1 proteins are not known. In other proteins, BRCT domains usually occur as tandem pairs and can function as a phosphopeptide binding module [194].

1.3.2 *Rap1 and telomere length regulation*

Telomere length regulation by Rap1 in budding yeast is conducted through its interaction with Rif1 and Rif2 (*R*ap1 *i*nteracting *f*actor *1* and *2*), as evidenced by the elongation of telomeres in their absence [195,196]. A proposed mechanism of Rif1 and Rif2 action in the negative regulation of telomere length is by interfering with recruitment of Tel1 (the ATM ortholog). The MRX (*M*re11-*R*ad50-*X*rs2) complex binds to telomeres in *S. cerevisiae* and recruits Tel1 [197,198]. Tel1 has

been shown to preferentially associate with short telomeres [199-201] and facilitate their elongation. Rap1 binding partners Rif1 and Rif2 are proposed to compete with Tel1 binding to the MRX complex, hence preventing the subsequent steps that allow for telomerase recruitment [202]. Additionally, while *S. pombe* Rif1 does not bind directly to Rap1, it localizes to the telomere and is involved in regulating telomere length [36]. Although a mammalian ortholog of Rif1 (not Rif2) has been identified, it does not localize to functional telomeres, nor is it involved in telomere length homeostasis [203]. Instead Rif1 localizes to DSBs and dysfunctional telomeres and promotes NHEJ by inhibiting resection downstream of 53BP1 [165,204-207]. Additionally Rif1 also participates in the intra-S phase checkpoint, responding to replication stress [203,208], and timing of replication origin firing [209,210]. Thus it seems unlikely that hRap1 follows the budding yeast Rap1 paradigm in using Rif1 to maintain telomere length homeostasis.

1.3.3 *Rap1 and end-protection*

In both *S. cerevisiae* and *S. pombe,* Rap1 is required for the prevention of NHEJ at chromosome ends [191,211]. Some mechanistic insight has been obtained from studies in *S. cerevisiae* that indicate Rap1 can protect telomeres from fusion via its C-terminal interactors Rif2 and Sir4, and also by its central domain (which includes the DNA binding domain) [212]. Despite not binding to telomeric DNA, Rap1 in *S. pombe* has also been shown to inhibit telomere fusions [211]. While mammalian orthologs of Sir4 and Rif2 do not exist, deletion of TRF2 and Rap1

from MEFs resulted in telomere fusions, suggesting mammalian Rap1 may have retained its function in repressing NHEJ [24]. Furthermore, human Rap1 can block NHEJ when it binds to TRF2 loaded on a telomeric end-joining substrate *in vitro* [213], and a Rap1-fusion protein can reduce telomere fusions when it is tethered to telomeres that are depleted of TRF2 [160].

In several species of budding yeast, namely *Kluyveromyces lactis* (kl) and *Candida albicans* (ca), Rap1 functions in repressing homologous recombination at the telomere. The *K. lactis* strain *ter1-16T* expresses a re-programmed telomerase that synthesizes telomeres lacking Rap1 binding sites, leading to elongated telomeres with an especially long 3' overhang. Electron microscopy of these cells revealed the formation of T-loop structures and an abundance of t-circles. When Rad52, a bona fide HDR component in budding yeast was absent, the incidence of t-circles decreased indicating that the t-circles were products of HDR, suggesting Rap1 binding to telomeres is required to inhibit recombination [214]. Complete deletion of caRap1 also exhibited an abundance of t-circles in comparison to wild type [215]. Depletion of TRF2 and Rap1 from Ku70 null cells resulted in T-SCEs, raising the possibility that mammalian Rap1 may also be required to repress HDR at the telomere [154].

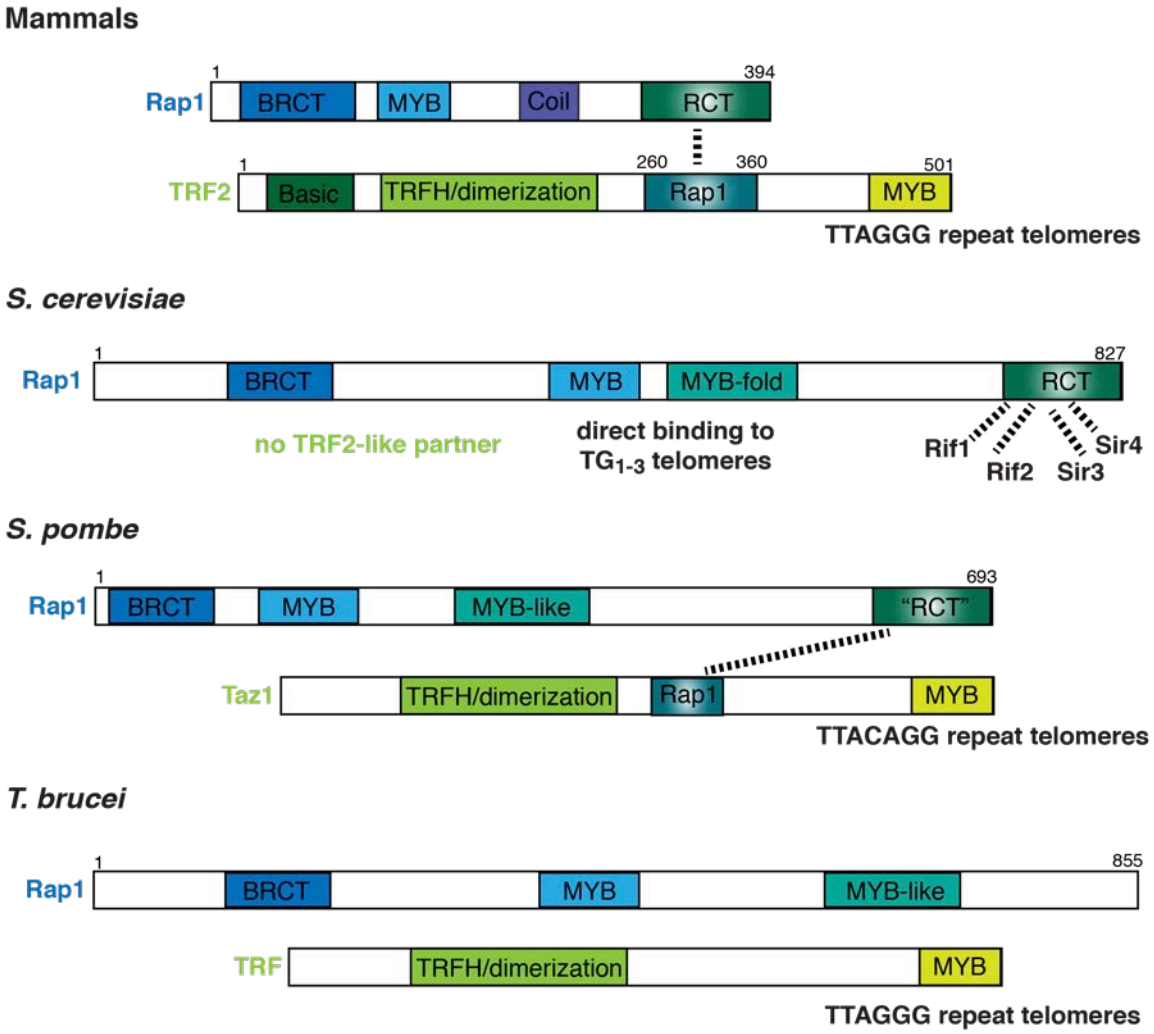

Figure 1.5 Mammalian Rap1 resembles yeast and trypanosome Rap1. Adapted from [227]. Schematic representation of conserved protein motifs of Rap1 and its TRF2-like partners in the indicated organisms. Amino acid positions indicated in schematic of mammalian Rap1 correspond to mouse Rap1. MYB indicates regions with a MYB sequence. MYB-fold indicates a motif that lacks sequence similarity to the MYB sequence but has a similar fold. MYB-like indicates sequence similarlity to the MYB-fold of *S. cerevisiae*, but their structure has not been determined. *S. cerevisiae* interacts with several factors important for its functions via its RCT domain. "RCT" of *S. pombe* indicates the region of Rap1 that is required for interaction with Taz1. It is not known whether *T. brucei* has a RCT domain, but the C-terminus of tbRap1 is not required for interaction with its TRF interacting partner.

1.3.4 *A role for Rap1 in meiosis and chromatin organization*

Telomeres are involved in chromatin reorganization during meiosis in yeasts, worms and mammals. During meiotic prophase I, telomeres attach to the nuclear envelope mediated by SUN/KASH-domain nuclear transmembrane complexes and other meiosis-specific protein complexes (reviewed in [216]). Following leptotene, telomeres cluster around the centrosome resulting in bouquet formation, proposed to stimulate homologous chromosome pairing and meiotic recombination. Rap1 in fission yeast is necessary for telomere clustering at the spindle pole body during the premeiotic horsetail stage, which in mammals is analogous to bouquet formation in meiosis [36,217,218]. During normal cell division, telomeres are tethered to the nuclear envelope during the process of nuclear assembly, potentially mediated by an interaction between Rap1 and SUN1 [219].

1.3.5 *Non-telomeric functions of mammalian Rap1*

Transcriptional regulation by Rap1 has been demonstrated in budding yeast as well in trypanosomes. Similar to budding yeast tbRap1 largely localizes to the telomere, but not exclusively. *T. brucei* normally express one variant surface glycoprotein (VSG) from subtelomeric loci in a monoallelic fashion. Knockdown of tbRap1 led to derepression of VSG expression sites causing simultaneous expression of multiple different VSGs [39].

Unlike in *S. cerevisiae,* where Rap1 interacts with sirtuins (Sir3p and Sir4p) that regulate transcription, mammalian Rap1 does not interact with the

sirtuins, however it has been shown to localize to over 30,000 chromosome-internal sites and control gene expression, affecting metabolism and body weight control [220-223]. ChIP-seq for Rap1 in MEFs indicated that it predominantly localized to chromosome internal loci with $[TTAGGG]_2$ as a consensus motif, suggesting TRF2-mediated recruitment to these sites. Rap1 was also detected at telomere sequences containing a mismatch that disrupts TRF2 binding, suggesting additional interacting partners and modes of recruitment for Rap1 [220]. Indeed, regulation of metabolic genes by Rap1 was independent of its ability to bind TRF2 [221]. Human Rap1 has also been reported to associate with chromosome internal loci, but the number of sites (~100) is much lower [223].

Another unanticipated function of Rap1 is its role in the modulation of NFκβ signaling. Rap1 was identified in a gain-of-function screen for regulators of NFκβ [224]. Despite the predominantly telomeric localization of Rap1, the authors observed a cytoplasmic fraction of Rap1 that is constitutively associated with Iκβ kinases (IKKs). IKKs are responsible for phosphorylation and subsequent degradation of inhibitors of NFκβ (Iκβ proteins). They found that Rap1 requires interaction with IKKs to activate NFκβ gene expression and suggested that Rap1 directs IKK activity specifically to p65, an inhibitory subunit of NFκβ. These results are surprising when taking into account data that shows that very little Rap1 is not bound to TRF2 [19], however it is possible that Rap1 has other interacting factors that recruit it to the cytoplasm, or Rap1 shuttles back and forth from the nucleus to the cytoplasm. Numerous Rap1-interacting factors have been

identified by mass spectrometry and proximity-based YFP fluorescence complementation screens, yet none of these interactions have been carefully characterized and it is unclear what roles they may play in protection and maintenance of telomeres [78,225,226].

1.4 Objectives

The first objective of this thesis was to understand the role of Rap1 in telomere end-protection. This was carried out using two independent methods: generation of a Rap1 conditional mouse knockout and analysis of a TRF2 mutant defective in Rap1 binding. These two approaches revealed that mouse Rap1 was required to inhibit HDR, but not NHEJ at the telomere.

The second objective, stemming from the discovery that Rap1 represses telomeric HDR, was to investigate the mechanism of this inhibition. Examination of a panel of Rap1 mutants indicated that the C-terminus of Rap1 was required to inhibit HDR. Further analysis suggested that Rap1 needs to be bound to TRF2 in order to repress HDR, although the mechanism by which Rap1/TRF2 act remains to be elucidated.

The third objective, facilitated by the development of efficient genome-editing technologies in human cells, was to query the discrepancy between the claimed functions of mouse and human Rap1. In contrast to mouse Rap1, *in vitro* and *in vivo* data had implicated human Rap1 in shielding telomeres from NHEJ. In addition, no deregulation of telomere length was noted in mouse cells lacking

Rap1, whereas human Rap1 had been implicated in telomere length homeostasis. To determine whether human Rap1 protects telomeres from NHEJ and negatively regulates telomere length, Rap1 knockouts were generated in a panel of human cell lines.

The fourth and final objective of this thesis was to construct human knockouts of POT1 to investigate its functions in and mechanisms of telomere protection, and to compare the role of human POT1 to those of mouse POT1a and POT1b.

Chapter 2: Loss of Rap1 Induces Telomere Recombination

2.1 Introduction

Previous loss-of-function studies that removed TRF2 from the telomere also noted concomitant loss of Rap1 [24,160]. Rap1 may therefore play a role in functions ascribed to TRF2, namely repression of the ATM kinase and inhibition of the DSB repair pathways, NHEJ and HDR [24,148,154,161]. In addition, overexpression and partial knockdown experiments revealed Rap1 as a potential regulator of telomere length [23,78]. In order to understand the contribution(s) of mammalian Rap1 to telomere protection two strategies were devised to remove Rap1 from the telomere and study the phenotypes of its loss. The two approaches taken were to 1) make a conditional mouse knockout of Rap1 and 2) to capitalize on the dependency of Rap1 on its telomeric recruitment by TRF2, by generating a TRF2-separation-of-function mutant that could fulfill all functions of TRF2 except interacting with Rap1. The results of these studies are reported here.

2.2 Results

2.2.1 *Deletion of Rap1 does not affect cell and organismal viability*

The gene for the mouse Rap1 protein is annotated as *TERF2IP (te*lomeric *r*epeat binding *f*actor *2 i*nteracting *p*rotein) but referred to as *Rap1* henceforth. Because the first exon of *Rap1* immediately abuts the essential KARS lysyl-tRNA-synthetase gene, a conditional knockout strategy was developed where a

Rap1 floxed (*Rap1*^{F}) allele was created by flanking exon 2 with LoxP sites (Agnel Sfeir, Figure 2.1A-C). Deletion of exon 2 by retroviral expression of Cre recombinase results in a premature stop codon in exon 3. The C-terminus of Rap1 is encoded by exon 3 and is required for its interaction with TRF2 and recruitment to the telomere. The resulting *Rap1*$^{\Delta ex2}$ allele can potentially encode a fragment containing the N-terminus of Rap1 (Agnel Sfeir, Figure 2.1A). Exogenous expression of FLAG-tagged Rap1-ex1 (*ex*on*1*) showed that this truncated form of Rap1, if it were produced, would not bind or localize to telomeres (Agnel Sfeir, Figure 2.1D-F). Indirect immunofluorescence (IF) on samples where nucleoplasmic proteins had been removed by treatment with Triton-X showed no visible signal of FLAG Rap1-ex1 (Agnel Sfeir, Figure 2.1E). Similarly, fractionation of cells expressing FLAG Rap1-ex1 showed that the protein was largely cytoplasmic and could not be detected in the chromatin bound fraction (Agnel Sfeir, Figure 2.1F).

Rap1$^{F/F}$ MEFs were isolated at embryonic day 13.5 and immortalized with *SV40 l*arge *T* antigen (SV40LT). IF and immunoblotting showed that Cre-treated SV40LT-immortalized *Rap1*$^{F/F}$ MEFs indeed lacked any detectable full-length or truncated Rap1 protein (Agnel Sfeir, Figure 2.2A-C) and *ch*romatin *i*mmuno*p*recipitation (ChIP) showed the loss of Rap1 from telomeres. The expression and localization of other shelterin components were not significantly affected (Agnel Sfeir, Figure 2.2D).

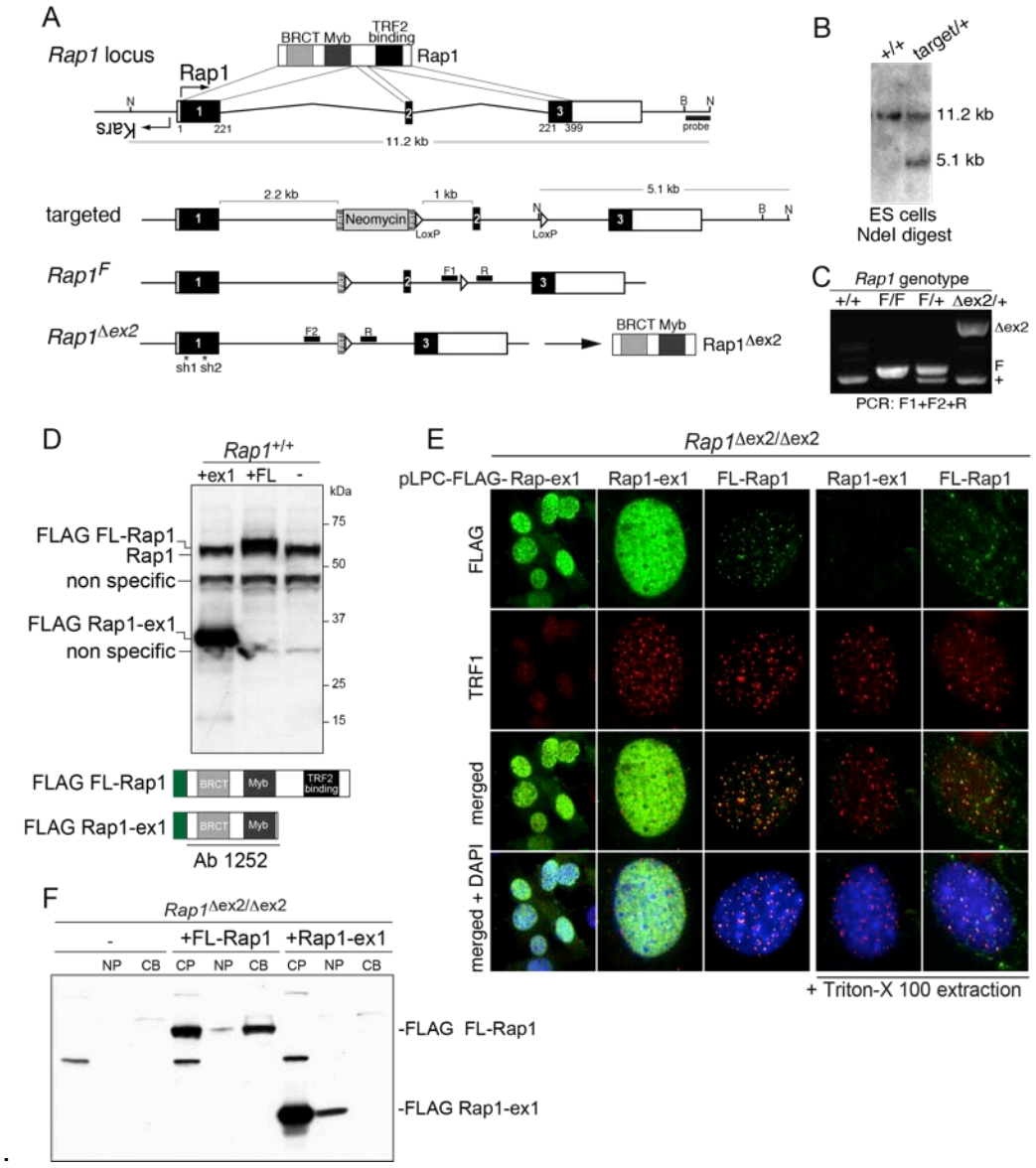

Figure 2.1 Strategy to conditionally delete mouse Rap1. (A) Schematic of Rap1, the mouse *Rap1* (*TERF2IP*) locus, the targeting construct, the floxed allele, and the Δex2 allele. N, NdeI; B, BamHI; F1, F2, and R, PCR primers. Rap1 shRNAs shown at the bottom. At right, Rap1Δex2-encoded protein. (B) Genomic blot of NdeI-digested DNA from ES cells. Probe in (A). (C) Genotyping of tail DNAs. Primers in (A). (D) Immunoblot for Rap1 in cells expressing FLAG FL-Rap1, FLAG Rap1-ex1, or vector control. The schematic below depicts full-length Rap1 protein (FLAG FL-Rap1) and the protein fragment encoded by exon 1 (FLAG Rap1-ex1). The antigenic region recognized by Rap1 Ab 1252 is indicated. (E) IF to monitor the localization of FLAG Rap1-ex1 and FLAG FL-Rap1. $Rap1^{\Delta ex2/\Delta ex2}$ MEFs expressing FLAG Rap1-ex1 or FLAG FL-Rap1 are stained with FLAG (green) and TRF1 (red). (F) $Rap1^{\Delta ex2/\Delta ex2}$ MEFs expressing FLAG Rap1-ex1, FLAG FL-Rap1 or vector control were fractionated as described in the materials and methods section and equal fractions of cytoplasmic proteins (CP), nucleoplasmic proteins (NP), and chromatin-bound proteins (CB) were analyzed by immunobloting with Rap1 Ab 1252.

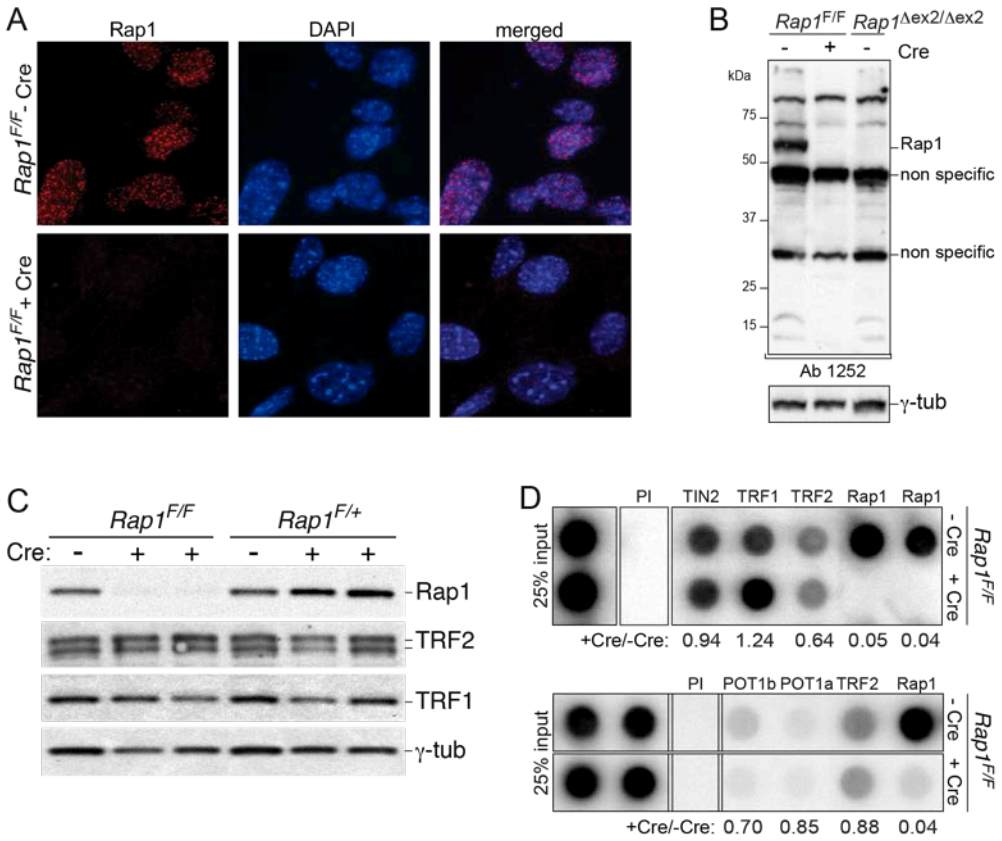

Figure 2.2 Deletion of Rap1 does not affect localization of other shelterin components to telomeres. (A) Loss of Rap1 IF signal from Cre-treated (day 5) Rap1F/F MEFs. Red, Rap1; green, telomeric FISH; blue, DNA (DAPI). (B) Western blot showing the disappearance of full-length Rap1 in cells deleted for exon 2. No new Rap1 protein was detected in cells bearing the Rap1Δex2 allele. (C) Immunoblots for Rap1 (Ab1252), TRF2 (Ab1254), and TRF1 (Ab1449) from *Rap1*$^{F/F}$ and *Rap1*$^{F/+}$ MEFs five days after Hit&Run-Cre (first lane) or pWZL-Cre (second lane). (D) Telomeric ChIPs on Cre-treated (day 5) *Rap1*$^{F/F}$ MEFs. Numbers represent ratios of % telomeric DNA in the ChIPs (pre-immune (PI) signal subtracted) on cells + and -Cre.

The growth rate of the SV40LT immortalized *Rap1*$^{\Delta ex2/\Delta ex2}$ MEFs was similar to control cells, and primary MEFs lacking wild type Rap1 did not show a growth arrest or p53 activation (Agnel Sfeir, Figure 2.3A-C). Furthermore, *Rap1*$^{\Delta ex2/\Delta ex2}$ mice were born at the expected frequencies and were fertile (Agnel Sfeir, Figure 2.3D). The survival of *Rap1*$^{\Delta ex2/\Delta ex2}$ cells and mice argues that *Rap1* deletion does not result in major telomere dysfunction, which is known to be lethal. While there was no evidence of translation of the truncated N-terminus of Rap1, to conclusively determine that no telomere-protection was being afforded by this fragment, *Rap1*$^{\Delta ex2/\Delta ex2}$ MEFs were infected with an shRNA targeting exon 1 (Agnel Sfeir, Figure 2.3E). Treatment with the shRNA targeting exon 1 did not induce a growth arrest or other phenotypes typical of telomere dysfunction further validating the previous conclusions.

In the second approach to remove Rap1 from telomeres, previously characterized *TRF2*$^{F/-}$*p53*$^{-/-}$ MEFs were used [24] to replace the endogenous TRF2 with a mutant that does not bind to Rap1. A short predicted helix at position 290 in the previously mapped Rap1 binding region (aa 260-360; [20]) was conserved in TRF2 orthologs but not in TRF1 (Figure 2.4A-B). Two mutations in this region (A289S and F290S) reduced the interaction between Rap1 and TRF2 in co-IP experiments (Giulia Celli, Figure 2.4C). To generate TRF2$^{\Delta Rap1}$, aa 284-297 were deleted (Megan van Overbeek, Figure 2.4D). TRF2$^{\Delta Rap1}$ failed to bind to Rap1 in co-IP experiments whereas it retained its previously reported interaction with Apollo (Megan van Overbeek, Figure 2.4E). TRF2$^{\Delta Rap1}$ was expressed in *TRF2*$^{F/-}$

p53$^{-/-}$ MEFs and the endogenous TRF2 was removed with Cre, resulting in depleted Rap1 protein levels (Megan van Overbeek, Figure 2.4F). Although TRF2$^{\Delta Rap1}$ localized to telomeres efficiently, IF and ChIP indicated that the telomeres lacked Rap1 (Figure 2.5A-B). Other shelterin components were affected to an extent (<2-fold; Figure 2.5B) that is not expected to be functionally significant as heterozygous MEFs and mice lacking one copy of *TRF1*, *TPP1*, *TRF2,* or *POT1a/b* display no telomere defect. Assessment of shelterin occupancy at telomeres by ChIP displayed some variability due to antibody quality and inexact experimental processing (Figure 2.5B). Despite this variability, on average less than 10% of residual Rap1 remained at telomeres in TRF2 null MEFs complemented with TRF2$^{\Delta Rap1}$, while levels of other shelterin components in these cells were approximately 85% or higher, compared to cells complemented with wild type TRF2 (Figure 2.5B). Consistent with the viability of *Rap1*$^{\Delta ex2/\Delta ex2}$ cells, cells expressing TRF2$^{\Delta Rap1}$ proliferated at the same rate as cells expressing wild type TRF2 (Megan van Overbeek, Figure 2.5C-D).

2.2.2 *No induction of DDR or NHEJ at telomeres lacking Rap1*

Rap1$^{\Delta ex2/\Delta ex2}$ cells did not show TIFs and phosphorylation of Chk1 and Chk2 (Chk1-P, Chk2-P) was not evident (Figure 2.6A-C). Further depletion of Rap1 mRNA with an shRNA also failed to elicit a DNA damage signal in *Rap1*$^{\Delta ex2/\Delta ex2}$ cells (Figure 2.6B). Consistent with these results, TRF2$^{\Delta Rap1}$ was equivalent to wild type TRF2 in its ability to repress TIFs in cells lacking

endogenous TRF2 (Figure 2.6D-F). The mutant form of TRF2 also repressed the induction of Chk2-P to the same extent as wild type TRF2 (Figure 2.6E). The low level of Chk2-P observed in Cre-treated TRF2- and TRF2$^{\Delta Rap1}$- expressing cells is likely due to Cre-induced DNA damage, since the phosphorylation of Chk2 was diminished when using a version of Cre (Hit&Run) that eventually disappears from the cells due to self-deletion (Figure 2.6F).

Telomere fusions were not induced by deletion of *Rap1* and TRF2$^{\Delta Rap1}$ had the same ability as wild type TRF2 to repress NHEJ at telomeres (Figure 2.7A-C). However, as previously discussed, NHEJ of telomeres lacking TRF2 requires active DNA damage signaling [148] thus the lack of telomere fusions could be due to the lack of ATM/ATR activation. In order to initiate DNA damage signaling specifically at the telomere, we used a TPP1 shRNA to activate the ATR kinase. This approach previously resulted in the reactivation of NHEJ at telomeres of TRF2- and ATM-deficient cells [148]. Despite ATR kinase signaling at telomeres and induction of TIFs elicited by the TPP1 shRNA (Figure 2.6B,D), Rap1 removal from telomeres did not induce their fusion (Figure 2.7B-C). Thus, Rap1 does not appear to be required in either the repression of NHEJ or ATM kinase signaling, explaining why the deletion of Rap1 does not curb cellular or organismal viability.

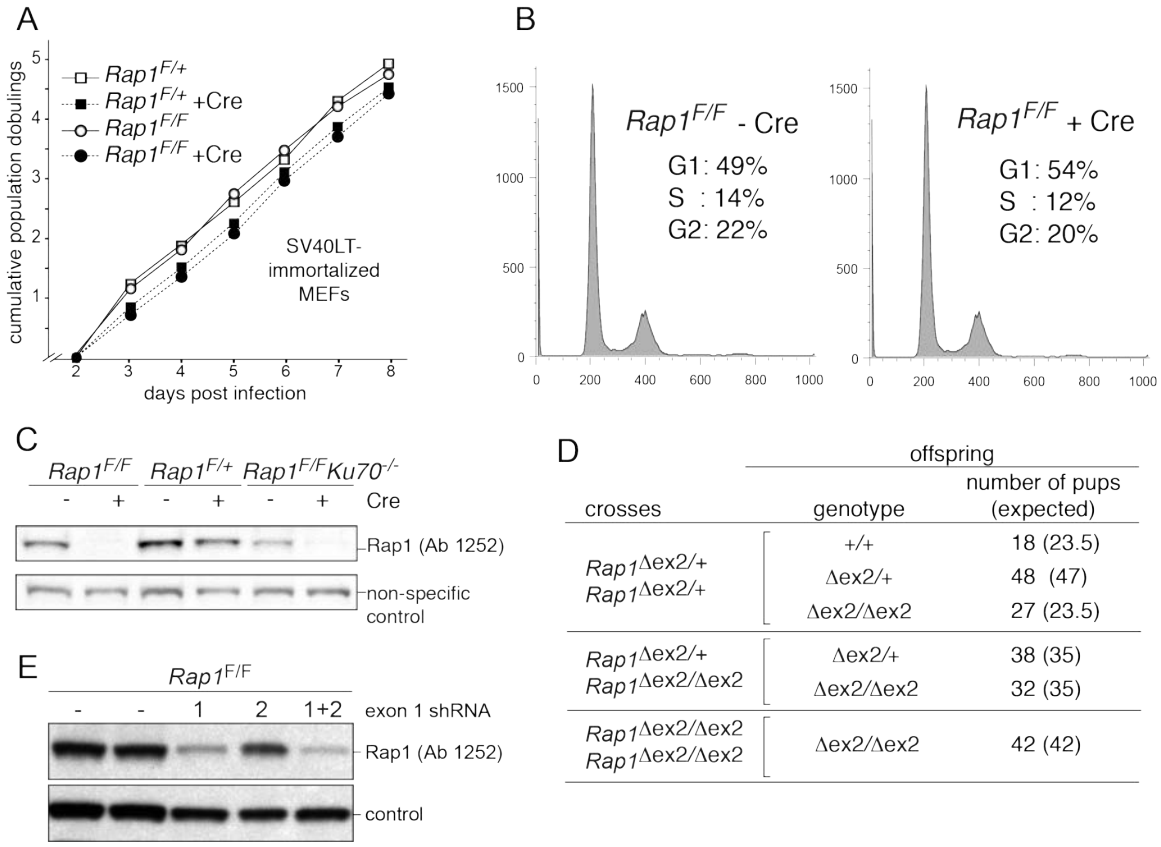

Figure 2.3 Rap1 deletion does not affect cell and organismal viability. (A) Proliferation of SV40LT-immortalized *Rap1*$^{F/F}$ and *Rap1*$^{F/+}$ MEFs infected as indicated. (B) FACS profiles of primary *Rap1*$^{F/F}$ cells infected with pWZL-Cre (left panel) or vector control (right panel), analyzed at day 5 after infection. The percentage of G1, S and G2 cells is noted within the FACS profile. (C) Immunoblot for Rap1 on MEFs with the indicated genotype, 96 hours after Cre treatment. (D) Offspring from *Rap1*$^{\Delta ex2/+}$ and *Rap1*$^{\Delta ex2/\Delta ex2}$ intercrosses. (E) Western blot showing the effect of Rap1 shRNAs 1 and 2 on Rap1 levels in wild type MEFs.

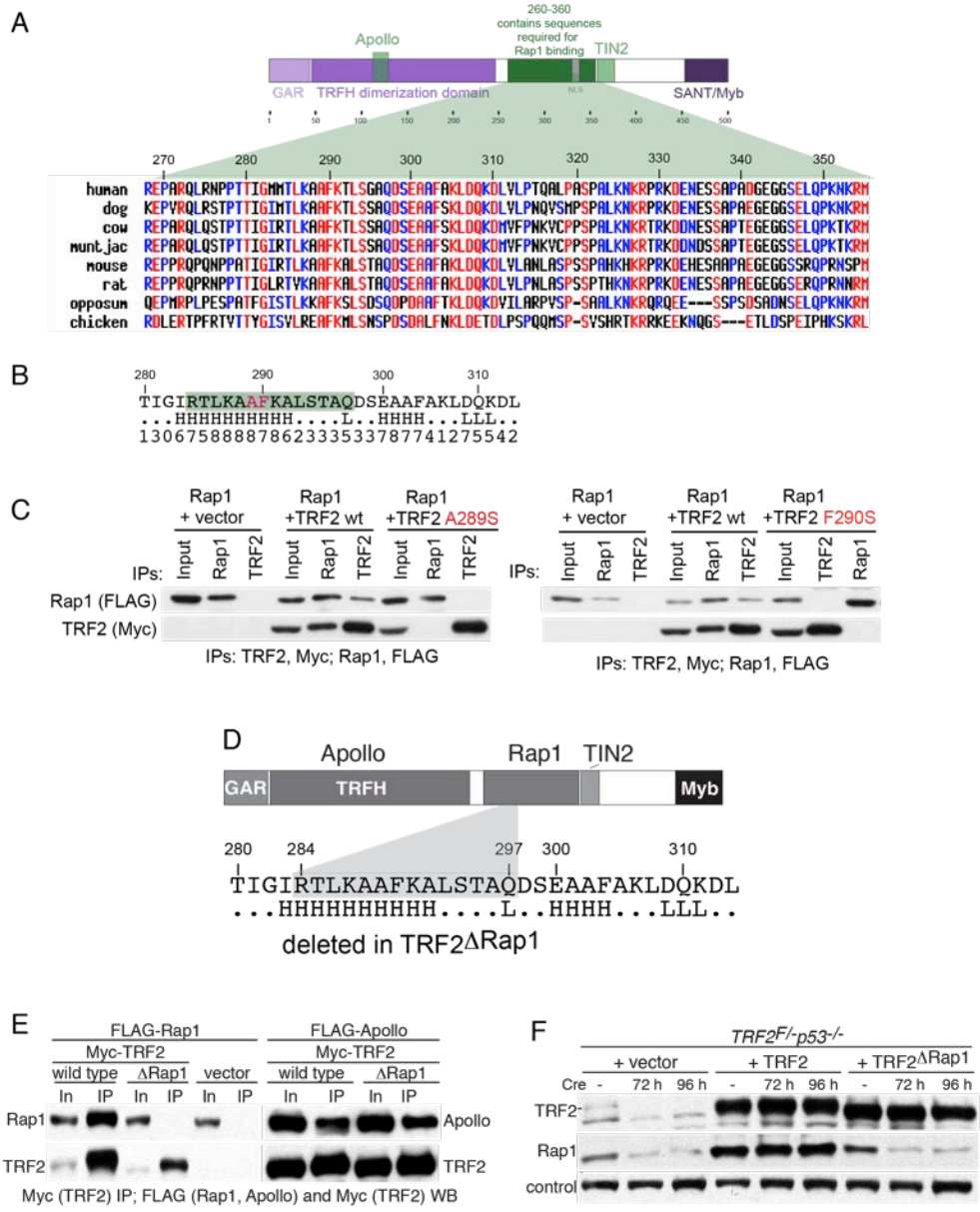

Figure 2.4 A TRF2 mutant deficient for Rap1 binding. (A) Schematic of TRF2 showing conservation of a subset of amino acids within the previously mapped Rap1 interaction domain. (B) Identification of a helical region within the conserved segment. Predicted protein structure from PredictProtein.org. (C) Co-IPs of FLAG-tagged Rap1 with wild type TRF2, TRF2 mutants or no protein. (D) The TRF2$^{\Delta Rap1}$ mutant. H, predicted helix. (E) Co-IP of Myc-TRF2 or Myc-TRF2$^{\Delta Rap1}$ with FLAG-Rap1 or FLAG-Apollo from co-transfected 293T cells. In, 2.5% of input. (E) Immunoblots for TRF2 and Rap1 from TRF2$^{F/-}$p53$^{-/-}$ MEFs expressing the indicated alleles at 72 and 96 hours after Hit&Run-Cre.

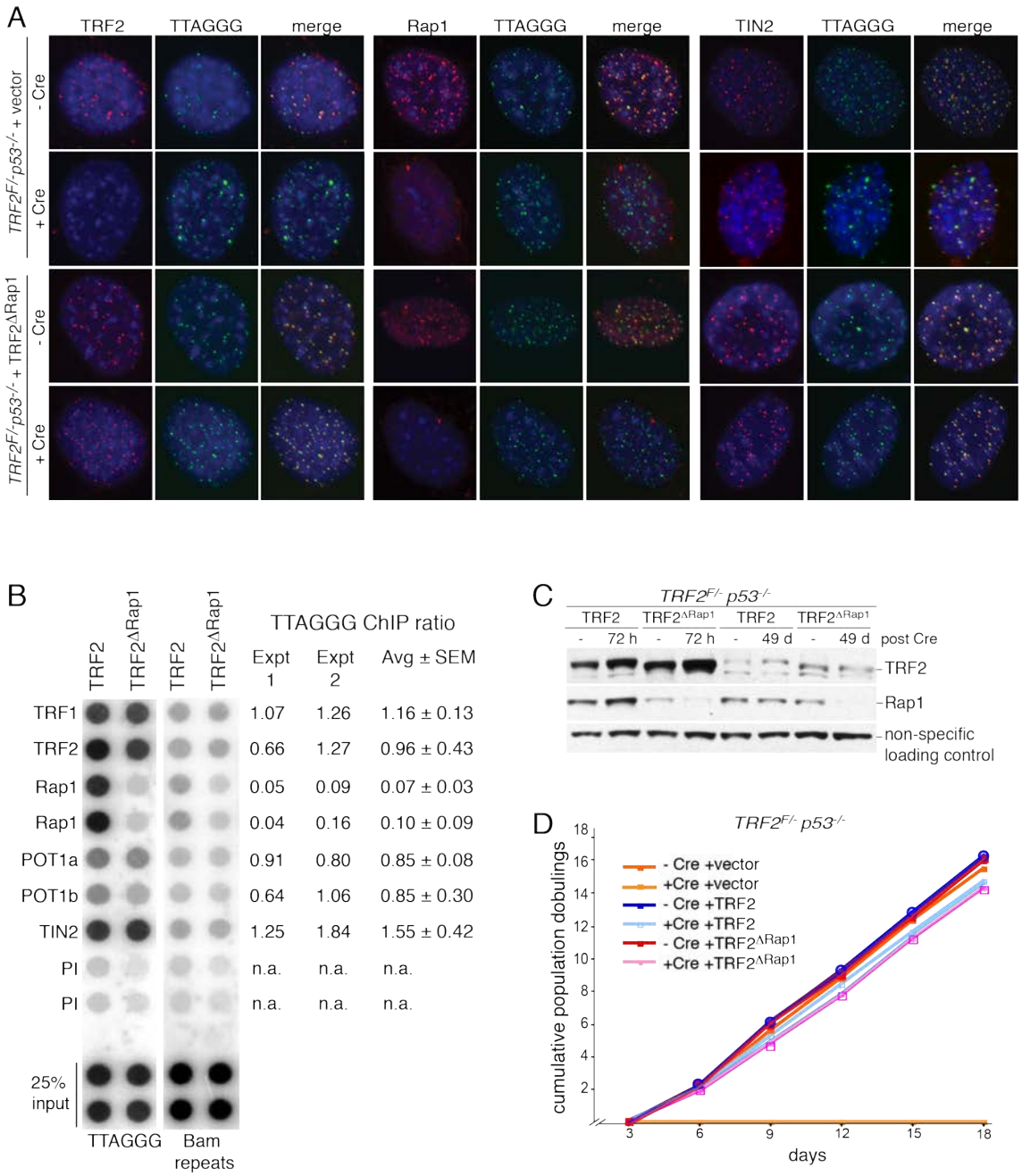

Figure 2.5 TRF2$^{\Delta Rap1}$ expression results in diminished levels of Rap1. (A) IF-FISH to monitor TRF2, Rap1, and TIN2 at telomeres in *TRF2$^{F/-}$p53$^{-/-}$* MEFs expressing TRF2$^{\Delta Rap1}$ or vector control at day 4 after Cre. (B) Telomeric ChIP of *TRF2$^{F/-}$p53$^{-/-}$* MEFs expressing TRF2 or TRF2$^{\Delta Rap1}$ at day 4 post Cre. Duplicate dot blots were probed for telomeric DNA or the dispersed BamHI repeats. ChIP ratios represent the % telomeric DNA recovered in TRF2$^{\Delta Rap1}$ vs. TRF2 expressing cells. ChIP ratios are shown from two independent experiments and averages with SEMs are listed to the right. (C) Immunoblots showing the expression of Rap1, TRF2, and TRF2$^{\Delta Rap1}$ in *TRF2$^{F/-}$p53$^{-/-}$* MEFs treated with pWZL-Cre for the indicated time-periods. (D) Growth curve of cells shown in (C) and the vector controls.

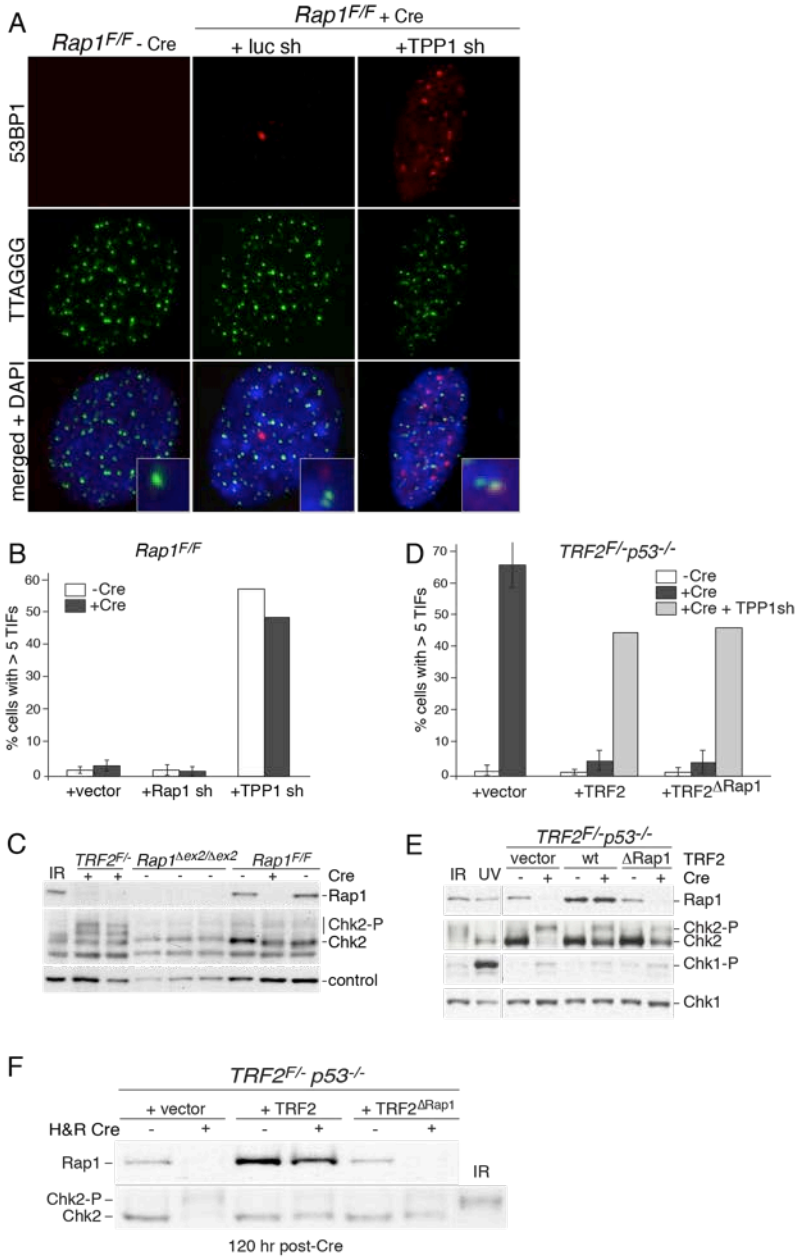

Figure 2.6 No DNA damage signaling at telomeres lacking Rap1. (A) TIF assay on Rap1F/F MEFs treated with Cre and the indicated shRNA. Red, IF for 53BP1; green, telomeric FISH; blue, DNA (DAPI). (B) TIF assay quantification. Averages of two independent experiments (n≥100 nuclei each) and SEMs. (C) Chk2-P in Rap1-deficient MEFs. TRF2 null cells and IR-treated cells (1 hr post 2 Gy,) serve as positive controls. (D) Quantification of TIF assays on TRF2F/-p53-/- cells expressing TRF2, TRF2ΔRap1 or vector control at day 4 post Cre. Mean of three independent experiments (n≥100 nuclei each) and SDs. (E) Chk1 and Chk2 phosphorylation in TRF2F/-p53-/- MEFs expressing TRF2, TRF2ΔRap1 or vector control. UV (1 hr post 25 J/m2) and IR (1 hr post 2 Gy) treated cells serve as positive controls. (F) Rap1 and Chk2 immunoblots of TRF2F/-p53-/- MEFs expressing TRF2, TRF2ΔRap1 or vector control, at 144 hours after treatment with Hit&Run-Cre.

A

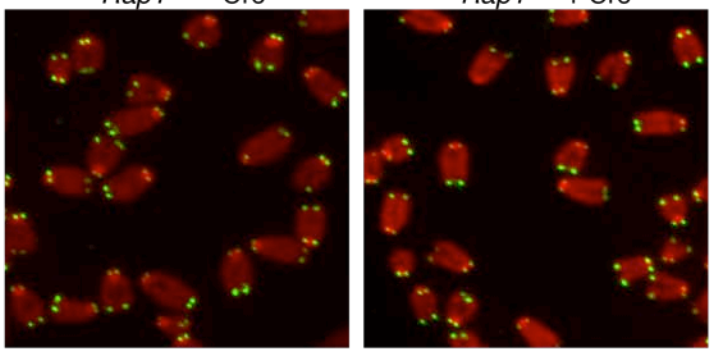

B

Rap1$^{F/F}$

Cre	shRNA	Telomeres scored	% fused (av)
-		800, 1030, 2124	0.13
+		2308, 4636, 5756	0.14
+	Rap1 sh	2720, 3452	0.19
-	TPP1 sh	1600, 2780	2.86
+	TPP1 sh	2240, 2860	2.93

C

TRF2$^{F/-}$p53$^{-/-}$

TRF2 allele	Cre	shRNA	Telomeres scored	% fused (av±SD)
vector	-		3848, 3660, 2092	0.13 ± 0.05
	+		1808, 2176, 2004	49 ± 6.3
	+	TPP1 sh	1240, 1488, 1060	51 ± 2.2
TRF2	-		3628, 4312, 2124	0.03 ± 0.05
	+		4552, 2020, 2196	0.15 ± 0.19
	+	TPP1 sh	2520, 2880, 1780	1.65 ± 1.2
TRF2$^{\Delta Rap1}$	-		3424, 4048, 2168	0.17 ± 0.07
	+		4428, 4140, 2212	0.06 ± 0.05
	+	TPP1 sh	2052, 2852, 1964	1.79 ± 0.2

Figure 2.7 Loss of Rap1 does not induce NHEJ. (A) Metaphase chromosomes from *Rap1$^{F/F}$* cells 5 days post Cre. Red, false colored DNA DAPI stain; green, telomeric FISH. (B) Quantification of telomere fusions, detected as in (A) in Rap1$^{F/F}$ MEFs with the indicated Cre and shRNA treatments. Average % of telomeres fused is given. (C) Quantification of telomere fusions in *TRF2$^{F/-}$p53$^{-/-}$* MEFs (+ or – Cre, day 4) complemented with TRF2 or TRF2$^{\Delta Rap1}$ or vector control and treated with TPP1 shRNA as indicated.

2.2.3 *Telomere length and chromatin unchanged in Rap1-deficient cells*

To assess the role of Rap1 in telomere length regulation, telomere length was examined over three generations of mouse breeding and over approximately 50 population doublings in cultured cells lacking Rap1 (Figure 2.8A-C). No overt changes in telomere length were detected. Furthermore, the amount of the single-stranded overhang remained unchanged in Rap1-deficient cells (Figure 2.8D).

Mammalian telomeres contain nucleosomes and epigenetic marks that are characteristic of heterochromatin, such as heavily methylated histones (reviewed in [228]). Rap1 was not required for the maintenance of telomeric nucleosomal organization or the methylation of telomeric H3K9 (Agnel Sfeir, Figure 2.9A-C). In addition, the level of telomeric lncRNA called TERRA (*te*lomeric *r*epeat-containing *R*N*A*; reviewed in [229]) was not affected upon deletion of Rap1 (Agnel Sfeir, Figure 2.9D).

2.2.4 *Rap1 is a repressor of telomere recombination*

Homology-directed repair threatens telomere integrity because unequal telomere-sister chromatid exchanges can change telomere lengths. T-SCEs are most frequent when either *TRF2* or *POT1a/b* are deleted from Ku-deficient cells [154,155], although low levels of T-SCEs have been reported for *POT1a* deficiency alone [32]. To determine whether Rap1 was required for TRF2-mediated repression of T-SCEs, TRF2$^{\Delta Rap1}$ was introduced into SV40LT-immortalized *TRF2$^{F/-}$Ku70$^{-/-}$*

MEFs, which display frequent T-SCEs upon deletion of *TRF2* with Cre. Whereas the telomeric exchanges were repressed by wild type TRF2, TRF2$^{\Delta Rap1}$ failed to block the telomeric HDR (Fig. 2.10A-C). The frequency of T-SCEs was the same whether the cells expressed TRF2$^{\Delta Rap1}$ or no TRF2 (Figure 2.10D). Furthermore, T-SCEs were induced by Cre-mediated deletion of Rap1 from *Rap1$^{F/F}$Ku70$^{-/-}$* cells (Figure 2.10E).

Notably, the T-SCEs occurred despite absence of TIFs in cells lacking both Ku70 and telomeric Rap1 (Figure 2.11A-B). Basal levels of Chk2-P were observed in cells lacking Rap1 and Ku70, but these were likely attributable to the Cre effect and Ku70 deficiency, as they were much lower than the induction of Chk2-P observed in the absence of TRF2 and Ku70 (Figure 2.11C-D). There appeared to be no effect on the terminal structure of telomeres in cells lacking Rap1 and Ku70 (Figure 2.11E).

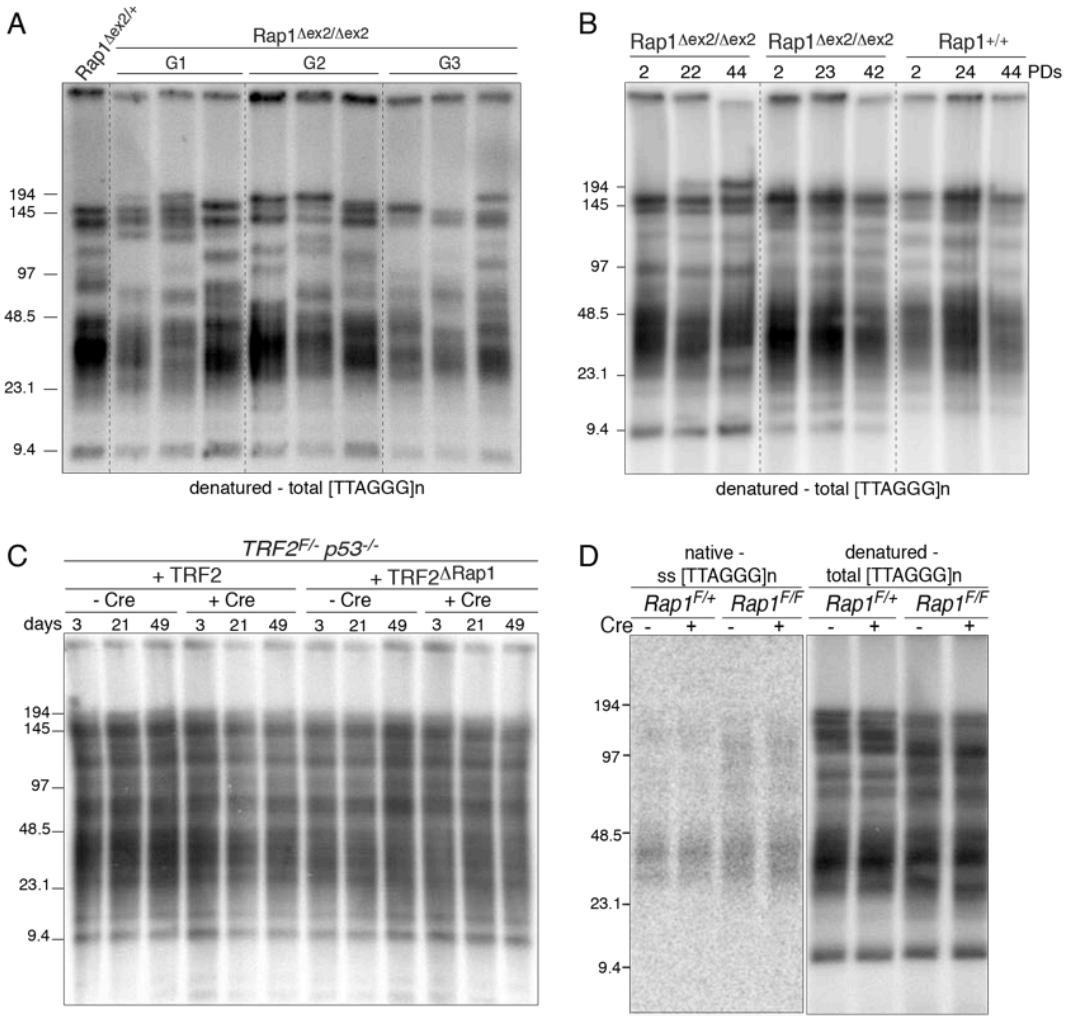

Figure 2.8 Rap1 does not affect telomere length maintenance. (A) Telomeric restriction fragment analysis on cells isolated from the liver of a *Rap1*$^{\Delta ex2/+}$ mouse and three successive generations of *Rap1*$^{\Delta ex2/\Delta ex2}$ mice. Telomeric DNA was detected by in-gel hybridization assays using a $(CCCAAT)_4$ probe under denaturing conditions. (B) Telomere length analysis on *Rap1*$^{\Delta ex2/\Delta ex2}$ MEFs and wild type cells at the indicated population doublings. (C) Telomere length analysis of *TRF2*$^{F/-}$ *p53*$^{-/-}$ cells expressing TRF2, TRF2$^{\Delta Rap1}$, or vector, plus or minus treatment with Cre. (D) Loss of Rap1 does not alter the telomeric single-stranded DNA. MEFs with the indicated genotypes were analyzed at day 5 post Cre treatment using in-gel hybridization to MboI digested DNA. The panel on the left shows the hybridization signal using a $(CCCAAT)_4$ probe under native conditions. The panel on the right represents total telomere signal after in situ denaturation of DNA and re-hybridization with the same probe. The numbers on the bottom represent the relative overhang signal normalized to the total telomeric repeat signal. Values of the normalized signal are compared between – Cre (set at 1) and +Cre samples.

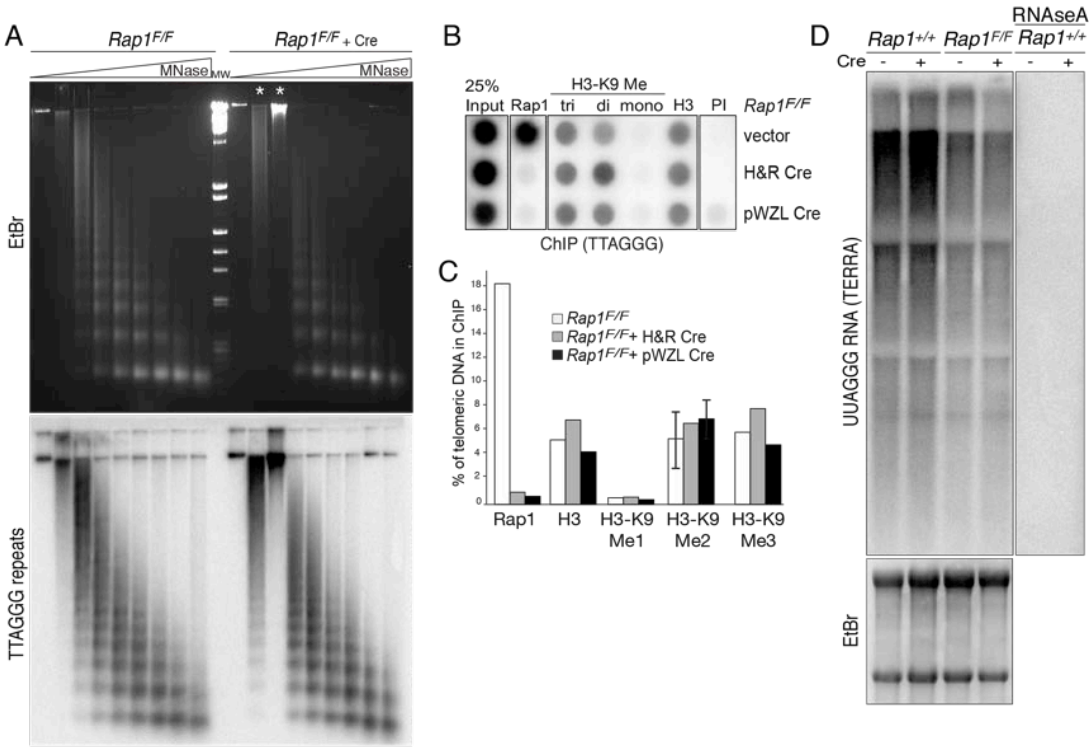

Figure 2.9 Telomeric chromatin and transcription unchanged upon Rap1 loss.
(A) Unaltered nucleosomal organization of telomeric chromatin upon loss Rap1. DNA from MNase digested nuclei of *Rap1*$^{F/F}$ MEFs (+ or – Cre treatment) fractionated on a 1% agarose gel and stained with ethidium bromide (upper panel) to monitor organization of bulk nucleosomes or blotted and hybridized with a ^{32}P-$(CCCTAA)_4$ probe (lower panel). The two DNA samples marked by (*) were switched. The concentration of MNase ranged from 5 – 600 U/ml. (B) Rap1 loss has no effect on the heterochromatic marks at telomeres. Telomeric ChIP analysis of Rap1$^{F/F}$ cells treated with pWZL Cre or Hit&Run Cre as indicated. Antibodies used are indicated on top. Pre-immune serum (PI) is used as a negative control. (C) Quantification of percentages of total telomeric DNA recovered in the ChIP shown in (B). (D) TERRA levels as detected by Northern blot analysis on Rap1 MEFs with the indicated genotype and Cre treatment. Ethidium bromide staining pattern serves as a loading control.

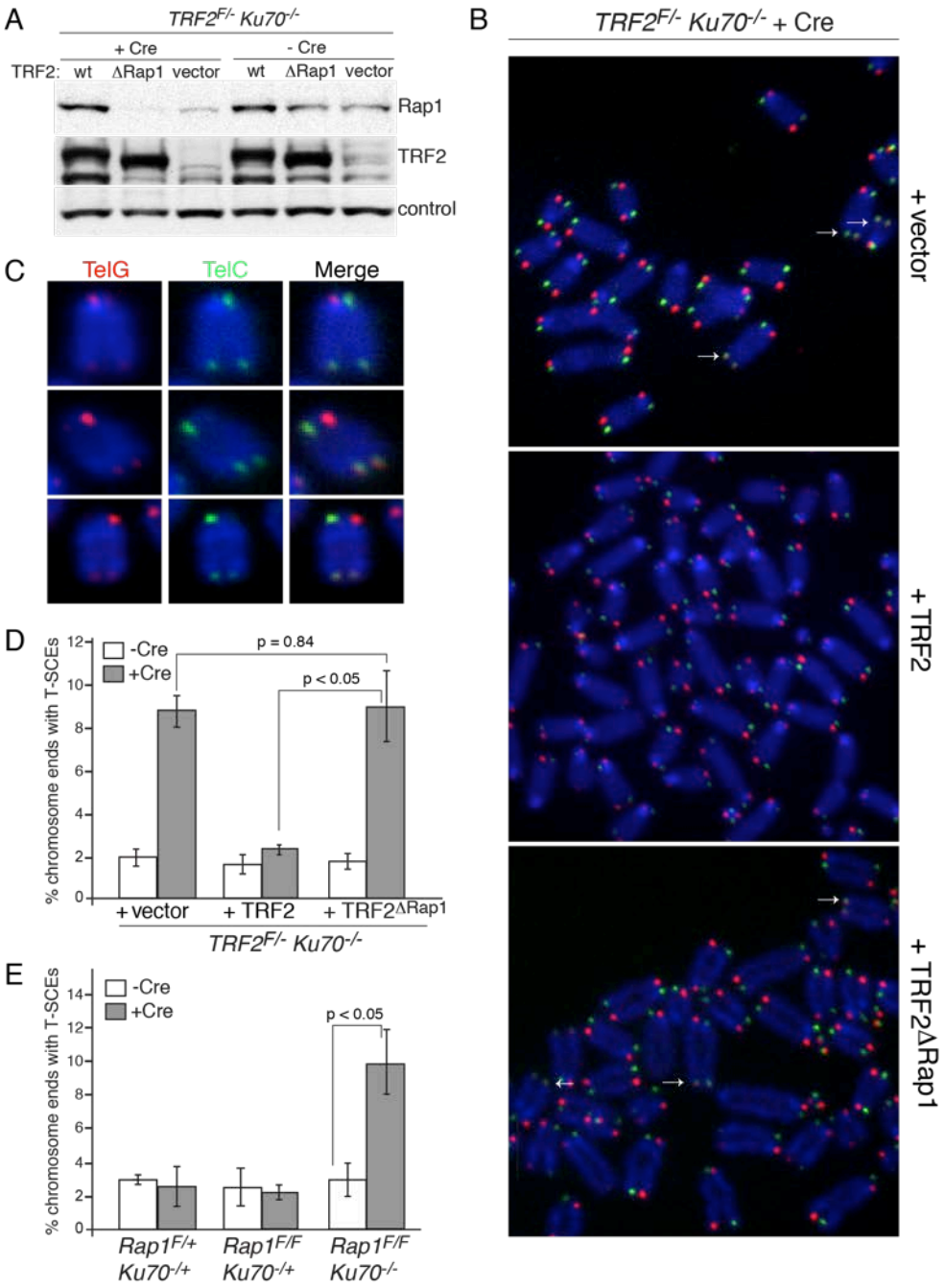

Figure 2.10 Rap1 is a repressor of telomere recombination. (A) Rap1 and TRF2 from *TRF2$^{F/-}$Ku70$^{-/-}$* MEFs expressing TRF2, TRF2$^{\Delta Rap1}$, or vector control analyzed 4 days after Cre. (B) CO-FISH analysis on cells in (A). Arrows: T-SCEs. (C) Enlarged T-SCE events in Cre-treated TRF2$^{F/-}$Ku70$^{-/-}$ MEFs expressing TRF2$^{\Delta Rap1}$. (D) Quantification of T-SCEs as assessed in (B). Bars represent averages from three independent experiments (n>1100 chromosome ends each) and SDs. P values based on Student's two-tailed t-test. (E) Quantification of T-SCEs as assessed in (B) in cells of the indicated Rap1 and Ku70 status. Method as in (D). Errors bars: SEMs except for SDs for *Rap1$^{F/F}$Ku70$^{-/-}$*.

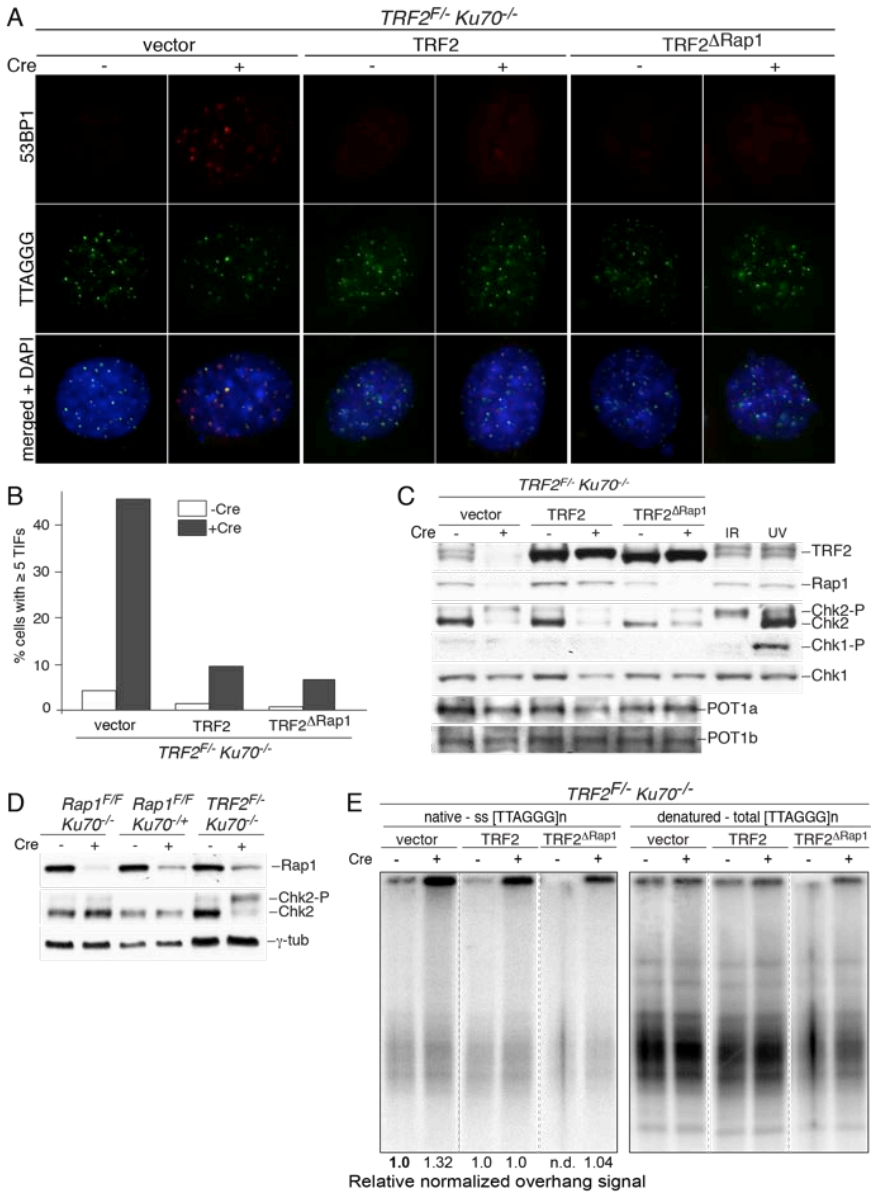

Figure 2.11 T-SCEs observed in Rap1-deficient cells despite no DNA damage signaling. (A) TIF assay on *TRF2$^{F/-}$ Ku70$^{-/-}$* SV40LT-immortalized MEFs expressing TRF2, TRF2$^{\Delta Rap1}$ or vector control, before or after treatment with Cre. Red, IF for 53BP1; green, telomeric FISH; blue, DNA (DAPI). (B) Quantification of TIF assay in (A). (C) Immunoblots for indicated shelterin components, Chk1 and Chk2 of same cells as in (A). IR (1hr post 2Gy) and UV (1hr post 25 J/m2) treated cells serve as positive controls. (D) Immunoblots for Rap1 and Chk2 on SV40LT immortalized MEFs with indicated genotypes, before and after treatment with Cre. γ-tubulin serves as loading control. (E) Loss of Rap1 in Ku-deficient SV40LT immortalized MEFs does not alter the telomeric single-stranded DNA. MEFs expressing TRF2, TRF2$^{\Delta Rap1}$, or vector control were analyzed using in-gel hybridization to MboI digested DNA before and 96 hours after treatment with Cre. Left, hybridization signal with $(CCCAAT)_4$ probe under native conditions; right, hybridization signal with same probe after denaturation. Overhang signal was normalized to the total telomeric repeat signal. Numbers represent the relative overhang signal as compared to TRF2 plus Cre (set as 1).

2.3 Summary of findings

These data indicate that Rap1 functions at mouse telomeres to repress HDR, which has the potential for generating shortened telomeres and can promote telomerase-independent telomere maintenance. Furthermore, these results underscore the functional compartmentalization within shelterin where each subunit is dedicated to distinct functions. As previously reported, replication of telomeric DNA is facilitated by TRF1 [156,157], TPP1/POT1 are required for the repression of ATR signaling [150,151], while TRF2 is the predominant repressor of both ATM signaling and NHEJ [24]. The current data show that these functions of TRF2 do not require Rap1. Instead, Rap1 is required to repress HDR. Interestingly, this division of roles revealed that telomeres can undergo HDR without being detected by the ATM and ATR kinase pathways. When HDR takes place at telomeres lacking TRF2 or POT1a/b, DNA damage signaling results in the formation of TIFs. In the case of Rap1 removal, however, the telomeres lack detectable TIFs, yet are susceptible to HDR. Thus, the formation of DNA damage foci at telomeres is not a prerequisite for HDR. How exactly Rap1 represses HDR and the action of Ku in this repression remains to be determined.

It is of interest to recall that expression of the TRF2$^{\Delta B}$ mutant allele leads to stochastic t-loop loss, presumably because the basic domain of TRF2 stabilizes Holliday Junctions and restrains the action of HJ resolvases [172-175]. However, if the basic domain of TRF2 cannot inhibit HJ resolution, a critical step in the generation of T-SCEs, the question arises as to why T-SCEs are not

observed in TRF2$^{\Delta B}$-expressing TRF2/Ku70-deficient cells [154]. One possibility is that Rap1 bound to TRF2 may repress the formation of HJs so that T-SCEs will not occur. For instance Rap1 and/or TRF2 may inhibit strand invasion into sister chromatids, or Rad51 filament assembly, thereby preventing HJ formation and potential exchange of sequence. In addition, it is possible that the basic domain of TRF2 blocks branch migration of TRF2, thereby also repressing HJ formation and preventing T-SCEs.

Rap1 was not required for the maintenance of several other features of mouse telomeres including the amount of the single-stranded overhang, the level of telomeric transcripts and the telomeric chromatin state and organization. In budding yeast, Rap1 has been proposed to facilitate heterochromatin assembly by recruitment of Sir3 and Sir4 that interact with the N-termini of histones H3 and H4 [231-233]. Despite a proximity-based screen identifying potential interactions between Rap1 and histones H2A and H4 [226], Rap1 does not seem to play a role in maintaining telomeric chromatin.

Surprisingly no gross aberrations in telomere length in Rap1 null cells were observed either, although small differences may be difficult to discern due to the long telomeres of mouse cells. Studies of Rap1's involvement in telomere length regulation may be more illuminating in human cells that have shorter telomeres.

Chapter 3: Elucidating the mechanism of HDR repression by Rap1

3.1 Introduction

How Rap1 represses HDR is not clear. It is possible that it functions by recruiting another protein with its BRCT domain or MYB motif, which are proposed to be protein-interaction domains (reviewed in [227]). Factors known to interact with Rap1 include the Rad50 and Mre11 components of the MRN complex [78], which contributes to 5' resection during HDR. However, the telomeric overhang is not altered in Rap1/Ku70-deficient MEFs [19], suggesting Rap1 does not play a major role in modulating resection at telomeres. Therefore it seems unlikely that Rap1 would inhibit telomeric HDR by limiting or preventing resection by MRN. The Rap1/TRF2 complex also interacts with the protein scaffold SLX4 [225], which binds to a HJ resolvase Mus81/Eme1. It is possible that Rap1 modulates the activity of one of the nucleases in the SLX4 complex to interrupt HDR.

In this chapter, Rap1 mutants were analyzed to determine which domains of Rap1 were required for repression of T-SCEs. These experiments identified the C-terminus of Rap1 as the important functional domain in the inhibition of HDR. Further investigation suggested that TRF2/Rap1 complex formation was necessary for HDR repression and preliminary experiments to assess the DNA-binding activity of this complex were conducted.

The repression of HDR also requires the presence of either of the two POT1 proteins [155]. POT1a/b bind to single-stranded telomeric DNA and may inhibit initiation of HDR by preventing loading of Rad51 onto ssDNA. In the

context of POT1a/b- and Ku70-deficiency, Rap1, which remains at telomeres, is incapable of repressing HDR. The converse is true of POT1a/b that remain at telomeres when Rap1 is deleted, but cannot inhibit HDR [19]. These data raise the possibility that Rap1 and POT1 may act together to repress HDR. To investigate whether Rap1 and POT1 are epistatic in their repression of HDR, an shRNA to TPP1 was used to remove POT1 from telomeres in Rap1/Ku70-deficient cells. No change in the level of T-SCEs would suggest that Rap1 and POT1 are epistatic, possibly acting together at the same step. For instance, Rap1 and POT1 may both interfere with Rad51 filament formation. Exacerbation of the occurrence of T-SCEs would suggest that Rap1 and POT1 act on distinct, non-linear aspects of homology-directed repair, for example HJ resolution by either Mus81/Eme1 or GEN1.

The lack of DNA damage signaling in Rap1/Ku70-deficient MEFs also provides a unique setting to study the consequences of ongoing HDR on telomere maintenance. As mouse cells constitutively express telomerase, this setting does not recapitulate ALT. However, the analysis of the long-term consequences of combined deficiency of Rap1 and Ku may still provide insights into the recombination-based mechanisms of telomere maintenance.

3.2 Results

3.2.1 *The C-terminus of Rap1 is required to repress telomeric HDR*

MYC-tagged alleles of mouse Rap1 containing deletions of the relevant motifs (BRCT, MYB, Coil) were constructed as illustrated in Figure 3.1A. Determination of amino acid positions of domains was based on analogous domain positions outlined in human Rap1 [20,23]. Based on the crystal structure of the hRap1 C-terminus in complex with a fragment of TRF2 ($TRF2^{RBM}$, *R*ap1 *b*inding *m*otif, aa 275-316) [18], the I318 residue in hRap1 was shown to be required for its interaction with TRF2. Co-IPs of transfected proteins from 293T cells showed that mutation of the analogous residue in mouse Rap1 (I312R) disrupted the interaction with mouse TRF2 (Figure 3.1B).

Rap1 mutants were retrovirally expressed in $Rap1^{F/F}Ku70^{-/-}$ MEFs and immunoblotting showed that most mutants were expressed at similar levels, except for MYC-I312R, which was significantly overexpressed, and MYC-ΔBMC, which was expressed weakly (Figure 3.1C). Rap1 protein levels are diminished upon TRF2 depletion, yet surprisingly the Rap1 I312R mutant, which could not bind TRF2, was overexpressed. Therefore, it seems that when Rap1 is not bound to TRF2, the I312 residue is bound by another factor that targets it for degradation. IF-FISH indicated that all mutants, except for MYC-I312R, localized to telomeres (Figure 3.1D). IF for MYC-I312R showed diffuse staining throughout the nucleus that disappeared upon extraction of nucleoplasmic proteins with

TritonX-100, indicating that the Rap1 I312R mutant was not associated with chromatin. (Figure 3.1D). CO-FISH analysis after removal of endogenous Rap1 with Cre revealed that all but the MYC-I312R mutant repressed T-SCEs, thus implicating the Rap1/TRF2 interaction in the inhibition of HDR (Figure 3.1E). Furthermore, the data showed that the BRCT, MYB and coiled domains of Rap1 are not required for the repression of homology-directed repair, either individually or together. Although the data argue against the N-terminus recruiting an HDR-repressing factor to telomeres, it is not excluded that the C-terminus of Rap1 binds to TRF2 and also recruits an HDR-repressor. However, since MYC-I312R cannot localize to telomeres, it is possible that its deficiency in repressing HDR is due to lack of telomeric recruitment of a factor involved in HDR inhibition. To address this latter possibility, we devised a strategy to tether Rap1 to telomeres in the absence of TRF2.

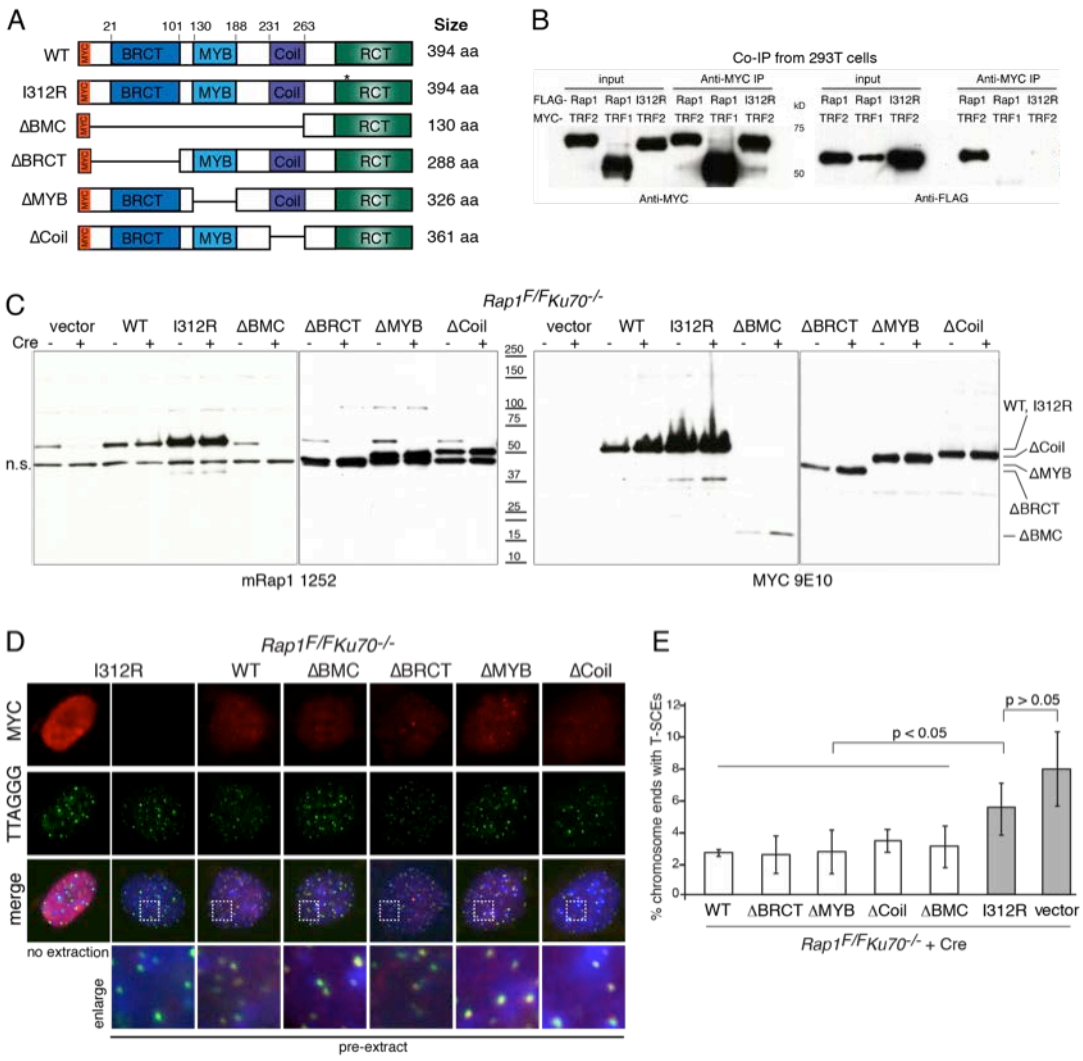

Figure 3.1 The C-terminus of Rap1 is required to inhibit HDR. (A) Schematic of Rap1 domain mutants. * indicates I312 to R mutation. ΔBMC, deletion of N-terminal 264 amino acids (aa), Rap1 protein coding started at aa 265. ΔBRCT, deletion of N-terminal 106 aa, Rap1 protein coding started at 107 aa. ΔMYB, deletion of aa 128-196, such that aa 127 was fused to aa 197. ΔCoil, deletion of aa 231-264, such that aa 230 was fused to aa 265. The Rap1 antibody was raised to full-length protein and detects multiple antigenic regions in the N-terminus of Rap1. (B) 293Ts were co-transfected with constructs as indicated and immunoprecipitated with a MYC antibody. Inputs and IPs were detected by the MYC antibody (left) and the FLAG antibody (right). MYC-TRF1 serves as a negative control for immunoprecipitation of FLAG-Rap1. (C) Immunoblots of MYC-tagged constructs in (A) expressed in *Rap1$^{F/F}$Ku70$^{-/-}$* MEFs, detected with Rap1 antibody (left) or MYC antibody (right). All constructs except ΔBMC contain an epitope(s) for the Rap1 antibody. n.s., non-specific band picked up by the Rap1 antibody. Running positions of constructs on gel are indicated on the right. (D) IF-FISH of constructs in (A) expressed in *Rap1$^{F/F}$Ku70$^{-/-}$* MEFs. Red, IF for MYC; green, telomeric FISH, blue, DAPI DNA stain. White square shows corresponding area enlarged below. (E) Quantification of T-SCEs. Bars represent averages from three independent experiments (n~1000 chromosome ends each) and SDs. P values based on Student's two-tailed t-test.

3.2.2 *Rap1 does not inhibit HDR at telomeres lacking TRF2*

Full-length TRF2 and a 41 amino acid fragment of TRF2 ($TRF2^{RBM}$) bind to Rap1 *in vitro* with similar affinities as determined by isothermal titration calorimetry [18]. The sequence encoding these 41 amino acids was inserted into MYC-tagged TRF1 ($TRF1^{RBM}$) with the aim of allowing TRF1 to recruit Rap1 to telomeres in the absence of TRF2 (Figure 3.2A). Expression of $TRF1^{RBM}$ in $TRF2^{F/F}Ku70^{-/-}$ MEFs showed that endogenous levels of Rap1 could be restored upon Cre-mediated deletion of TRF2 (Figure 3.2B). ChIP confirmed retention of Rap1 at telomeres despite removal of TRF2, while the telomeric occupancy of other shelterin components was not affected (Figure 3.2C-D). IF-FISH further illustrated that both endogenous Rap1 and $TRF1^{RBM}$ co-localized with telomeres (Figure 3.2E). IF for MYC displayed an unusual staining pattern of circular patches in the nucleus due to non-specific association of the secondary antibody, however magnification of insets show that MYC-tagged $TRF1^{RBM}$ localized to telomeres (Figure 3.2E). Expression of $TRF1^{RBM}$ in TRF1-deficient MEFs repressed the occurrence of fragile telomeres (Figure 3.3A-B), which are induced upon loss of TRF1 [156,157]. Thus, introduction of the RBM sequence into TRF1 did not disrupt normal functions of TRF1 and allowed for the retention of Rap1 at telomeres lacking TRF2. However, despite the presence of Rap1 at telomeres, T-SCEs were not repressed when TRF2 was deleted from $TRF2^{F/F}Ku70^{-/-}$ MEFs (Figure 3C-D), pointing to a requirement for the interaction between Rap1 and TRF2 in the inhibition of HDR. Rap1 binding to TRF2 may be required for a

conformational change of the complex that facilitates recruitment of an additional protein involved in the repression of homology-directed repair. Alternatively, Rap1 may change the DNA binding activity of TRF2, perhaps by changing its affinity to DNA structures that resemble substrates for HDR, such as the telomere terminus.

In addition to induction of telomere-sister chromatid exchanges, a low percentage of alt-NHEJ mediated telomere fusions are also observed in TRF2/Ku70-deficient MEFs [120]. Placement of Rap1 at telomeres by TRF1^{RBM} did not inhibit these fusions (Figure 3.3E) indicating that Rap1 does not play a role in the repression of alt-NHEJ. In contrast to these results, another study shows that tethering Rap1 to HeLa (a human cervical carcinoma cell line) telomeres by a fungal telomere-binding domain can repress c-NHEJ-mediated fusions when TRF2 is depleted [160]. It remains to be seen whether retention of Rap1 by TRF1^{RBM} can inhibit c-NHEJ mediated telomere fusions in TRF2-null MEFs.

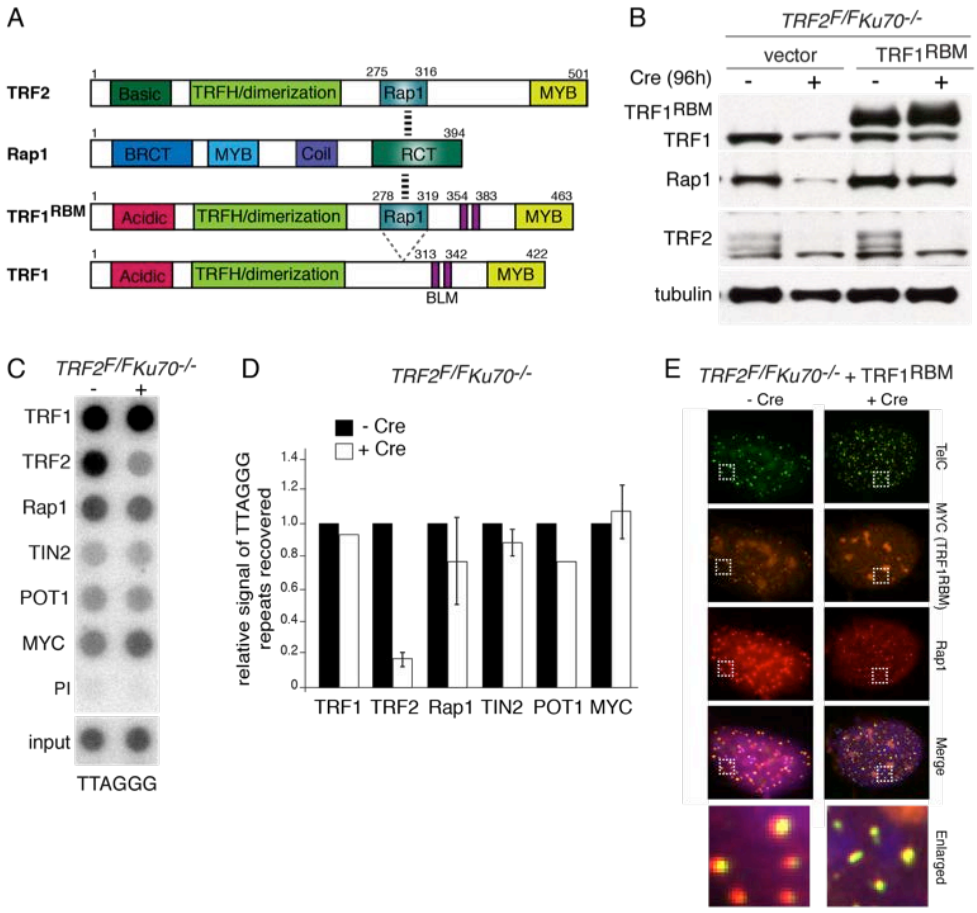

Figure 3.2 Tethering Rap1 to telomeres in the absence of TRF2. (A) Schematic illustrating composition of the TRF1^{RBM} allele. 41 aa encoding RBM was inserted into TRF1 at position aa 278. This did not interfere with the Bloom (BLM) helicase interaction sites shown in purple, or disrupt any other known interaction or nuclear localization signal. (B) Immunoblot showing expression of TRF1^{RBM} in *TRF2$^{F/F}$Ku70$^{-/-}$* MEFs and levels of Rap1 before and 96 hours after deletion of TRF2 with Cre. (C) ChIP for shelterin components and MYC-tagged TRF1^{RBM} at telomeres before and 96 hours after deletion of TRF2. Dot blot was probed with TTAGGG repeats. (D) Relative telomeric ChIP signals obtained as in (C) were expressed as the ratio of signal in minus and plus Cre samples. Minus Cre set to 1. Values with error bars represent averages of two experiments. Error bars represent SEM. (E) Combined IF for MYC (orange) to detect TRF1^{RBM}, for Rap1 (red) and FISH for telomeres (green). Blue in merged image: DAPI DNA stain. White square corresponds to area of enlarged image below.

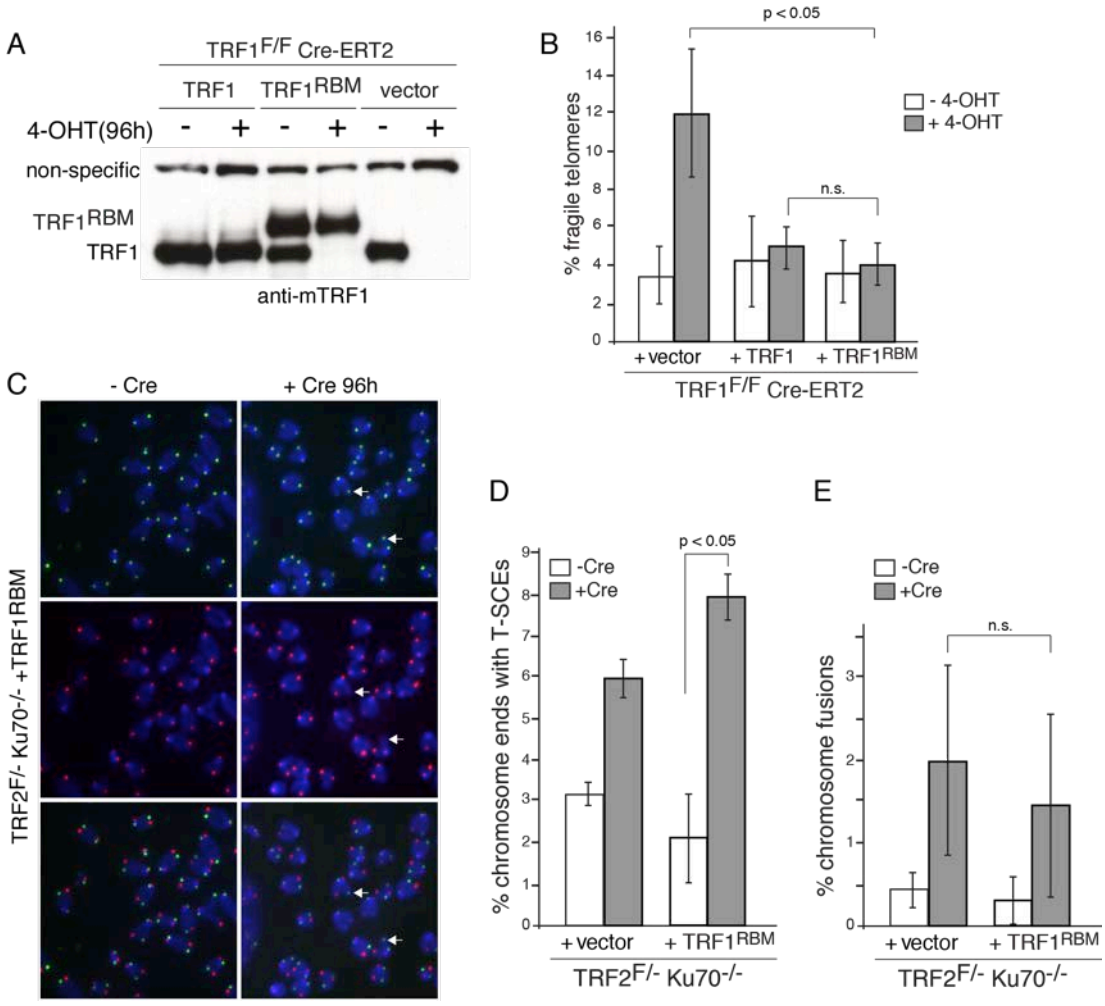

Figure 3.3 Rap1 cannot repress HDR in the absence of TRF2. (A) Immunoblot of TRF1^{RBM} expressed in TRF1$^{F/F}$ Cre-ERT2 (tamoxifen inducible Cre expression) MEFs where endogenous TRF1 was deleted by treatment with 4-hydroxytamoxifen (4-OHT). (B) Quantification of fragile telomeres of cells in (A) before and 96h after treatment with 4-OHT. Bars represent mean values of three independent experiments with SDs. P values derived from two-tailed Student's t-test. (C) COFISH of TRF1^{RBM}-expressing TRF2$^{F/F}$ Ku70$^{-/-}$ MEFs before and 96 hours after treatment of Cre. White arrows point to T-SCEs. (D) Quantification of T-SCEs as shown in (C). Bars represent mean values of three independent experiments with SDs. P values derived from two-tailed Student's t-test. (E) Quantification of chromosome fusions on metaphase spreads of cells in (D). Bars represent mean values of three independent experiments with SDs. Student's t-test indicated lack of significance between Cre-treated TRF2$^{F/F}$ Ku70$^{-/-}$ MEFs expressing vector control or TRF1^{RBM}.

3.2.3 *Rap1 confers an increase in TRF2 DNA binding affinity.*

To test the hypothesis that Rap1 changes the interaction of TRF2 with certain DNA substrates, nickel-affinity purifications of baculovirus-expressed His-Rap1, His-TRF2, and the His-Rap1/TRF2 complex were performed (Figure 3.4A). For purification of the Rap1/TRF2 complex, His-hRap1 and hTRF2 were co-expressed in Sf9 insect cells. Immunoblotting of the co-purified Rap1/TRF2 complex showed the expected 1:1 stoichiometry of Rap1 and TRF2 (Figure 3.4B). *E*lectrophoretic *m*obility *s*hift *a*ssays (EMSAs) with a duplex telomeric substrate with 12 repeats showed the Rap1/TRF2 complex had a slight increase in DNA binding affinity (less than 2-fold) over TRF2 alone (Figure 3.4C). Mixing of separately purified Rap1 and TRF2 did not result in this improved binding affinity and the pattern of the shifted probe looked very similar to TRF2 alone, suggesting that Rap1/TRF2 complex formation was not efficient *in vitro* (Figure 3.4C). Analysis of binding to a ds-ss 'junction' indicated that the co-purified complex bound to the junction substrate with a higher affinity than TRF2 alone (Figure 3.4D). Binding of TRF2 to the junction probe was variable with an affinity ranging from 2.5- to 6-fold less than that of the Rap1/TRF2 complex. Despite the ability of Rap1/TRF2 to bind to the junction probe better than TRF2 alone, its affinity for a telomeric junction was very similar to its affinity for duplex telomeric DNA. Therefore, while Rap1 clearly increases the DNA binding affinity of TRF2, it is unclear whether it is this activity of Rap1 that confers its inhibition of HDR. The length of the telomere tract did not affect Rap1/TRF2 binding ability, as EMSAs

with a duplex DNA substrate with three telomere-repeats (like the junction probe) did not show a change in DNA-binding affinity. Rap1 has previously been shown not to bind duplex telomeric DNA [20] and similarly did not exhibit any DNA binding to the junction probe (Figure 3.4D). Taken together these data suggest that Rap1 binding to TRF2 improves its ability to bind telomeric DNA. However, a significant difference was not observed in the binding affinity of Rap1/TRF2 to a ds-ss telomere junction relative to duplex telomeric DNA. Therefore it remains unclear whether Rap1 inhibits HDR by altering the DNA binding activity of TRF2.

3.2.4 *HDR is not aggravated by dual absence of Rap1 and POT1*

To test whether Rap1 and POT1 repress HDR at the same step, I created and analyzed cells in which both Rap1 and POT1 were removed from telomeres. An shRNA to TPP1 was used to deplete POT1a/b from telomeres in $Rap1^{F/F}Ku70^{-/-}$ MEFs. As a control, TPP1 was also depleted in $Rap1^{F/F}Ku70^{+/-}$ MEFs, where the presence of one allele of Ku is sufficient to inhibit T-SCEs. The level of TPP1 knockdown could not be assessed by immunoblotting due to lack of a good antibody for mouse TPP1. However, the TPP1 shRNA was effective in POT1a/b removal as indicated by the induction of TIFs (Figure 3.5A-B) as well as the appearance of T-SCEs in Ku70-deficient cells (Figure 3.5D-E). Deletion of Rap1 with Cre (Figure 3.5C) in TPP1-depleted cells did not exacerbate the T-SCE phenotype (Figure 3.5D-E). In fact the levels of T-SCEs observed in a Ku70-deficient background when Rap1 or POT1 alone were depleted, was very similar

to telomeres lacking both Rap1 and POT1. Telomeres remained shielded from HDR when Rap1 and POT1 were removed in Ku70-proficient cells. These data suggest that Rap1 and POT1 act together to repress HDR.

One caveat to consider with the interpretation of these results is whether it is possible to observe an exacerbation of the T-SCE phenotype. Theoretically, assuming HDR intermediates can be equally shuttled into pathways that dissolve the Holliday junction or resolve it resulting in crossover, the maximal number of T-SCEs we would expect to detect is 50%. Current levels of T-SCEs observed are rarely above 15%. Various efforts to knockdown BLM or TOP3α to remove the dissolution arm of HDR and skew resolution of HDR intermediates into crossovers were unsuccessful, therefore it remains to be seen what the threshold of detection for T-SCEs is.

Despite this caveat, these results raise the possibility that Rap1 and POT1 repress HDR as a subcomplex of shelterin. Indeed it has been shown that TRF2 and POT1 are capable of forming a detectable complex [21,152,185,234]. However, coimmunoprecipitation experiments failed to detect a stable interaction between MYC-POT1a or –b and FLAG-Rap1 (Figure 3.5F).

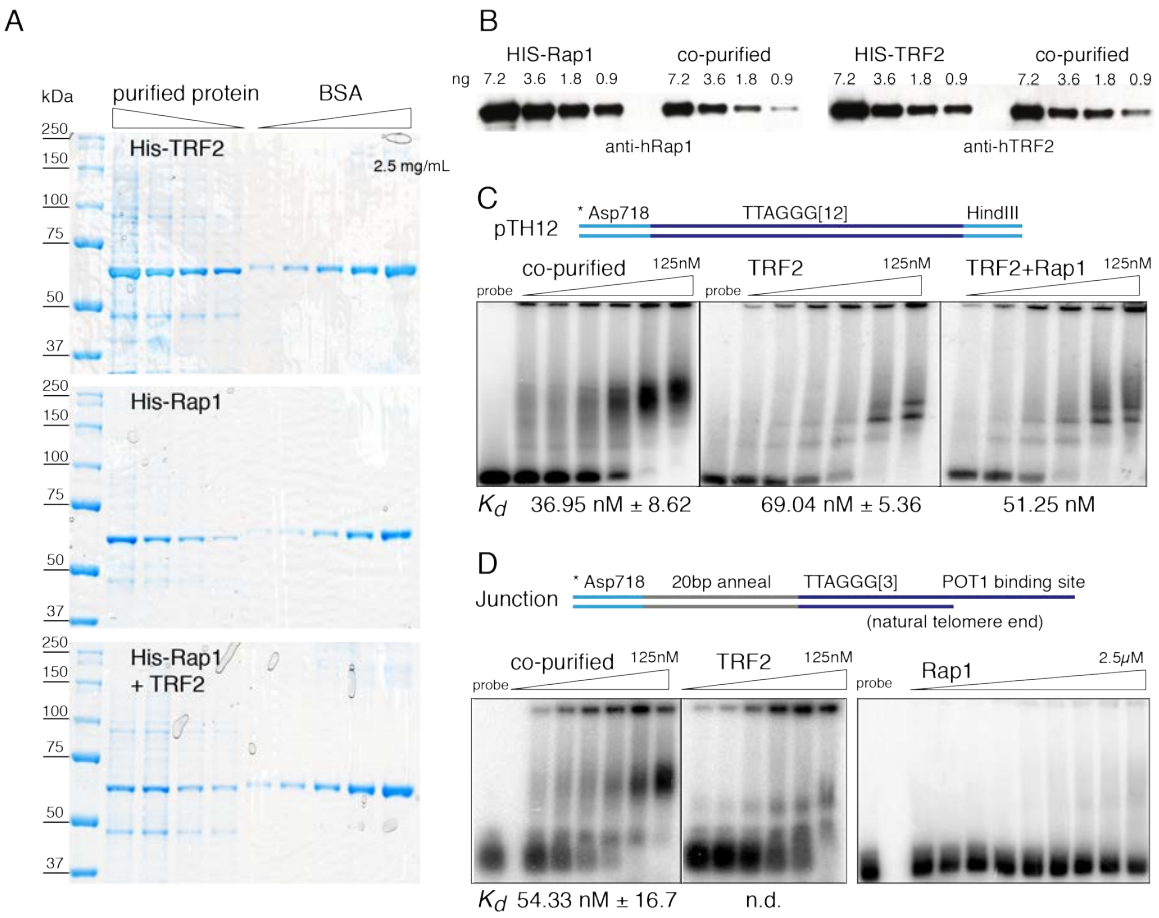

Figure 3.4 Rap1 confers an increase in the telomere binding affinity of TRF2.
(A) Coomassie stained SDS-PAGE gels of purified His-tagged proteins as indicated. 2-fold serial dilutions of purified protein and *B*ovine *s*erum *a*lbumin (BSA) were run on the same gel to quantify protein amounts. (B) Immunoblotting of quantified protein amounts to calculate stoichiometry of Rap1 and TRF2 in the co-purified sample. (C) Top, schematic of probe (restriction fragment containing 12 TTAGGG repeats) used for EMSAs below. Bottom, EMSAs with 2-fold serial dilutions of indicated proteins; probe, no protein added. Dissociation constants (K_d) calculated below. Values for co-purified and TRF2 are mean of three experiments with SDs. (D) Top, schematic of probe with 3 TTAGGG repeats, a 3' overhang containing the minimal binding site for POT1 (5'-GGTTAGGGTTAG-3'), and a natural telomere end (ATC-5'). Bottom, EMSAs with probe above using 2-fold serial dilutions of indicated proteins; probe, no protein added. Dissociation constant (K_d) calculated below. Value for co-purified is mean of three experiments with SDs; n.d., not determined.

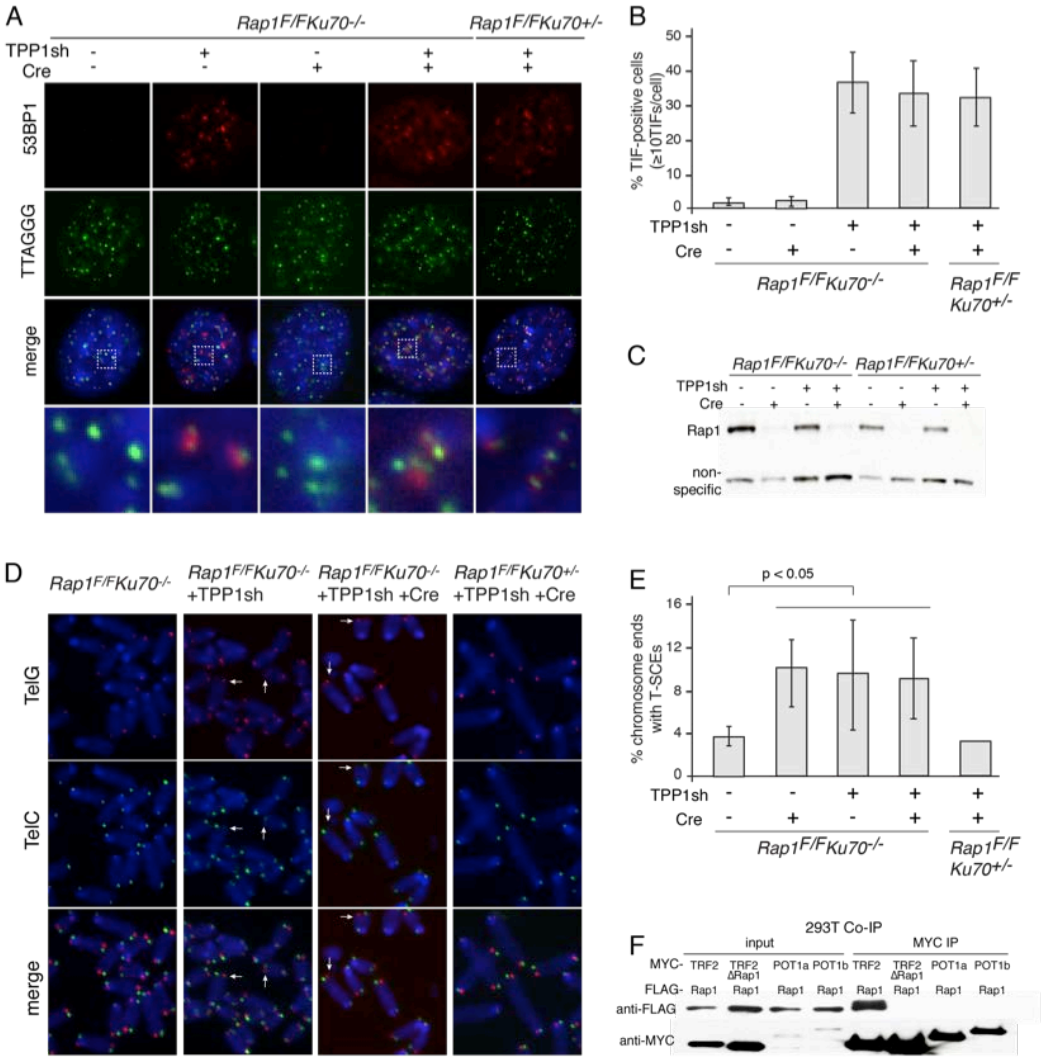

Figure 3.5 No exacerbation of T-SCE levels upon removal of Rap1 and POT1. (A) TIF assay on *Rap1*$^{F/F}$*Ku70*$^{-/-}$ or *Rap1*$^{F/F}$*Ku70*$^{+/-}$ MEFs treated with Cre and or a TPP1 shRNA as indicated for 96 hours. White square indicates area enlarged below. (B) Quantification of TIF-positive cells as in (A). Cells with ≥ 10 TIFs were considered TIF-positive. Bars represent mean values of three independent experiments with SDs. (C) Immunoblot for Rap1 in cells as described in (A). (D) CO-FISH assay on cells as described in (A). White arrows indicate T-SCEs. (E) Quantification of CO-FISH in (D). Bars represent mean values of three independent experiments with SDs. P-values calculated based on Student's t-test. (F) MYC-immunoprecipitation from 293T cells co-transfected with MYC-tagged constructs as indicated and FLAG-tagged Rap1. MYC-TRF2$^{\Delta Rap1}$ was used as a negative control and MYC-TRF2 was used as a positive control for interaction with Rap1.

3.2.5 *Deletion of Rap1 and TRF1 does not induce T-SCEs*

TRF1 loss results in inefficient replication of telomeric DNA [156] and potentially introduces replication intermediates that are susceptible to resolution by homology-directed repair. However, T-SCEs are not observed when telomeres lack TRF1, possibly due to repression of HDR by Ku70/80. Indeed, preliminary analysis of MEFs lacking TRF1 and Ku80 showed an induction of T-SCEs (Figure 3.6A), suggesting that telomeres are also vulnerable to HDR during DNA synthesis.

Mass spectrometry and ChIP experiments using human cells have implicated shelterin components TRF1, TRF2 and Rap1 in interacting with and potentially recruiting Ku to telomeres [78, 265, 283], although Ku has also been shown to bind directly to telomere repeats *in vitro* [284]. To explore potential redundancy in the recruitment of Ku to telomeres, we decided to delete both Rap1 and TRF1 from telomeres. If T-SCEs were observed in Rap1/TRF1 null MEFs, this would suggest that Ku is unable to repress HDR in this setting. Alternatively, removing both Rap1 and TRF1 could lead to an increase in telomere substrates vulnerable to HDR and result in T-SCEs regardless of whether co-repression of HDR by Ku was functional or not.

Analysis of metaphases lacking Rap1 and TRF1 in a Ku-proficient setting showed an increase of fragile telomeres and telomere sister associations which are characteristic of TRF1 loss (Figure 3.6B-C). Despite the presence of telomere replication problems, no induction of T-SCEs was observed (Figure 3.6C),

suggesting that Ku was still able to repress HDR. A low level of telomere fusions were also detected in MEFs where Rap1 and TRF1 had been deleted (Figure 3.6C), potentially due to minor destabilization of TRF2 binding to telomeres.

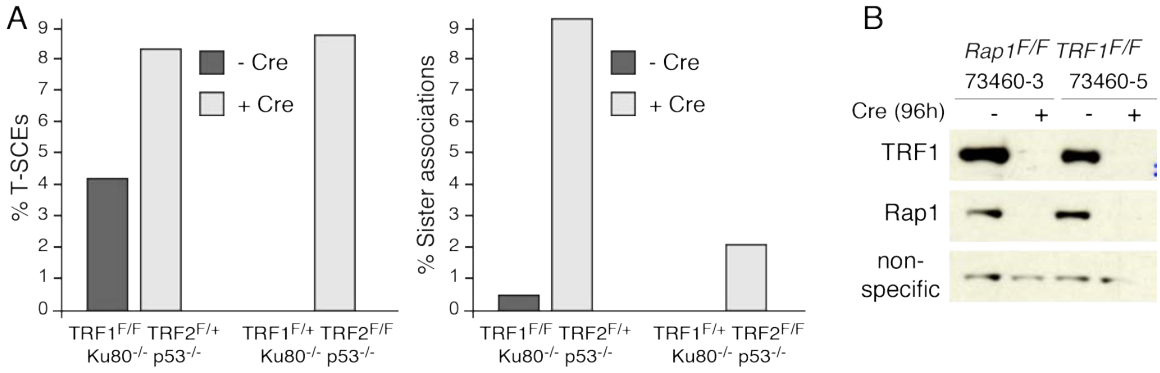

C

Rap1/TRF1 status	Telomeres analyzed	Fragile telomeres % ± SD	Sister associations % ± SD	T-SCEs % ± SD	Chromosome fusions % ± SD
+	1028, 1050, 1034	3.6 ± 0.56	2.3 ± 0.48	3.7 ± 0.47	0
-	1070, 1064, 1050	11.9 ± 2.3	20.0 ± 4.3	2.9 ± 0.23	3.5 ± 0.99

Figure 3.6 Ku represses T-SCEs in TRF1 null cells, as well as in MEFs lacking both Rap1 and TRF1. (A) Quantification of T-SCEs (left) and telomere sister associations (right) on metaphase spreads, before and 96 hours after treatment with Cre. Genotypes as indicated. (B) Western blot of two littermate controls with genotypes as indicated, before and 96 hours after treatment with Cre. Antibodies used for detection of proteins are indicated on left. (C) Quantification of aberrant structures on metaphase spreads in Rap1F/F TRF1F/F MEFs before and 96 hours after treatment with Cre. Data represents averages and standard deviations from analysis of three independently derived cell lines.

3.2.6 *HDR is repressed in late-passage Ku70-deficient MEFs*

The induction of homology-directed repair in absence of DNA damage signaling and cell cycle arrest in Rap1/Ku70-deficient MEFs allowed examination of the consequences of unbridled HDR on telomere maintenance. $Rap1^{F/F}$ $Ku70^{-/-}$ (or $Rap1^{F/\Delta}$ $Ku70^{-/-}$) MEFs were isolated and immortalized with SV40LT. The immortalization process is variable and takes approximately 15 to 20 PDs for cells to escape crisis and proliferate at a steady pace. The number of PDs cells undergo during immortalization is a reproducible estimate, but cannot be exactly calculated due to cell death or senescence that primary MEFs undergo during the immortalization process. After immortalization, at approximately PD 20, $Rap1^{F/F}Ku70^{-/-}$ (or $Rap1^{F/\Delta}Ku70^{-/-}$) MEFs were further cultured to 70 PDs with and without Cre treatment (Figure 3.7A-B). Cells were harvested at various time-points to assess the level of T-SCEs. Surprisingly, T-SCE events began to diminish as early as PD 30 and were reduced to basal levels similar to Rap1-proficient cells by PD 50 (Figure 3.7C). T-SCEs were also no longer induced when Rap1 was deleted from late passage $Rap1^{F/F}$ $Ku70^{-/-}$ showing that Ku70-deficient MEFs exhibit downregulation of telomeric HDR when cultured extensively.

To determine whether HDR was downregulated in general or just at the telomere, efforts were made to use a transient reporter assay developed in the Jasin lab [171] that assesses HDR-mediated repair events of a break induced by expression of I-SceI (a site-specific endonuclease). However this assay did not

work robustly in MEFs, due to difficulty in achieving high transfection efficiencies and minimal cell death.

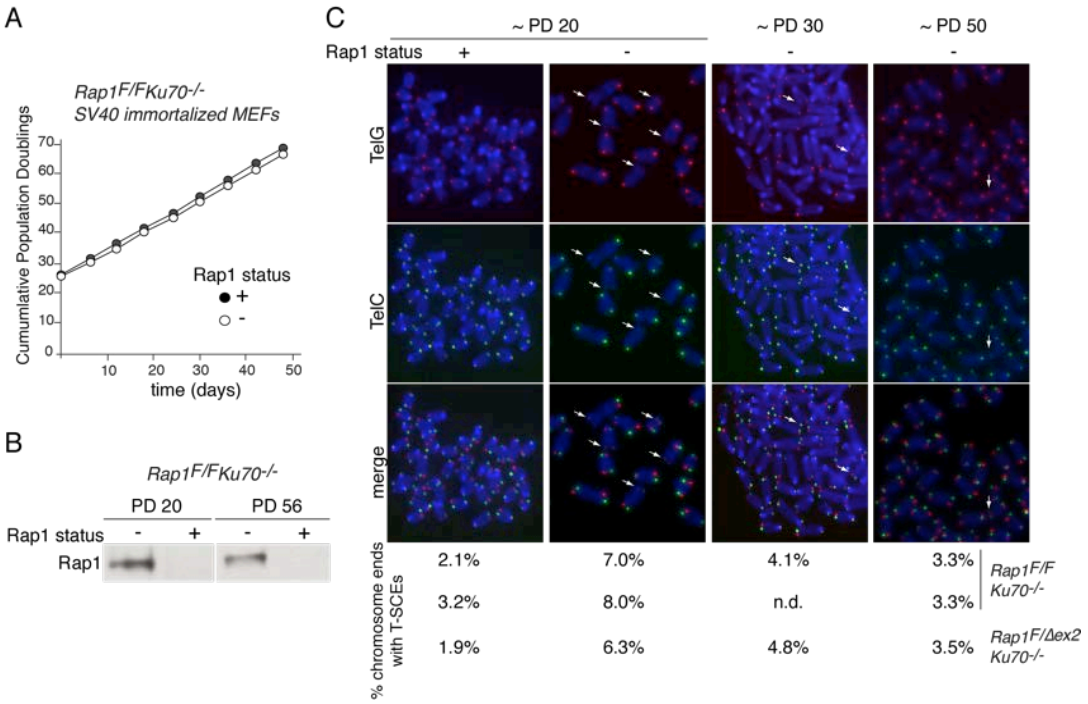

Figure 3.7 HDR is repressed in late-passage Ku70-deficient MEFs. (A) Growth curve of *Rap1*$^{F/F}$*Ku70*$^{-/-}$ MEFs with and without deletion of Rap1 by Cre. (B) Western blot indicating Rap1 levels in the two cell lines shown in (A) at the indicated PDs. (C) CO-FISH analysis of Ku70 deficient MEFs with or without Rap1 at the indicated PDs. White arrows point to T-SCE events. Quantification of chromosome ends with T-SCEs for three independent experiments is listed under corresponding CO-FISH panels.

3.3 Summary of findings

The data presented here show that Rap1 requires its interaction with TRF2 to repress HDR. Recruitment of Rap1 to telomeres by $TRF1^{RBM}$ in the absence of TRF2 did not prevent T-SCEs. It is possible however, that experimentally induced binding of Rap1 to $TRF1^{RBM}$ may disrupt Rap1's interaction with another factor required for repression of HDR. Additionally, the specific localization of Rap1 at telomeres by $TRF1^{RBM}$ may be subtly, yet impactfully different compared to its placement byTRF2.

The Rap1/TRF2 complex may bind to a protein involved in HDR inhibition that Rap1 alone or TRF2 alone may be unable to bind to. Alternatively, Rap1 may enhance the DNA binding affinity of TRF2 to HDR substrates and prevent loading of components required for repair. Preliminary gel-shift assays indicated that Rap1 may enhance the overall binding affinity of TRF2 to telomeric DNA, but this effect was minor and it is unclear whether it would be physiologically relevant. However, one report showed that the Rap1/TRF2 complex binds to ds-ss telomere junctions 10-fold better than duplex DNA [235]. The discrepancy between this study and the results reported here could be due to changes in the activity or oligomeric state of the purified proteins, as well as the different substrates used. In addition, another study reported Rap1 conferred no advantage to TRF2 to bind ds-ss telomere junctions, but instead improved the specificity of TRF2 binding to telomeric DNA [236].

Rap1 and POT1a/b seem to inhibit HDR via the same pathway as no increase in the number of T-SCEs was observed when Rap1 and POT1a/b were all removed from telomeres in a Ku70-deficient setting. Further assessment of Rap1/TRF2 DNA-binding needs to be conducted in the context of the shelterin complex, as POT1 binding to the overhang together with Rap1/TRF2 binding to the ds-ss junction may contribute to the repression of telomeric HDR.

Lastly, the surprising finding that Ku70-deficient cells eventually downregulate HDR suggests that when Ku is unable to inhibit HDR other factors may be enlisted to regulate HDR. Efforts to determine whether this repression of HDR was global or telomere-specific have thus far been unsuccessful and warrant further study.

Chapter 4: TALEN gene knockouts of human Rap1

4.1 Introduction

Two discrepancies exist concerning the function of Rap1 in mammals. *In vitro*, human Rap1 can block NHEJ when it binds to TRF2 loaded on an end-joining substrate [213]. *In vivo*, a Rap1-fusion protein can reduce telomere fusions when it is tethered to telomeres that are depleted of TRF2 [160]. On the other hand, mouse cells lacking Rap1 show no telomere fusions and Rap1-deficient mice are alive and fertile [19,220]. The only telomere deprotection phenotype in Rap1-deficient mouse cells is a propensity for telomere-telomere recombination when Ku70/80 are also absent [19].

In addition, it is unclear whether Rap1 has a conserved role in telomere length homeostasis in mammals. In support of a role in telomere length control, shRNAs to human Rap1 induce telomere lengthening [78], as does overexpression of several Rap1 truncation mutants [23]. Furthermore, overexpression of Rap1 mutants lacking its BRCT domain or MYB motif exhibit diminished telomere length heterogeneity, suggesting Rap1 also has a role in regulating distribution of telomere length. However, Rap1 knockout mice show no change in telomere length, even after three generations [19].

To determine the function(s) of human Rap1, Transcription Activator Like Effector Nucleases (TALENs) were used to knockout the *Rap1* gene. Analysis of several independent Rap1-deficient cell lines demonstrated that human Rap1 was not required for telomere protection, telomere length regulation, and other

aspects of telomere function. Instead, changes were observed in the transcription of several genes upon loss of Rap1.

4.2 Results

4.2.1 *Efficient TALEN-mediated knockout of human Rap1*

Similar to the mouse, the human Rap1-encoding gene (*TERF2IP,* referred to as *Rap1*) shares its promoter region with the essential *KARS* (lysyl-tRNA synthetase) gene located just upstream of exon 1 (Figure 4.1A). To avoid disrupting the *KARS* gene, a targeting strategy analogous to the one used for mouse *Rap1* [19] was implemented and TALENs were employed to delete exon 2. Deletion of exon 2 should result in an mRNA encoding a 226 aa ORF that ends prematurely in a stop codon at the beginning of exon 3. As exon 3 encodes the TRF2-binding domain, the truncated Rap1 protein is not expected to localize to telomeres. Taking advantage of the small size of exon 2 (125 bp) and anticipated resection of TALEN-induced DSBs [237,238], a neomycin or blasticidin donor construct was designed containing 5' and 3' arms homologous to the surrounding introns. HDR using the donor construct should result in deletion of exon 2 and insertion of the neomycin cassette (Figure 4.1A).

Rap1 was targeted in two near-diploid cancer lines (HCT116 colorectal carcinoma and HT1080 fibrosarcoma), a subclone of the near-triploid cervical carcinoma HeLa cell line (HeLa1.3 [22]), the diploid ARPE-19 retinal pigment

epithelial cell line, and primary BJ fibroblasts transformed with SV40LT. With the exception of BJ-SV40LT, all cells expressed telomerase. For HCT116, HT1080, and ARPE-19 cells, neomycin resistant clones were obtained, analyzed by PCR, and then evaluated by Southern blotting to verify the correct neomycin insertion (Figure 4.1B-C). For HeLa1.3 and BJ-SV40LT, the blasticidin donor construct was used and clones were analyzed by immunoblotting for Rap1. These analyses identified clones that lacked the wild type *Rap1* gene and expressed no detectable Rap1 protein (Figure 4.1C-D). Polypeptides representing the remaining ORF of the targeted *Rap1* gene were not detected (Figure 4.2A-C), perhaps due to nonsense-mediated decay.

Unexpectedly, immunoblotting revealed the complete loss of Rap1 in heterozygous clones with one neo insertion (Figure 4.1B-C). Telomeric ChIP of two such clones (HT1080 c21 and HeLa1.3 c28) confirmed that Rap1 was absent from telomeres (Figure 4.2D-G). Sequencing revealed small deletions close to the TALEN site in these and other Rap1-deficient clones with only one neo-containing *Rap1* gene (Figure 4.3A-B). Most mutations had ablated Rap1 by deleting the exon 2 splice acceptor site or had created a frame-shift mutation, indicating that errors generated during NHEJ had inactivated the *Rap1* gene (Figure 4.3C). As a result, the frequency of the *Rap1 k*nock*o*uts (KOs) is much higher than deduced from PCR genotyping. Taking the deleterious repair events into account, the ablation of Rap1 occurred at 20-65% efficiency in HCT116, HT1080, and ARPE-19 cells (Figure 4.3D). The HCT116 cells showed the

highest KO frequency consistent with their propensity for HDR (reviewed in [239]). The actual KO frequency is probably even higher as only clones with a neo cassette in the *Rap1* gene were analyzed.

The high KO frequency allowed screening of HeLa1.3 and BJ-SV40LT clones by Rap1 immunoblotting. Sequencing of Rap1-negative HeLa1.3 clones revealed that all three alleles in these clones contained inactivating mutations near the TALEN cut site (Figure 4.3B). Prolonged culturing of clones in blasticidin resulted in cell death, suggesting that the pEF blasticidin cassette did not confer long-term resistance. The KO frequency was lower in BJ-SV40LT fibroblasts with only one blasticidin-resistant clone showing absence of Rap1 protein. This clone was not analyzed because it perished in telomere crisis, as did many of the Rap1-proficient BJ-SV40LT clones.

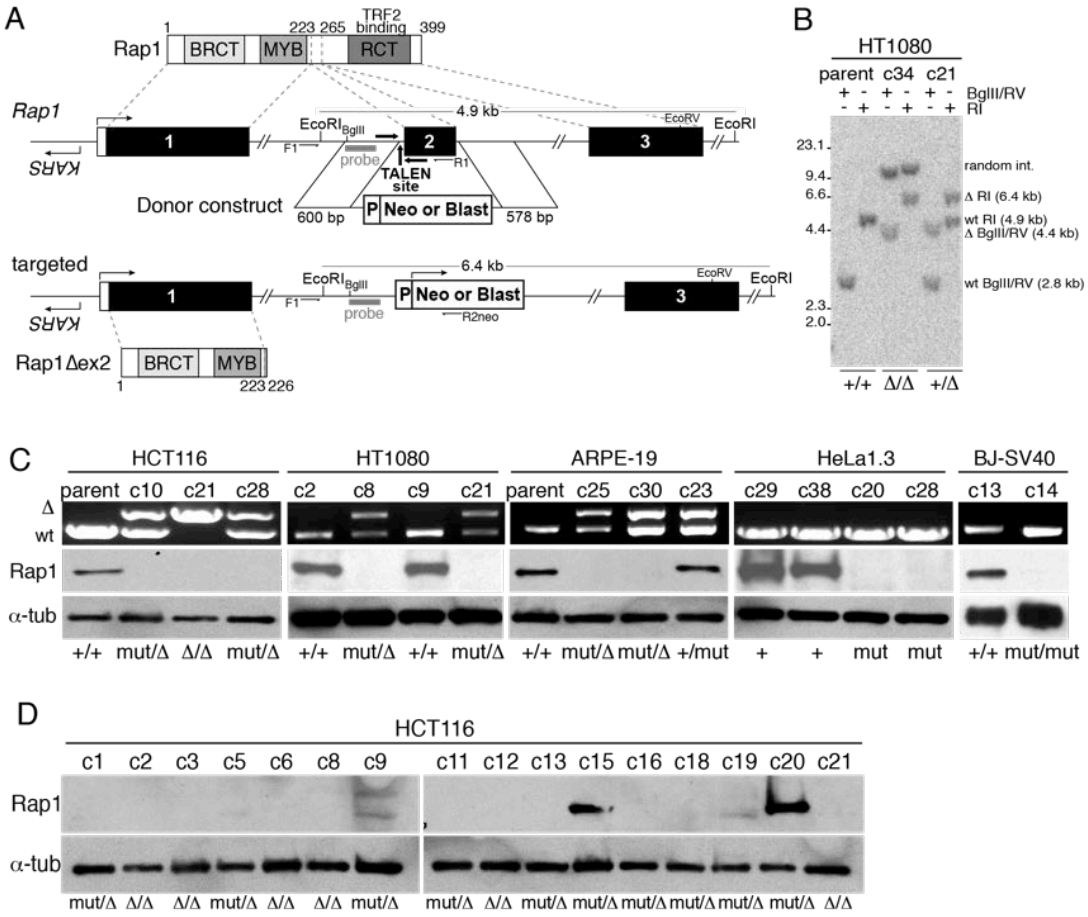

Figure 4.1 TALEN-mediated inactivation of the gene for human Rap1. (A) Schematic of human Rap1, the *Rap1* locus, the targeting construct, and the resulting knockout allele. F1, R1, and R2neo: PCR primers for genotyping. Arrows in bold: TALEN binding and cut sites. (B) Southern blot of EcoRI (RI)- or BglII/EcoRV (RV)-digested genomic DNA from targeted HT1080 clones. Probe shown in (A). (C) PCR genotyping of the *Rap1* gene and western blotting for Rap1 in the indicated clones. +, WT allele; Δ, targeted allele; mut, mutation resulting in loss of Rap1. (D) Immunoblotting of protein from targeted homozygous and heterozygous HCT116 clones showing absence of Rap1 in a large proportion of heterozygous clones. Genotypes indicated below.

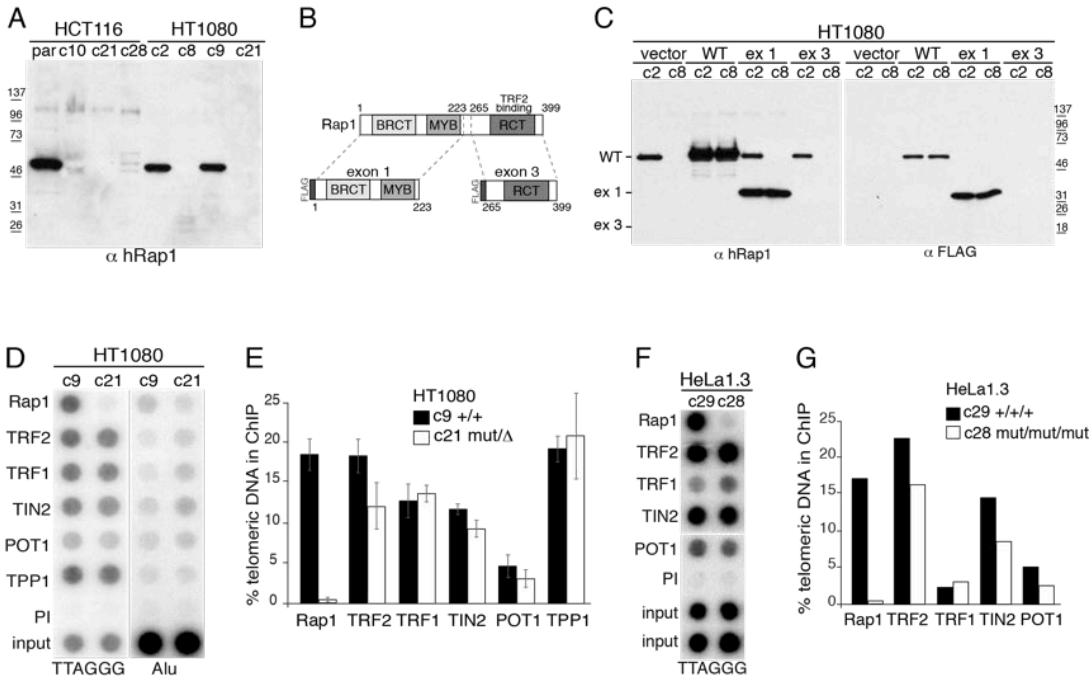

Figure 4.2 Loss of Rap1 in targeted clones. (A) Immunoblots of HCT116 and HT1080 KO clones probed with anti-hRap1 showing the absence of detectable truncated Rap1 proteins. (B) Schematic of retroviral constructs expressing FLAG-tagged exon 1 (ex 1) and FLAG-tagged exon 3 (ex 3). (C) Immunoblotting for the expression of constructs in (B) in HT1080 KO and WT clones. The protein fragment encoded by exon 1 is expressed and detected by the Rap1 antibody. The protein fragment encoded by exon 3 contains epitopes that the Rap1 antibody can recognize, but lack of detectable signal indicates that it is not expressed. (D) Telomeric ChIP of WT and targeted HT1080 clones. Duplicate dot-blots were probed for telomeric or Alu repeats. (E) Average percentage of telomeric DNA recovered in ChIPs with the indicated antibodies (two independent experiments). Error bars: SEMs. (F) Telomeric ChIP of HeLa 1.3 WT and KO cells. (G) Quantification of the percent of telomeric DNA recovered in each ChIP.

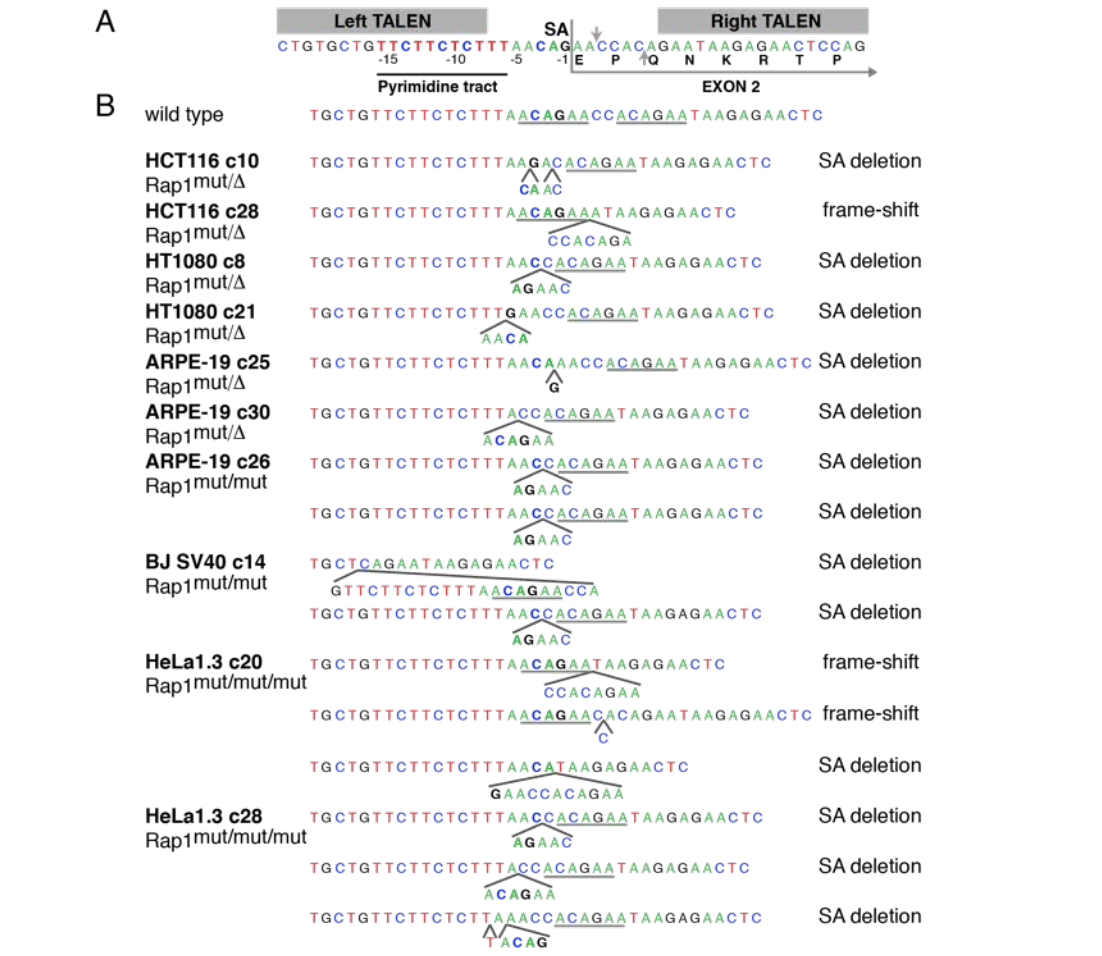

D

Cell line	Primary screening	Clones w/o Rap1 protein (% of total)	Clones w/ neo in both alleles	Clones w/ muts in one allele	Clones w/ muts only
HCT116	PCR (neo)	10 (65%)	3	7	n/a
HT1080	PCR (neo)	11 (36%)	1	10	n/a
ARPE-19	PCR (neo)	6 (24%)	0	6	n/a
HeLa1.3	Immunobl	8 (21%)	0[a]	0	8
BJ-SV40(neo)	Immunobl	1[b](3%)	0[a]	0	1

[a] no insertion of the blasticidin cassette into the Rap1 locus ;
[b] this clone succumbed in crisis

Figure 4.3 TALEN-induced mutations in the *Rap1* locus. (A) Schematic illustrating TALEN binding sites, their predicted cutting site (grey arrows), the pyrimidine tract, splice acceptor (SA), and the location of exon 2 in the Rap1 locus. A short repeat (underlined in grey) is frequently mutated in the mutant alleles. (B) Relevant sequences of the indicated clones. Predicted consequences of the mutations are indicated on the right. (C) Schematic illustrating NHEJ and HDR after TALENs cutting. (D) Table indicating number of Rap1 knockout clones acquired and the genetic alterations in *Rap1*.

4.2.2 *Rap1-deficient cell proliferate and maintain fully protected telomeres*

The Rap1-deficient cell lines proliferated normally (Figure 4.4A) and lacked a significant level of TIFs (Figure 4.4B-C), indicating that removal of Rap1 from telomeres does not result in a DNA damage response. Cells lacking Rap1 also did not show a significant induction of DSB repair at telomeres. Metaphase spreads of Rap1 KOs lacked chromosome end fusions, a read-out for telomeric NHEJ (Figure 4.5A-B). CO-FISH to monitor HDR-mediated T-SCEs established that recombination remained repressed at telomeres (Figure 4.5C-D). Analysis of telomere-sister chromatid exchanges in cells lacking Rap1 was conducted in a Ku-proficient background. Similar to the mouse, human Ku70/80 are also required to repress telomere recombination. However, unlike the mouse, deletion of Ku70/Ku80 is lethal in human somatic cells [240,241], thus it was not possible to test a setting where both Rap1 and Ku70/80 were deleted. While the contribution of human Rap1 to the repression of HDR in the context of Ku70/80-deficiency remains to be determined, our data indicate that human telomeres remain protected from NHEJ and HDR in absence of Rap1.

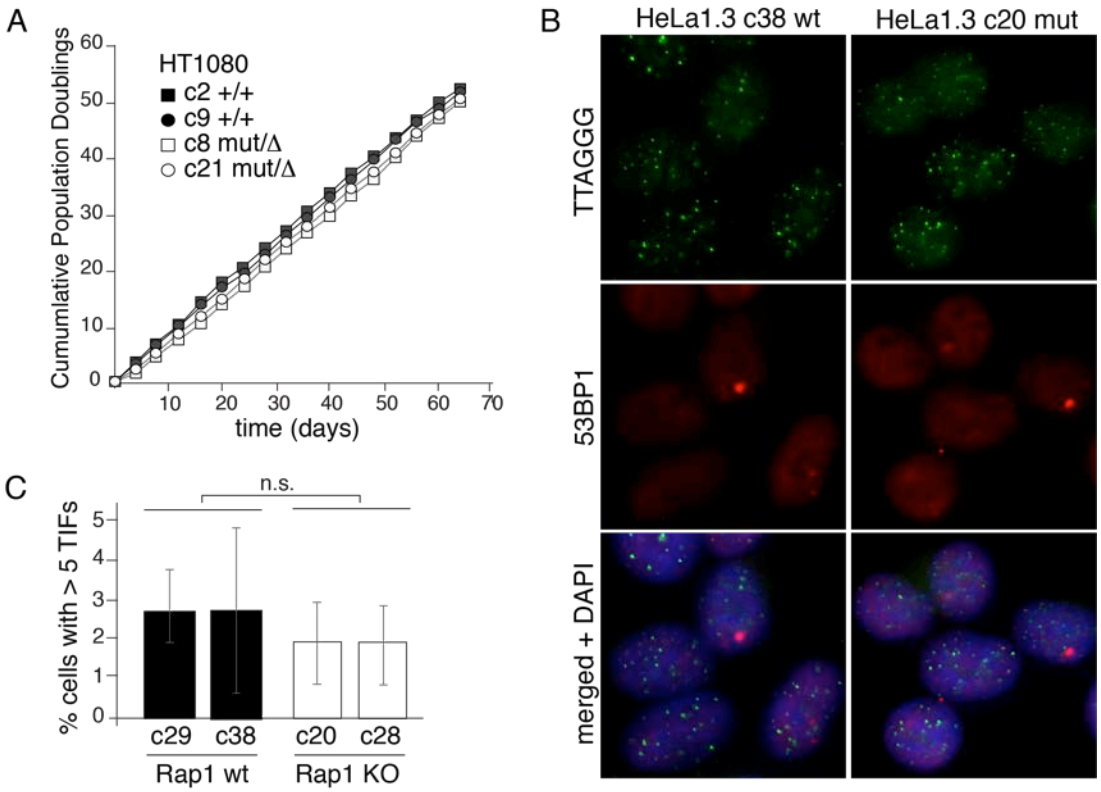

Figure 4.4 Rap1-deficient cells proliferate and do not induce DNA damage signaling.
(A) Growth curves of WT and Rap1 KO HT1080 clones. (B) TIF assay on WT and KO HeLa1.3 clones. Green, telomeric FISH; red, IF for 53BP1; blue, DNA (DAPI). (C) Quantification of TIFs assay (see (B)). Error bars: SDs of three independent experiments (n≥100 nuclei per clone). P values from a two-tailed paired t-test combining WT and KO datasets. n.s.: not significant.

A

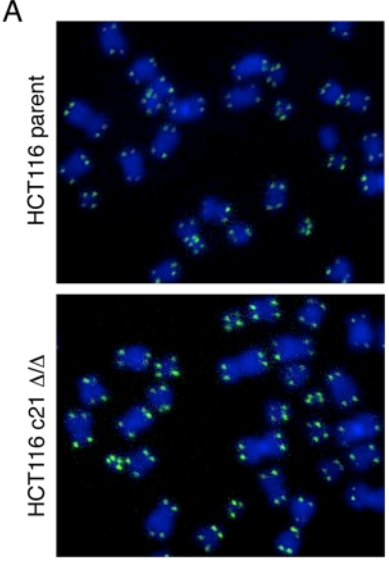

B

Cell line	Rap1 status	number of telomeres scored	% of telomeres fused (av±SD)
HeLa1.3 c29	+/+/+	1084, 932, 1008	0.27±0.2
HeLa1.3 c38	+/+/+	1002, 1110, 1004	0.40±0.4
HeLa1.3 c20	mut/mut/mut	1028, 1002, 1060	0.85±0.5
HeLa1.3 c28	mut/mut/mut	1010, 992, 1044	0.92±1.0
HCT116 parent	+/+	952, 920	0.21
HCT116 c8	mut/Δ	1100, 600	0.18
HCT116 c21	Δ/Δ	1068, 852	0.23
ARPE-19 c23	+/+	956	<0.1
ARPE-19 c25	mut/Δ	1008, 800	0.2
HT1080 c9	+/+	1020	0.39
HT1080 c21	mut/Δ	1120	0.36

p=0.084

C

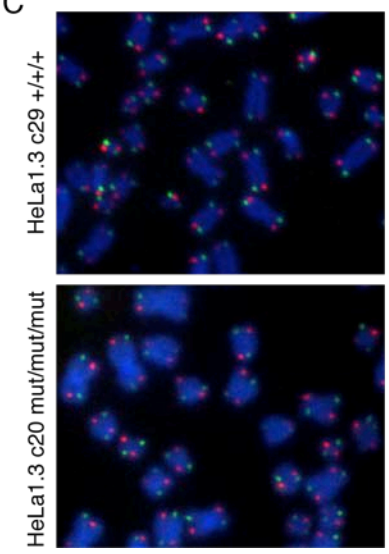

D

Cell line	Rap1 status	number of telomeres scored	%T-SCE
HeLa1.3 parent	+/+/+	1232	3.3
HeLa1.3 c29	+/+/+	1876	3.3
HeLa1.3 c38	+/+/+	2112	3.0
HeLa1.3 c20	mut/mut/mut	1298	4.3
HeLa1.3 c27	mut/mut/mut	1074	1.9
HeLa1.3 c28	mut/mut/mut	1746	4.5
HeLa1.3 c35	mut/mut/mut	2148	3.0

p=0.8

Figure 4.5 Telomere protection in Rap1-deficient cells. (A) Metaphase chromosomes from the indicated WT and Rap1 KO cells. Green, telomeric FISH; blue, DNA (DAPI). (B) Quantification of telomere fusions, detected as in (A), in the indicated clones. P values from a two-tailed paired t-test on combined WT and KO datasets. (C) CO-FISH analysis on the indicated WT and KO HeLa clones. (D) Table showing the percentage of telomeres showing T-SCEs as assayed in (C) in the indicated clones. P value from unpaired two-tailed t-test.

4.2.3 *Unaltered telomere length dynamics in absence of Rap1.*

To determine whether Rap1 affected telomere length homeostasis, two HT1080 Rap1-deficient clones were cultured for 50 PDs alongside two Rap1-proficient clones selected for their matching telomere lengths (Figure 4.6A). All clones exhibited a mild increase in telomere length (Figure 4.6B). The two Rap1-deficient clones lengthened their telomeres at a similar modest rate (1-2 bp/PD) whereas the two Rap1-proficient clones differed in the rate of telomere lengthening (28 and 4 bp/PD) (Figure 4.6B). Given the clonal variation and small differences in telomere length changes, the removal of Rap1 did not appear to have a strong effect on telomere length dynamics in HT1080 cells.

Similarly, Rap1 did not affect the telomere length dynamics of HCT116 clones (Figure 4.6C). Two Rap1-deficient clones showed telomere shortening at variable rates (-3 to -32 bp/PD). Given that the telomere shortening in the parental cells (-27 bp/PD) is similar to that of one of the Rap1-deficient clones (c10), it can be concluded that Rap1 did not strongly affect telomere dynamics in HCT116 cells either.

Finally, three Rap1-deficient ARPE-19 clones (c26, c25, and c30) showed wide variations in telomere dynamics, ranging from slight shortening (-18 bp/PD) to slight elongation (9 and 16 bp/PD) (Figure 4.6D). The single Rap1-proficient clone (c23) showed telomere shortening at a rate of -34 bp/PD. Thus, there is considerable variability in the telomere dynamics in ARPE-19 clones but no consistent effect of Rap1 deletion.

Given the lack of consistent shortening or lengthening phenotypes in multiple Rap1 knockouts, the simplest interpretation is that Rap1 does not play a major role in telomere length regulation. Deletion of Rap1 also did not induce an obvious change in the telomere length heterogeneity (Figure 4.6A and 4.7A), which was affected by Rap1 mutants in overexpression studies [20]. Removal of Rap1 from several cell lines also did not appear to affect the 3' telomeric overhang. The amount of ss telomeric DNA was determined by in-gel hybridization of a labeled C-strand telomeric repeat probe to native telomeric restriction fragments. Quantification of normalized single-stranded telomeric DNA signals indicated that Rap1 status had no significant impact on the 3' overhangs in HT1080, HCT116, and ARPE-19 cells (Figure 4.7A-B).

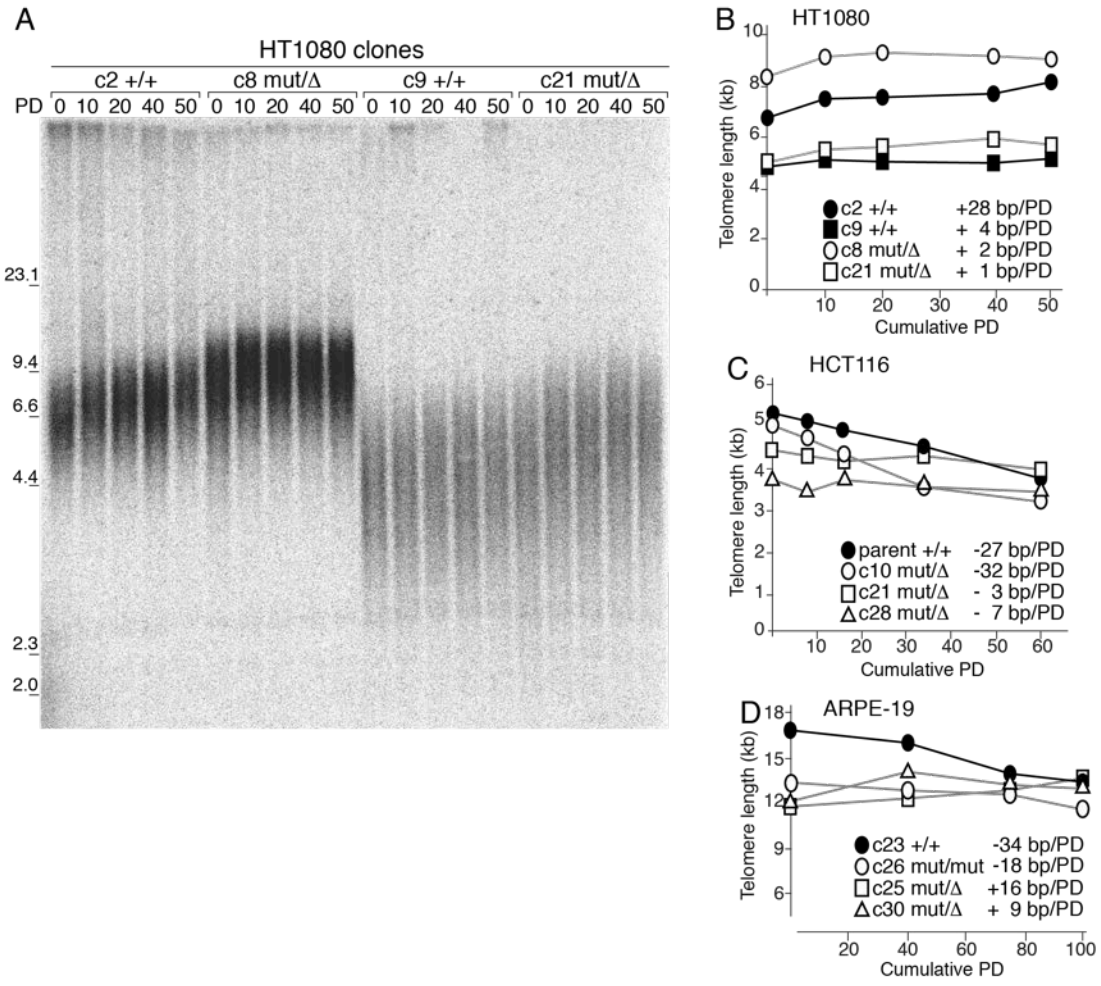

Figure 4.6 Rap1 knockouts exhibit no systematic changes in telomere length. (A) Southern blot of telomeric restriction fragments from two WT and two KO HT1080 clones at the indicated PDs.(B-D) Curves of average telomere lengths at indicated PDs in HT1080, HCT116, and ARPE-19 clones, respectively.

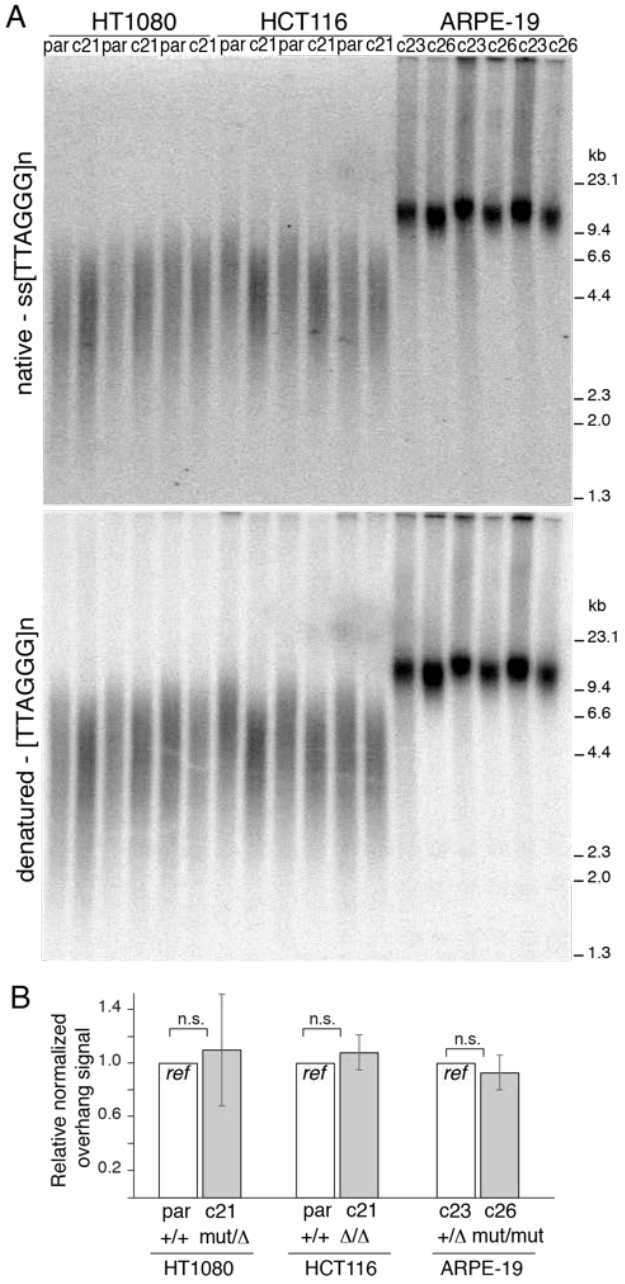

Figure 4.7 Loss of Rap1 does not affect telomere structure. (A) Telomeric DNA analysis of WT and KO clones in three different cell lines. Top, in-gel detection of native telomeric restriction fragments with a C-strand telomeric probe revealing the G-strand overhang signals; bottom, same gel rehybridized after in situ denaturation of the DNA, revealing the total telomeric DNA in each lane. Three biological replicates of each cell line were run adjacent to each other on the same gel. (B) Overhang signals were normalized to total telomeric signals in each lane and plotted as a ratio compared to the WT overhang signal of the corresponding cell line. Error bars represent SDs. Lack of statistical significance derived from two-tailed paired t-tests using the three independent experiments conducted with each cell line.

4.2.4 *Telomeric positioning in Rap1 null cells*

To determine whether Rap1 is involved in the peripheral positioning of telomeres in newly formed G1 cells [219], mitotic shake-off was used to analyze HeLa1.3 daughter cells in early G1. HeLa cells were used due to the ease of detection of their long telomeres, and the same method of telomere position analysis had been previously conducted in HeLa cells [219], thereby enabling a fair comparison to published data.

Using Lamin A to mark the nuclear envelope (NE) and FISH to visualize telomeres, the subnuclear position of the telomeric signals was determined and compared between Rap1-proficient and -deficient cells (Figure 4.8A-B). The distribution of telomeres in the nucleus and median distance from the nuclear envelope was similar for two Rap1-proficient and -deficient clones in two independent experiments. Moreover, the percentage of telomeres present in a zone defined arbitrarily as the nuclear periphery (within 10% distance from the NE) was also similar regardless of Rap1 status, illustrating that Rap1 is not required for the more peripheral positioning of telomeres in early G1.

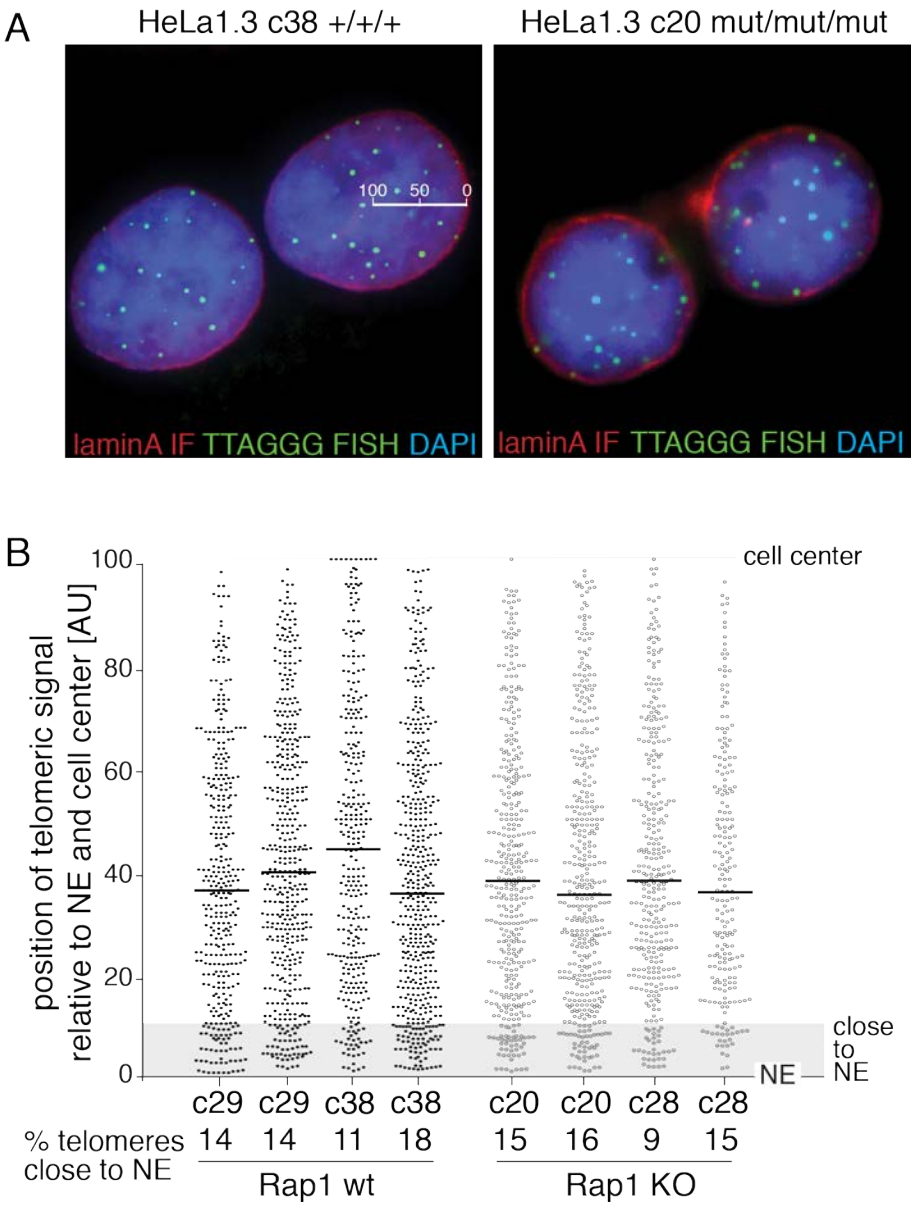

Figure 4.8 Effects of Rap1 on telomere position. (A) Combined IF for lamin A (red) and FISH for telomeres (green) in early G1 nuclei of WT and Rap1 KO HeLa1.3 clones. The scale in one nucleus indicates how the position of the telomeric signals was determined. Blue: DAPI DNA stain. (B) Distance of telomeres from nuclear envelope (NE) in arbitrary units. For each nucleus imaged in a single plane, the ratio between the distance of each telomere from the center and the radius (center to NE) was plotted. Median distance for each clone is indicated by horizontal line. % telomeres at periphery reflects telomeres within 10% of the distance from the NE. Two independent experiments for each clone are shown.

4.2.5 *No change in telomeric chromatin or transcription upon Rap1 loss*

Mammalian telomeres contain nucleosomes and epigenetic marks that are characteristic of heterochromatin, such as H3K9me3, H4K20me3 and the loading of *h*eterochromatin *p*rotein *1* (HP1, reviewed in [228]). Rap1 also had no detectable effect on general markers for the chromatin status at telomeres, as evidenced by ChIP for methylation of H3K9, acetylation of H4, and HP1α, HP1β and HP1γ (Figure 4.9A-B). In addition there was no significant effect of Rap1 on the abundance of the telomeric lncRNA TERRA (Figure 4.9C-D). This finding is consistent with the unaltered TERRA levels after deletion of mouse Rap1 [19].

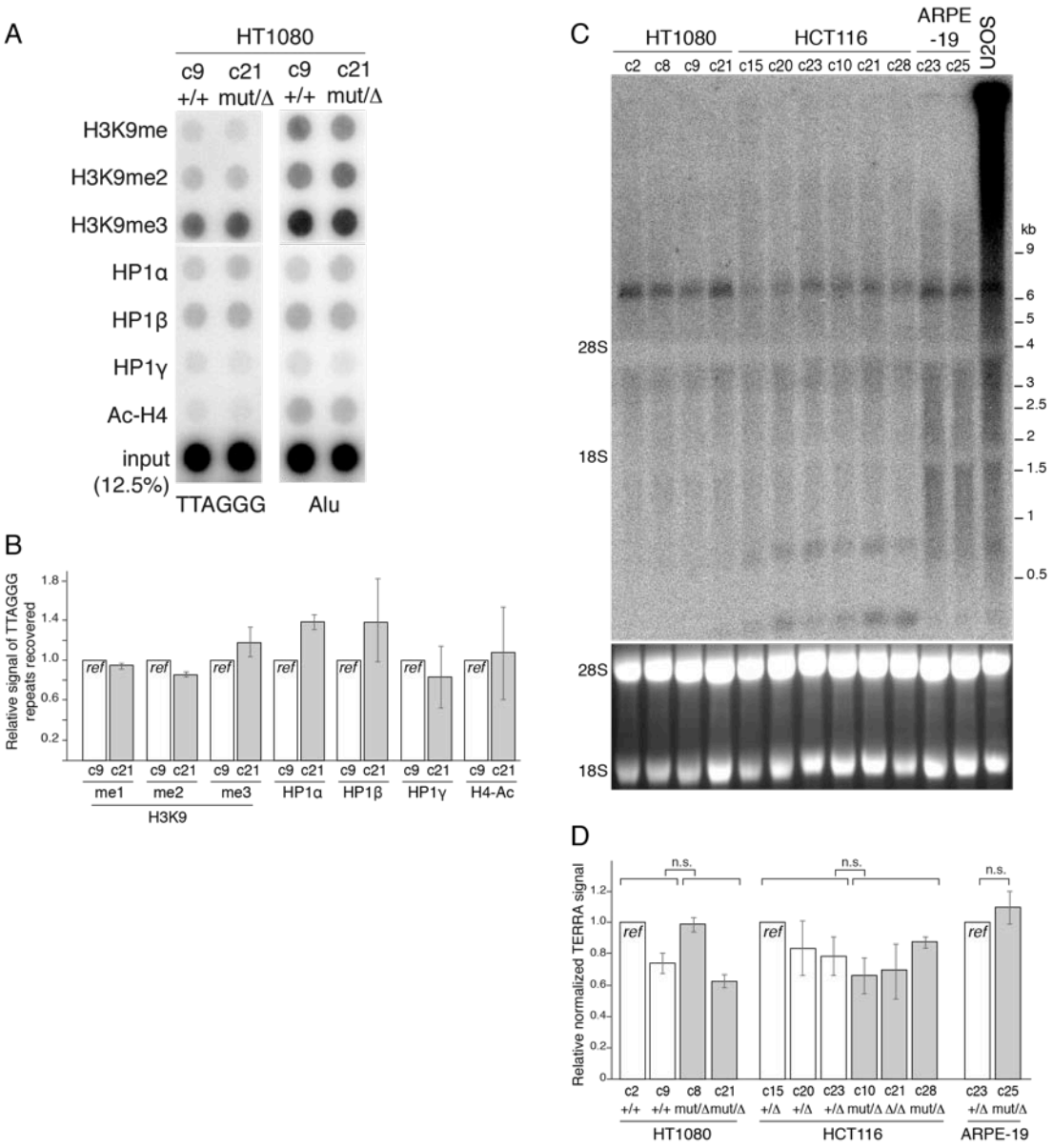

Figure 4.9 No change in telomeric chromatin or transcription in Rap1-deficient cells.
(A) ChIP for modified histones at telomeres in WT and Rap1 KO cells. Duplicate blots were probed for telomeric DNA or Alu repeats. (B) Relative telomeric ChIP signals obtained as in (A) were expressed as the ratio of signal in KO and WT clones (WT set to 1). Values represent averages of two experiments. Error bars: SEMs. (C) Northern blot hybridized with a telomeric probe showing TERRA levels of Rap1 WT and KO clones in the HT1080, HCT116 and ARPE-19 cell lines. U2OS serves as a positive control for TERRA expression. Ethidium bromide staining of ribosomal RNA serves as a loading control. (D) TERRA signals were normalized using the 18S ribosomal RNA and plotted as a ratio compared to the WT TERRA signal of the corresponding cell line. Error bars represent SDs. Two-tailed unpaired t-tests of 3 independent experiments illustrates lack of statistical significance between Rap1 WT and KO TERRA expression levels.

4.2.6 *Rap1 affects transcriptional regulation*

Mouse Rap1 localizes to over 8600 gene-associated loci, affecting transcription of numerous genes [220-222], while human Rap1 is found at ~63 gene loci [223]. To query the effect of Rap1 on the transcriptome, microarray profiling was performed on seven Rap1 WT and KO clones derived from three different cell lines, ARPE-19, HT1080 and HCT116. A number of differentially regulated genes were identified (Tables 4.1-4.3). The three Rap1-regulated genes in the ARPE-19 cells (LHX2, LRRC17 and CDO1) were validated by quantitative RT-PCR (qRT-PCR) and their response to Rap1 deletion was further confirmed on an additional ARPE-19 Rap1 KO clone (c26) (Figure 4.10A-C). The Rap1-regulated genes varied between the different cell lines, most likely due to the different origins of the cell lines. Gene ontology analysis was uninformative, because of the low number of genes identified by this limited analysis. However, one Rap1-regulated gene in the HT1080 cells was among the human Rap1-associated loci in the HT1080-derived HTC75 cell line [223]. Taken together, these data are consistent with a role for Rap1 in transcriptional control in human cells.

Table 4.1 Microarray expression analysis for ARPE-19.

Cell Line	**Gene (chromosome) [LogFC][a]**		
KO v WT	LHX2 (chr9)	LRRC17 (chr7)	CDO1 (chr5)
c25 v c23	-3.3	-5.1, -3.4	-3.5
c30 v c23	-2.7	-5.1, -3.4	-3.8
c25 v par	-4.2	-4.6, -3.1	-3.3
c30 v par	-3.7	-4.5, -3.0	-3.5

[a],Multiple LogFC values reflect data from multiple probes for the corresponding gene.

Table 4.2 Microarray expression analysis for HT1080.

Cell Line	**Gene (chromosome) [LogFC][a]**							
KO v WT	ATP9A (chr20)	CDCP1[b] (chr3)	CYP2J2 (chr1)	FAIM3 (chr1)	MGC 39900	NELL2 (chr12)	PTGR1 (chr9)	TERF2IP (chr16)
c8 v c2	3.0	3.4, 1.8, 2.5, -	2.0	-3.4	-2.1	3.0	2.0, 1.7	-2.9
c21 v c2	3.1	3.7, 1.9, 2.4, 3.0	2.2	-3.6	-2.3	2.2	2.1, 1.9	-2.3
c8 v c9	3.8	3.6, 1.8, 2.3, -	1.6	-2.0	-2.7	2.9	2.0, 1.7	-2.9
c21 v c9	3.9	3.9, 1.8, 2.3, 2.8	3.5	-2.2	-2.9	2.2	2.1, 1.9	-2.3

[a],Multiple LogFC values reflect data from multiple probes for the corresponding gene. [b] CDCP1 was identified as a Rap1 associated locus by ChIP-seq in a subclone of HT1080 [223] .

Table 4.3 Microarray expression analysis for HCT116.

Cell Line	**Gene (chromosome) [LogFC] [a]**		
KO v WT	BMP4 (chr14)	SLC2A3 (chr12)	SUSD2 (chr22)
c10 v c15	-2.0	-3.4	-2.6
c21 v c15	-2.1	-2.7	-2.2
c28 v c15	-1.9	-2.3	-2.1
c10 v c20	-2.0	-2.7	-2.0
c21 v c20	-2.0, -2.5	-2.0	-1.6
c28 v c20	-1.8	-1.5	-1.5
c10 v c23	-1.8	-2.9	-2.8
c21 v c23	-1.9, -2.4	-2.1	-2.5
c28 v c23	-1.7	-1.7	-2.3

[a],Multiple LogFC values reflect data from multiple probes for the corresponding gene.

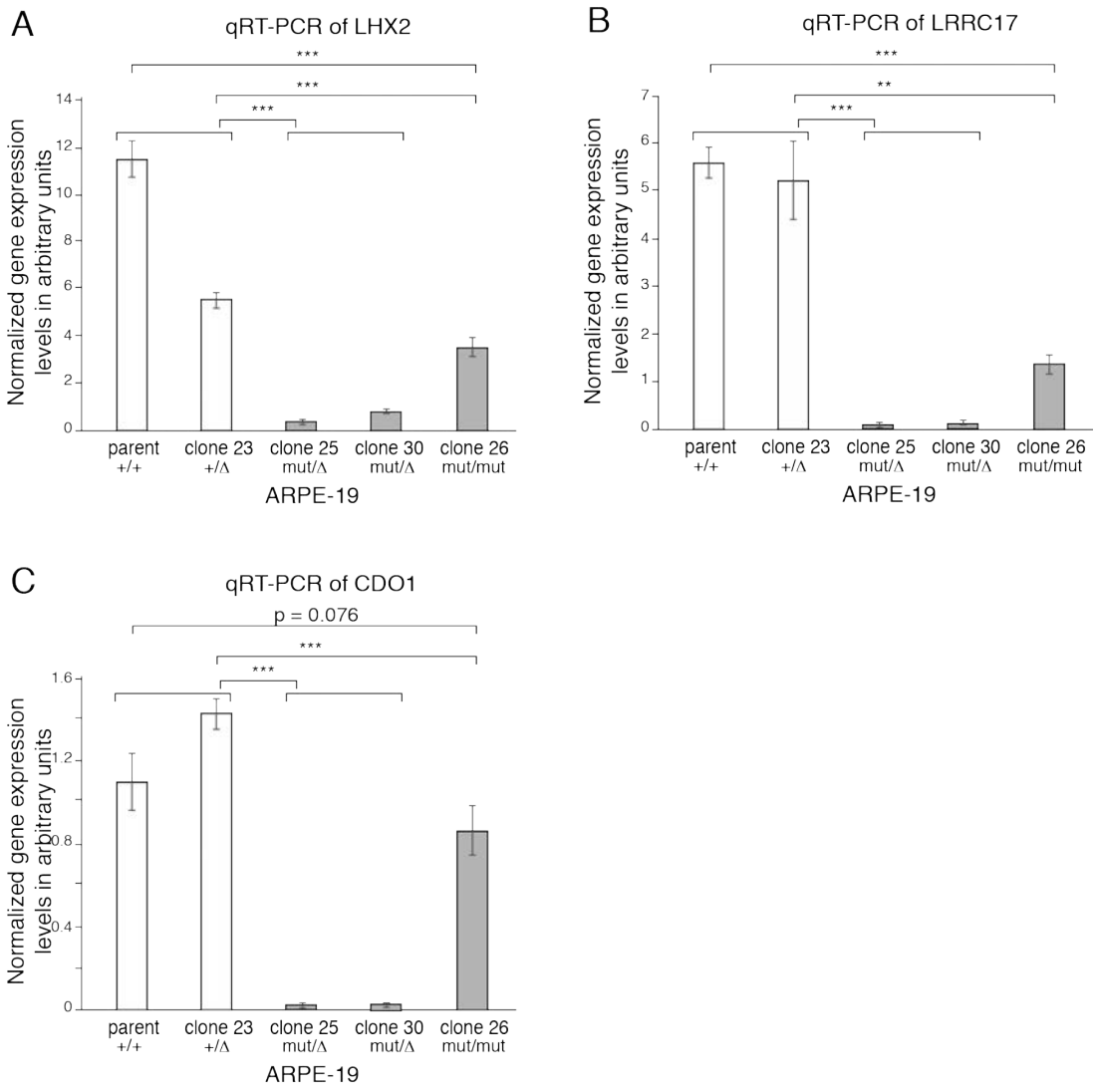

Figure 4.10 Validation of Rap1 as a transcriptional regulator. (A-C) Quantitative RT-PCR illustrates differential expression of three genes ((A) LHX2, (B) LRRC17, (C) CDO1) in Rap1 WT and KO ARPE-19 cells. Gene expression was normalized to GAPDH and mean expression level for each gene as determined by the ΔCt method from 3 independent replicates is graphed in arbitrary units. Error bars represent SDs. Significance was calculated by two-tailed unpaired T-Tests. *** indicates $p \leq 0.001$.

4.3 Summary of findings

Based on the genetic data presented here, human Rap1 is not required for the protection of telomeres from NHEJ and has no obvious effect on telomere length regulation, contrary to what was anticipated from other studies [23,78,160,213]. The results in this chapter point to the difficulty in interpreting experiments in which telomeric phenotypes are observed upon overexpression of shelterin (mutant) proteins or their partial inactivation by shRNAs. The prior finding of changes in telomere length and heterogeneity upon overexpression of Rap1 mutants [23] may have been due to nucleoplasmic titration of factors away from the telomere that (indirectly) influence these phenotypes. Similarly, the artificial tethering of Rap1 to telomeres may have had an effect on NHEJ that does not reflect the normal function of the protein [160].

In addition, telomeres lacking Rap1 remained protected from DNA damage signaling and HDR, and had a normal 3' overhang. These findings are in agreement with the mouse Rap1 KO, which revealed no obvious phenotype other than that of telomeres becoming prone to undergo HDR when Ku70/80 was absent [19]. Whether human telomeres lacking Rap1 also recombine more readily in a Ku70/80-deficient setting is difficult to assess since deletion of human Ku70/80 leads to rapid telomere loss and cell death [240,241].

Human Rap1 was surprisingly dispensable for telomere protection, however its role in transcriptional regulation appears to be conserved. Due to the low number of deregulated genes identified in vastly differing cell types, it was

difficult to assess what transcriptional programs Rap1 participates in. Examination of Rap1 deletion in cell lines with high metabolic activity, such as hepatocytes, would help identify whether human Rap1 affects metabolism similar to mouse Rap1.

These data indicate that while mammalian Rap1 has functionally diverged away from its yeast predecessors, mouse and human Rap1 are very similar. Both Rap1 knockout mice and human cells are viable, lack hallmarks of telomere dysfunction, and have no overt change in telomere length settings. While the Rap1 components of human and mouse shelterin are indistinguishable, it will be important to query the functions of other shelterin components and associated factors to gain a complete understanding of telomere maintenance and protection in human cells.

Chapter 5: Investigating the role of human POT1 at telomeres

5.1 Introduction

As discussed in the general introduction, the deletion of mouse POT1a and –b leads to embryonic and cellular lethality, elicits a telomeric ATR dependent DNA damage response, increases 3' telomere overhangs, and results in infrequent post-replicative telomere fusions and telomere sister associations [31,32,182].

In human cells, two isoforms of POT1 are detected by immunoblotting with molecular weights of 71 kDa and 55 kDa [184]. The protein that migrates at 71 kDa corresponds to full-length POT1 (POT1-FL). The isoform with the molecular weight of 55 kDa (POT1-55) lacks the first N-terminal OB fold of POT1 and is unable to bind telomeric DNA [34]. POT1-55 is almost identical to a mutant allele of POT1 (POT1ΔOB). POT1ΔOB cannot bind to telomeric DNA but retains its interaction with TPP1. When overexpressed, POT1ΔOB acts as a dominant-negative [79], presumably by binding to TPP1 and displacing endogenous POT1. Endogenous expression levels of POT1-FL are approximately 10-fold more abundant than POT1-55 [184], and no function has been ascribed to POT1-55 as of yet.

Partial depletion of POT1-FL with shRNAs impairs the growth of primary but not transformed cells [184]. Furthermore, there is a modest reduction (~30%) in the overhang signals and the precise nature of the 5' end of the telomeres is disrupted [184,185]. Knockdown of both POT1-FL and POT1-55 results in low levels

of TIFs, where ~40% of cells are TIF-positive, occurring during the G1 phase of the cell cycle [184].

In addition to protecting telomeres from the DNA damage response and modulating the nature of the telomere terminus, POT1 has been implicated in the cis-acting negative regulation of telomerase. Depletion of POT1 with shRNAs [29] or expression of the POT1ΔOB allele leads to telomere elongation [79]. The POT1 binding partner TPP1, on the other hand, interacts with telomerase and promotes the recruitment of the enzyme to telomeres in vivo and enhances the processivity of the enzyme in vitro [81].

Although the functions of POT1a and POT1b have been examined in detail, it is as yet unclear to what extent the single human POT1-FL protein incorporates these functions, and what role POT1-55 plays, if any. To understand the role of human POT1 in telomere protection, we used TALENs with the aim to generate human knockout cell lines lacking POT1. The preliminary analysis of these human POT1-deficient cells is reported here.

5.2 Results

5.2.1 *The human POT1 targeting strategy*

Mouse *POT1a* and *–b* share greater than 70% amino acid identity with human POT1 [31]. Human *POT1*, *POT1a*, and *POT1b*, have transcripts comprised of 19, 18 and 17 exons respectively, 15 of which are coding exons (annotated by

Ensembl). Here, coding exons are numbered sequentially with exon 1 containing the ATG. A strategy analogous to the mouse knockouts was employed to create knockouts of human *POT1*. The mouse knockouts of *POT1a* and *–b* were generated by deletion of exon 3, which results in an ORF with a premature stop codon in exon 4 [31]. In that study, exons 1 and 2 were not targeted because this could bring a putative alternate start site in the 5' UTR into frame with exon 3 coding sequences. Similar to the mouse genes, deletion of human exon 3, which encodes aa 41 to 85, is predicted to lead to a premature stop codon in the POT1 ORF at a position four codons into exon 4. Thus, we decided to delete exon 3 in human cells to generate a POT1-FL knockout. Neomycin, blasticidin and zeocin donor constructs were designed with 5' and 3' arms homologous to the introns surrounding exon 3 (Figure 5.1B). The anticipated resection at the TALEN-induced DSB and the small size of exon 3 should allow processing to extend into the surrounding introns such that the 5' and 3' arms can be used for homology-dependent repair, such that the repaired allele lacks exon 3.

In silico analysis of potential exon skipping products indicated that the ORF could be put back into frame if splicing were to occur from the exon 2 splice donor site to exon 7, 8, 10, 12, or 14. The potential truncated products generated by the exon skipping events would lack most of the N-terminal OB-folds that confer the ssDNA binding activity to POT1. Therefore, some of these versions of POT1 (splicing of exon 2 splice donor site to exon 7, 8, or 10) might still be recruited to telomeres via their C-terminal TPP1 binding region (encoded by

exons 10-15; see Figure 5.1A) and could potentially act as dominant-negative mutants due to loss of their OB folds [79]. To circumvent the formation of these truncated proteins, the donor construct was endowed with a 'STOP cassette' composed of an array of four copies of the SV40 poly (A) addition site [242-244], which should halt transcription beyond the second intron (Figure 5.1B). Furthermore, introduction of the STOP cassette will also disrupt transcription of the POT1-55 allele, effectively knocking out both isoforms of POT1.

Finally, given the lethality of deleting POT1a and -b in the mouse, we considered the likely cell lethal phenotype of cells lacking both alleles human POT1, which might be generated by TALENs (see Chapter 4). Therefore, HT1080 fibrosarcoma cells were first infected with a retrovirus containing cDNA encoding MYC-tagged full-length POT1 expressed from a CMV promoter (Figure 5.1B), and the retrovirus also conferred hygromycin resistance. Because the POT1 rescuing allele is flanked with LoxP sites, exogenous POT1 can be excised by Cre recombinase after the endogenous POT1 loci have been targeted. Hygromycin resistant clones were isolated with the initial intent to use western blot analysis to determine whether the exogenously expressed POT1 could be efficiently deleted. However, the antibody used in previous studies [29] (that detects endogenous POT1-FL and POT1-55) [184] was no longer functional. Therefore a single clone, 20.3, was selected at random for further targeting. Eventual identification of a commercial antibody that was able to detect POT1-FL, but not POT1-55 (see Figure 5.1A), was used to determine that clone 20.3 expressed

exogenous POT1-FL at similar levels to endogenous POT1-FL, and could be effectively deleted upon treatment with Cre (Figure 5.2A-B). In addition, as shown previously [79], the levels of POT1 protein seem to be regulated such that overexpression of POT1 resulted in repression of protein production from the endogenous allele (see c20.3 in Figure 5.2B).

A TALEN pair was designed to bind a site starting in intron 2-3 and extending into exon 3, such that the nuclease would not target the exogenous floxed POT1 cDNA. In addition, inclusion of the intron-exon junction near the predicted cleavage site enhances the likelihood of deleterious mutations that give rise to either splicing errors or frame-shifts.

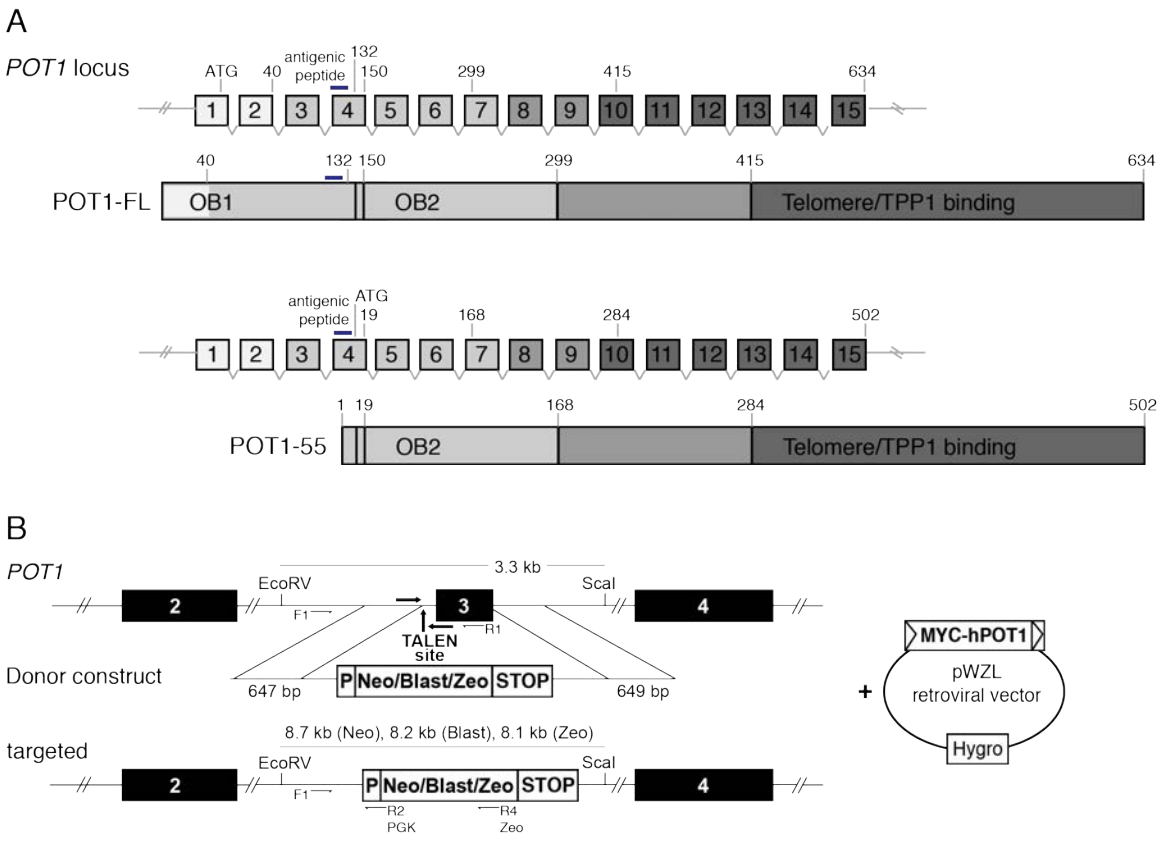

Figure 5.1 TALEN-mediated inactivation of the gene for human *POT1*. (A) Schematic of the human *POT1* locus, and the two reported isoforms and their respective ATGs. POT1-FL, full-length POT1 protein; POT1-55, POT1 protein lacking the first OB fold. Exons not drawn to scale, coding exon numbers indicated (as annotated by Ensembl). Shading of exons corresponds to protein regions they encode. Known structures of and binding sites in POT1 are indicated. Navy line corresponds to peptide used to generate POT1 antibody used in this study (Abcam). (B) The *POT1* locus, the targeting construct, and the resulting knockout allele. F1, R1, R2-PGK, R4-Zeo: PCR primers for genotyping. Arrows in bold: TALEN binding and cut sites. Schematic of MYC-tagged hPOT1 cDNA with flanking LoxP sites (triangles), cloned into the pWZL retroviral vector (confers hygro resistance).

5.2.2 *TALEN-mediated deletion of full-length human POT1*

HT1080 clone 20.3, expressing the floxed MYC-POT1 rescuing allele, was co-transfected with the aforementioned TALEN pair and the neomycin donor construct (Figure 5.1B). Cells were then selected with neomycin to enrich for POT1 alleles that had been targeted by the TALENs and repaired by HDR, resulting in deletion of exon 3 and acquisition of neomycin resistance. PCR analysis of neomycin resistant clones showed that 4 out of 34 (~12%) clones had integrated the donor cassette into one allele of POT1 (Figure 5.2B). Treatment of these heterozygous clones with Cre showed that 3 (c3, c5, c17) of the 4 clones expressed no detectable endogenous POT1-FL protein, which migrates slightly slower than the MYC-tagged POT1, suggesting bi-allelic disruption of the gene (Figure 5.2B). The efficiency of Cre-mediated deletion of POT1 varied between experiments (compare Figure 5.2A to 5.2B). Therefore, POT1-FL deletion was verified by immunoblotting for all experiments conducted, and only experiments that had less than 10% to undetectable levels of residual POT1 protein were analyzed.

Sequencing of uninterrupted alleles in these heterozygous clones lacking endogenous POT1 revealed that clones c3, c5 and c17 all contained mutations close to the TALEN cut site (Figure 5.2C). Mutations had ablated POT1-FL by creating a frame-shift or a defect in splicing, indicating that errors generated during NHEJ-mediated repair of the TALEN-induced break had inactivated the second allele of *POT1*. However, these NHEJ-mediated mutated alleles lacked

integration of the STOP cassette and could still be transcriptionally active. Therefore, while these clones served as knockouts for full length POT1, the POT1-55 protein and potential exon skipping products generated by these mutated alleles might still be translated. Furthermore, POT1-55 and potential exon skipping products would not be detected by the POT1 antibody used in this study, as it recognizes an epitope in exon 4 that is absent from the predicted peptides (indicated in Figure 5.1A). RT-PCR with primers to exon 2 and exons 4, 9, 13 and 15 was therefore performed to determine whether POT1-55 was being expressed. No products generated by exon skipping were detected, but products derived from the POT1-55 isoform were visible (Figure 5.2D). Therefore POT1-FL cannot be generated from the endogenous POT1 locus in clones c3, c5 and c17, but POT1-55 is still transcribed and presumably translated in these clones. No product was amplified in two lanes of the RT-PCR (asterisks in Figure 5.2D), likely due to experimental error, as amplification from the cDNA was detected in other lanes.

Telomeric ChIP on clone 17 (neo/mut) confirmed the loss of the exogenously expressed MYC-POT1 after the retroviral introduction of Cre recombinase, while levels of other shelterin components at telomeres were not affected (Figure 5.3A-B). Both control and targeted HT1080 clones exhibited slower growth when treated with Cre**,** presumably a consequence of Cre-induced DNA damage [245] (Figure 5.3C). The POT1-targeted clones had a mild proliferative defect, but did not cease proliferating. Immunoblotting of cells lacking

endogenous POT1-FL collected at four time-points during the growth curve, showed the reappearance of MYC-POT1 at approximately 6 days after Cre treatment (Figure 5.3C). The reappearance of MYC-POT1 was likely due to the outgrowth of some cells that escaped Cre infection. Retention of the exogenous allele of MYC-POT1 presumably provided these cells a proliferative advantage over POT1 null cells. Furthermore, MYC-POT1 was not detected at any time-point after Cre infection in cells that had the wild type endogenous POT1 gene (Figure 5.3D). Taken together, these data suggested that POT1-deficiency challenged the cells. However, a puzzling aspect of the growth curve was that no plateau or trough was observed, which would be expected if POT1-deficient cells struggled to proliferate while POT1-proficient cells underwent enough population doublings (at least 6 PDs, if we assume 1% cells escaped Cre) to constitute majority of the culture. Moreover, at day 12 after ~10 PDs, MYC-POT1 expressing cells had still not completely overtaken the culture, suggesting POT1-deficient cells were still proliferating. At day 20 after Cre, complete repopulation of the culture by POT1-proficient cells was observed. Therefore, POT1-deficiency appears to be detrimental for cells; however from the data presented here, we cannot conclude that it is lethal.

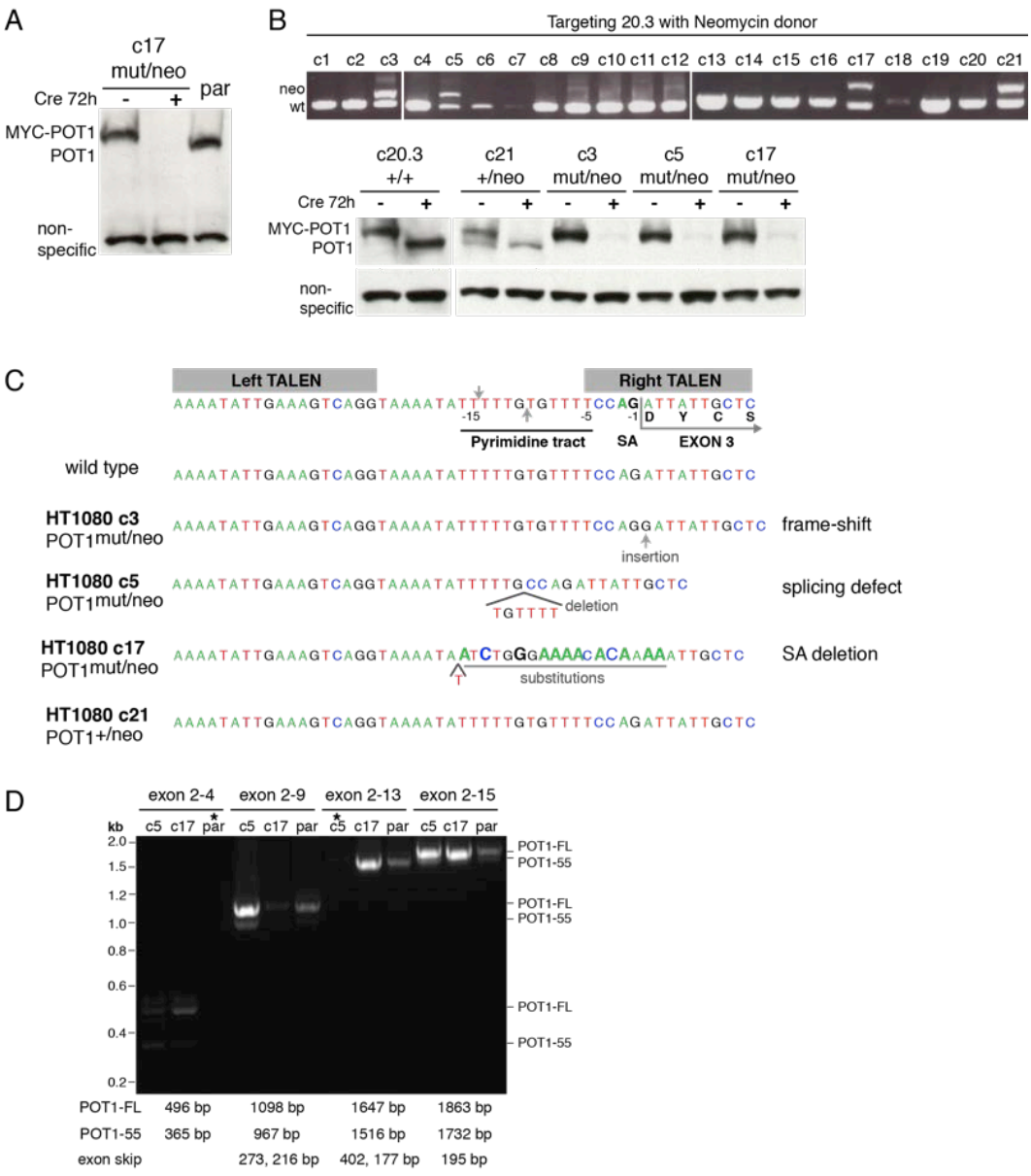

Figure 5.2 Loss of POT1-FL in targeted clones. (A) Immunoblotting for POT1 (Abcam antibody) indicated that MYC-POT1 migrates more slowly than endogenous POT1, allowing us to distinguish between exogenous and endogenous forms of POT1. Bands corresponding to MYC-POT1 and endogenous POT1 are indicated. Non-specific band serves as loading control; par, parental HT1080 population. (B) Top, PCR of neo resistant clones with F1, R1 and R2-PGK primers. Bottom, immunoblot of HT1080 clones with genotypes as indicated, before and 72 hours after treatment with Cre. Blot probed with anti-hPOT1 (Abcam). (C) Top, schematic illustrating TALEN binding sites, their predicted cutting site (grey arrows), the pyrimidine tract, splice acceptor (SA), and the location of coding exon 3 in the *POT1* locus. Bottom, relevant sequences of the indicated clones. (D) RT-PCR on RNA from clones c5, c17 and the parental HT1080 cell line (par). Exons amplified as indicated. Bottom, expected sizes for the two known isoforms of POT1, and predicted sizes of potential products generated by exon skipping. Asterisks indicate lanes where no amplification was observed.

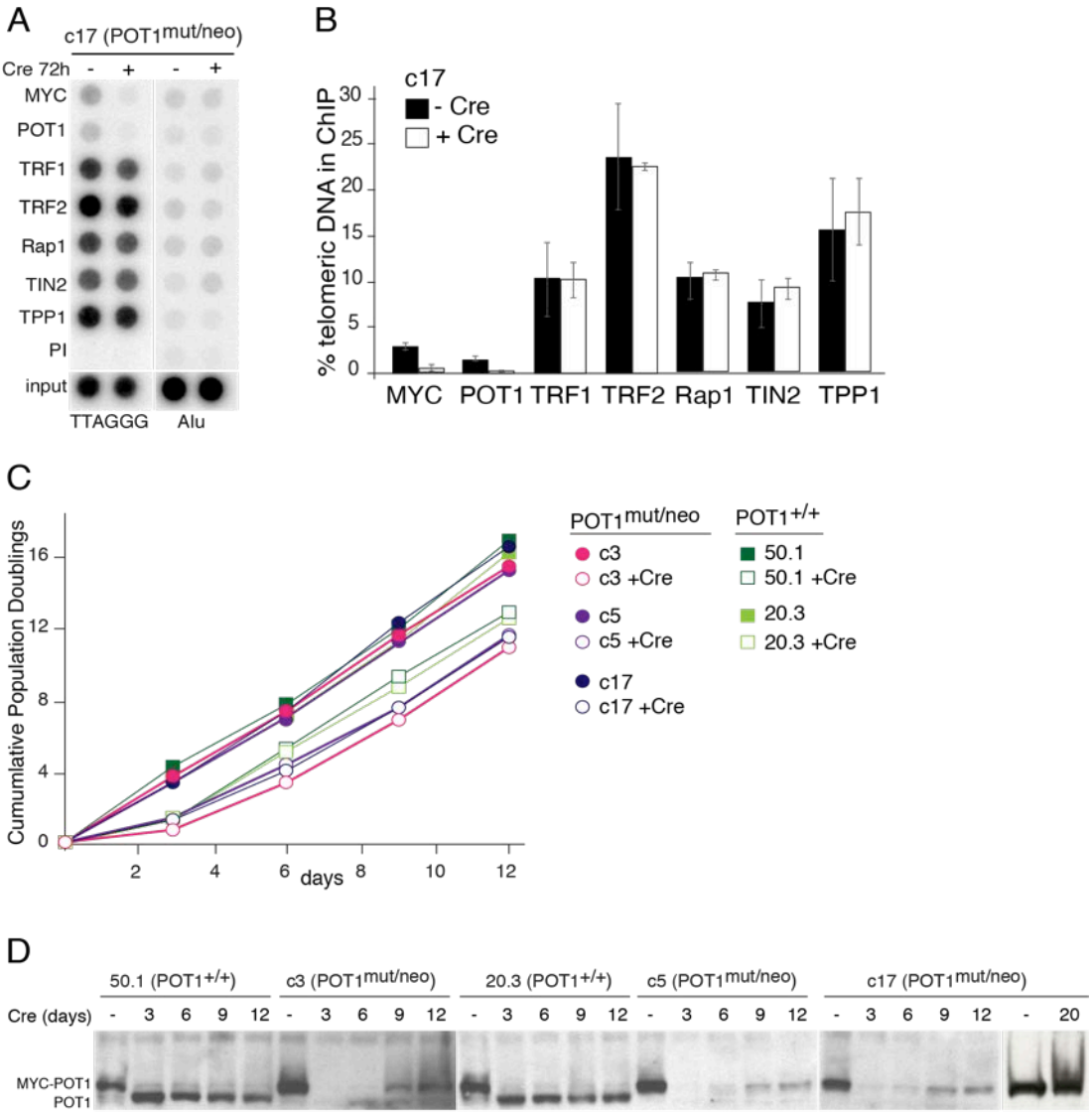

Figure 5.3 Deficiency of POT1-FL is not tolerated. (A) Telomeric ChIP of targeted HT1080 c17 with and without Cre treatment. Duplicate dot-blots were probed for telomeric or Alu repeats. (B) Average percentage of telomeric DNA recovered in ChIPs with the indicated antibodies (two independent experiments). Error bars: SEMs. (C) Growth curves of targeted and WT HT1080 clones, plotted as cumulative population doublings over time (days) after Cre treatment as indicated. Genotypes of cell lines as indicated above. (D) hPOT1 (Abcam) immunoblot of cells in (C) at different time-points after Cre treatment as indicated.

5.2.3 *Telomere deprotection in POT1-deficient cells*

Removal of full-length POT1 resulted in deprotected telomeres as revealed by the induction of a strong TIF response (~65%)(Figure 5.4A-B), similar to when mouse POT1a and –b are deleted (~75%) [31]. Depletion of POT1-FL and POT1-55 by shRNA results in only 40% of TIFs that occur in the G1 phase of the cell cycle [184]. It is not clear whether the lower level of TIFs is due to incomplete knockdown of POT1, or whether POT1-55 may contribute to TIF formation in the POT1-FL knockout cells (see Chapter 6). The cell cycle dependency of TIF formation in cells deficient for POT1-FL has not yet been tested, however, considering 65% of cells were TIF positive, it is likely that TIFs persist through most of the cell cycle. DNA damage signaling remained repressed in clones 20.3 (homozygous for WT POT1) and c21 (heterozygous for WT POT1), indicating that one allele of POT1 is sufficient to inhibit DNA damage signaling at telomeres (Figure 5.4B), consistent with previous observations showing that POT1a and POT1b are haplosufficient [31]. A partial, but significant reduction of TIFs is observed when POT1 is depleted by shRNA in ATR-deficient HCT116 cells or MEFs [148]. Treatment with an ATR inhibitor almost entirely repressed the occurrence of TIFs in the POT1-deficient c17 clone, confirming that human POT1-FL is required to repress activation of the ATR kinase at telomeres (Figure 5.4B).

Metaphase spreads of cells lacking POT1-FL showed no gross chromosomal aberrations. An increase in telomere sister associations was

observed (Figure 5.4C-E), which also occurs upon deletion of mouse POT1a and -b [31]. Metaphase spreads also showed several chromosome ends lacking one (sister loss) or two (signal free ends) telomeric signals. However, this was likely due to difficulty in detection of these telomeres by FISH, as WT cells showed the same phenotype (Figure 5.4D). There was no significant induction of NHEJ at the telomeres lacking POT1, as evidenced by the lack of telomere fusions (Figure 5.4E). Fragile telomeres, a readout for telomere replication problems [156], are not observed at telomeres lacking POT1a/b, and have not yet been assessed in this study[31]. The propensity of POT1-deficient cells to undergo HDR was complicated to test for two reasons. First, due to the short telomeres of HT1080 cells, the telomeric fluorescent signals are weak, making the analysis of CO-FISH difficult. Second, telomere recombination in MEFs lacking POT1a and –b is observed only when Ku is also absent. However, since Ku-deficiency is lethal in human cells, we were unable to co-delete Ku and POT1 [240,241].

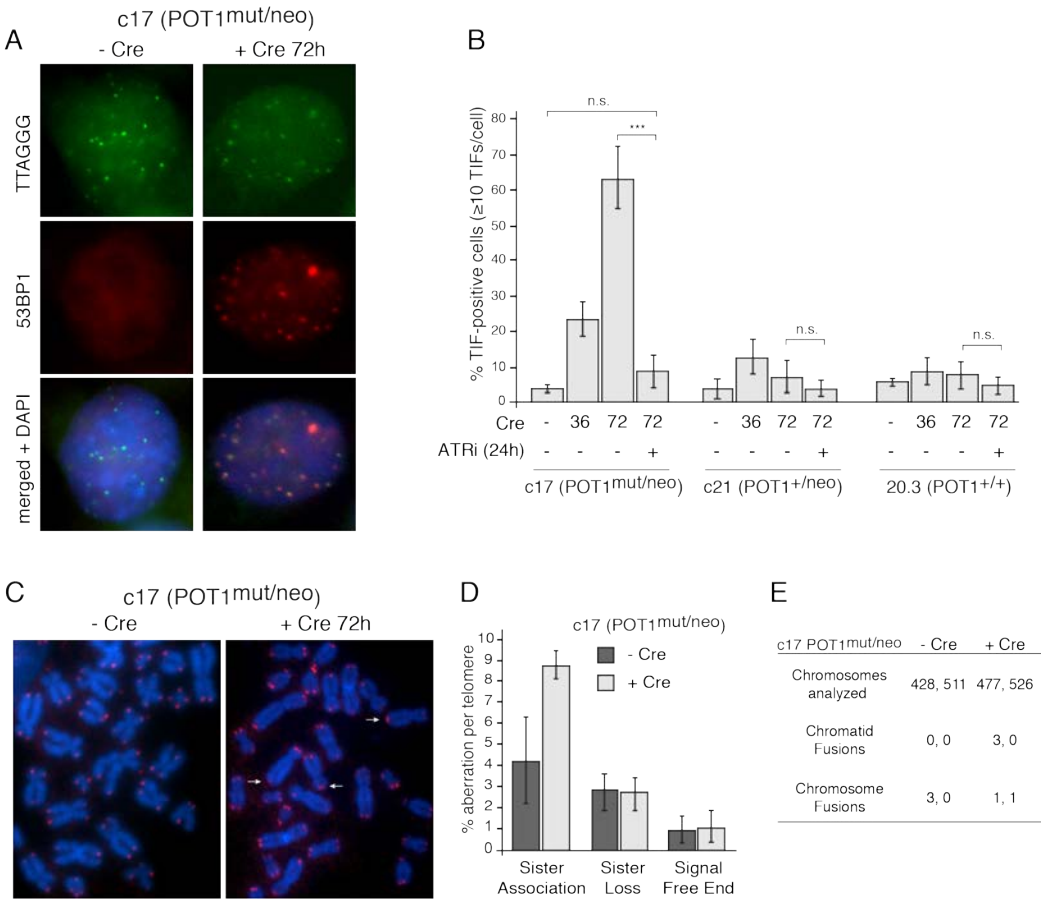

Figure 5.4 ATR-dependent DNA damage signaling induced upon loss of full-length POT1. (A) TIF assay on HT1080 c17 before and after deletion of POT1 with Cre. Green, telomeric FISH; red, IF for 53BP1; blue, DNA (DAPI). (B) Quantification of TIFs assay as in (A). TIF analysis was performed on three cell lines 36 and 72 hours after treatment with Cre. ATR inhibitor ETP-46464 [254] was added to indicated cells 48 hours after Cre treatment at a final concentration of 1μM, for 24 hours. Values represent mean from three independent experiments with SDs. Calculations of significance based on paired two-tailed Student's T-Test (C) Metaphase spreads of c17 cell line before and after treatment with Cre as indicated. White arrows point to examples of telomeric 'sister associations'. (D) Aberrant features of metaphase spreads as in (C) were scored. Values represent mean of two independent experiments, where > 400 chromosomes were scored. Error bars: SEM. (E) Table showing occurrence of telomere fusions as detected in (C).

5.2.4 *Maintenance of telomere overhangs*

Removal of both mouse POT1 proteins (or POT1b alone) results in extended 3' telomere overhangs [31,52,150], whereas knockdown of human POT1-FL, but not POT1-55, leads to a reduction in overhang signal [184,185]. Expressing mutant alleles of POT1a or POT1b that lack their first OB fold, similar to POT1-55, results in increased overhang signals, presumably due to displacement of endogenous POT1a/b by competing for binding to TPP1 [246]. Interestingly, the amount of single-stranded DNA at chromosome ends was unchanged upon loss of POT1-FL (Figure 5.5A-B) based on detection of the single-stranded telomeric DNA by in-gel hybridization of a labeled C-strand telomeric repeat probe to native telomeric restriction fragments. The *E. coli* 3' exonuclease, ExoI, was used to confirm that the detected signal was derived from terminal 3' overhangs (Figure 5.5A). Despite observing increased overhangs in the presence of DNA damage signaling in the POT1a/b double knockout MEFs [31], we considered the possibility that the DDR response at human telomeres interferes with overhang processing. However, treatment with an ATR inhibitor to repress DNA damage signaling at deprotected telomeres in POT1-deficient cells showed no change in the telomere overhang signals (Figure 5.5C-D).

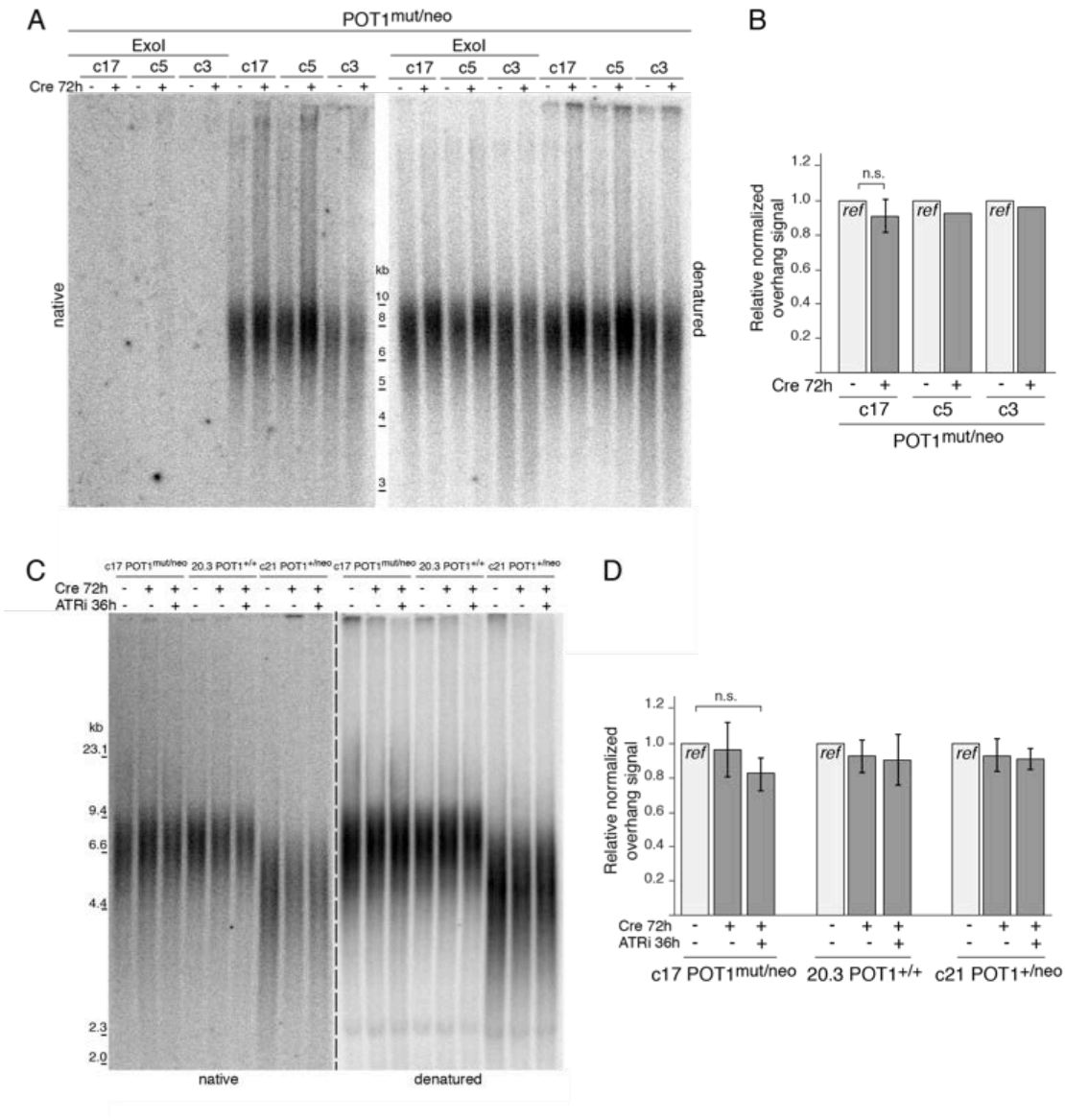

Figure 5.5 No change in 3' telomere overhangs upon loss of POT1-FL. (A) Overhang analysis of clones lacking functional endogenous POT1 loci, before and after removal of exogenous POT1 with Cre as indicated. Left, in-gel detection of native telomeric restriction fragments with a C-strand telomeric probe revealing the G-strand overhang signals; right, same gel rehybridized after in situ denaturation of the DNA, revealing the total telomeric DNA in each lane. Samples were treated with ExoI (Exonuclease I) as indicated. (B) Overhang signals from (A) were normalized to total telomeric signals in each lane and plotted as a ratio compared to the WT overhang signal of the corresponding cell line, labeled as *ref*. Values plotted for clones c5 and c3 are from one experiment. Value plotted for c17 is the mean of 3 independent experiments with SD. Lack of statistical significance derived from two-tailed paired t-test. (C) Overhang analysis of clones with indicated genotypes, Cre treatment and ATR treatment as described in Figure 5.4B. Detection of native (left) and denatured (right) telomeric restriction fragments as described in (A). (D) Quantification of overhang signals in (C) using the same methodology as in (B). Values represent means of three independent experiments with SDs. Lack of statistical significance derived from two-tailed paired t-test.

Mouse POT1b recruits CST to telomeres, presumably to perform fill-in synthesis [52]. Human POT1 interacts with CST [247,248] and may serve a similar function of recruitment. As a positive control for alterations in overhang maintenance, we examined the effect of a mutant of POT1 (S322L), proposed to disrupt the POT1-CST interaction and result in extended overhangs (Hiro Takai, unpubl.). FLAG-tagged constructs of wild type POT1 or the mutant POT1-S322L were retrovirally expressed in clones c5 and c17 (Figure 5.6A). Overhang analysis showed that expression of POT1-S322L in cells lacking POT1-FL indeed resulted in an increase in overhang signal (Figure 5.6B-C), perhaps due to the lack of CST-mediated fill-in. Although this positive control showed that the effects of POT1 on overhang maintenance could be detected in these clones, it remains puzzling that there is no overhang phenotype upon the deletion of POT1. POT1 might therefore be required to both stimulate resection and regulate CST mediated fill-in to obtain the correct overhang length.

Partial knockdown of POT1-55 yields no overhang phenotype, and shRNA targeting both POT1-FL and POT1-55 shows no additive change in overhang signal as compared to depletion of POT1-FL alone [184]. To confirm that POT1-55 does not play a role in overhang maintenance, clone c21 (heterozygous for WT POT1) was subjected to a second round of targeting with TALENs and the blasticidin or zeocin donor constructs. Blasticidin and zeocin resistant clones were screened by PCR to identify clones where both alleles of POT1 had been targeted (Figure 5.7A). RT-PCR of homozygous targeted clones confirmed the

lack of the POT1-55 isoform mRNA, while it was still present in clone c17, which had a single-integration of the STOP cassette (Figure 5.7B). Similar to the earlier observation that endogenous POT1-FL was repressed upon overexpression of MYC-POT1 (Figure 5.3D), detection of the POT1-55 isoform by RT-PCR was enhanced after removal of MYC-POT1 with Cre treatment (Figure 5.7B). Therefore, regulation of POT1 protein levels might be mediated by up- or down-regulation of transcription, as opposed to proteasome-mediated degradation, but the mechanism of how this occurs is unknown. However, multiple RT-PCR replicates need to be performed to confirm this finding of potential crosstalk between protein levels of POT1 and transcription of its locus.

POT1-FL was also still detected by RT-PCR after Cre treatment, albeit at much lower levels (Figure 5.7B), probably due to a low percentage of cells that had not completely deleted the exogenous MYC-POT1 rescue allele. Quantitative RT-PCR showed that expression of POT1-FL was significantly attenuated after treatment with Cre (Figure 5.7C), and was confirmed by immunoblotting (Figure 5.7D). Overhang analysis of clones lacking both isoforms of POT1 showed no change in overhang signal, indicating that POT1-55 did not contribute to overhang maintenance.

A recurrent phenotype that was observed on these overhang gels was mild telomere elongation after deletion of POT1-FL (Figure 5.5A, Figure 5.6B, Figure 5.7E). Given the role of POT1 in the negative regulation of telomerase [29,79,249], this lengthening could be due to the action of telomerase. Interestingly,

telomere elongation was not observed after deletion of both POT1-FL and POT1-55 (Figure 5.7E), which would suggest that telomere extension is mediated by POT1-55 when POT1-FL is deleted. Additional replicates need to be performed to corroborate this observation.

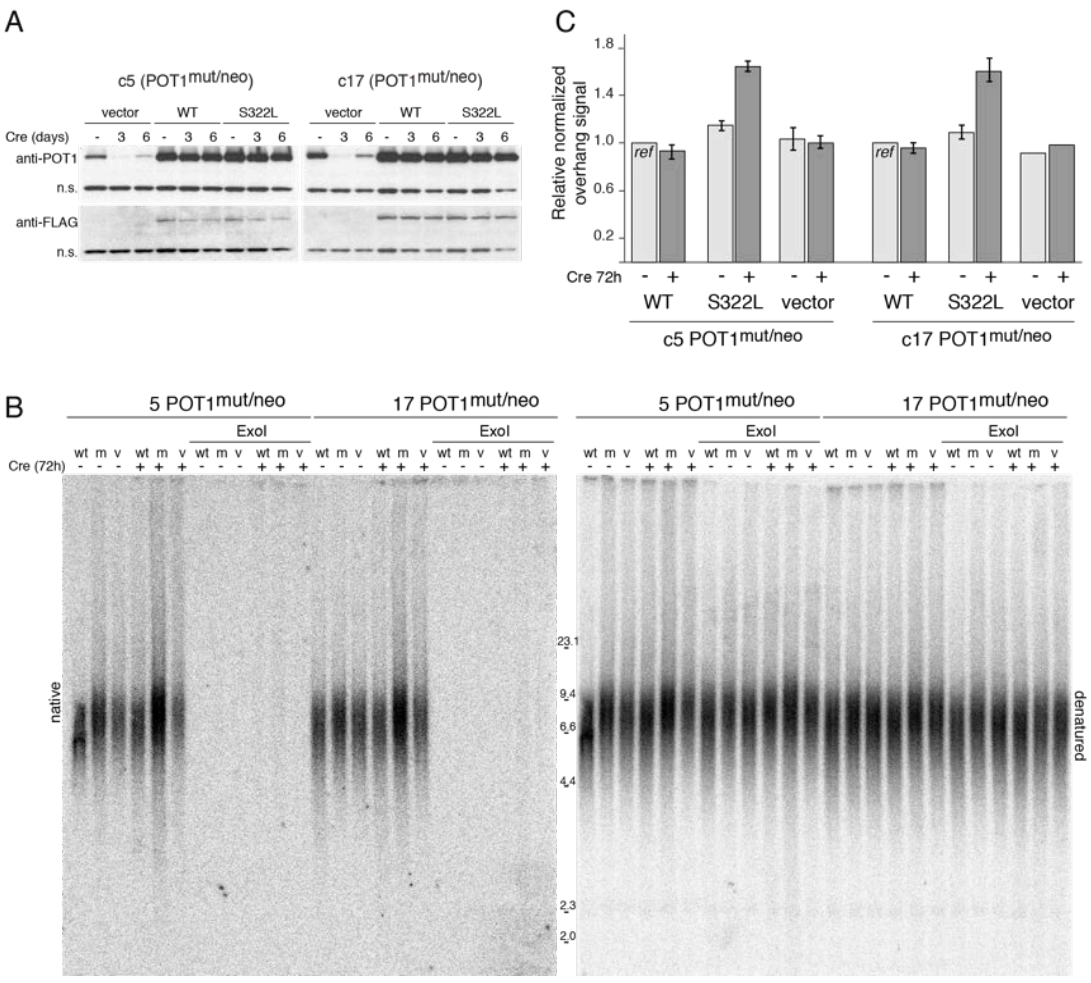

Figure 5.6 Extended overhangs in POT1-deficient cells expressing the S322L mutant.
(A) Immunoblot for FLAG and hPOT1 in clones expressing FLAG-POT1-FL (WT), FLAG-POT1-S322L (S322L) or vector control. Treatment with Cre (as indicated) removes expression of MYC-POT1-FL, which all cell lines also express. n.s., non-specific band detected by the antibody serves as a loading control. (B) Gel for overhang analysis as previously described in Figure 5.5A. Cre treatment and ExoI treatment as indicated. Left, native gel; Right, denatured gel. wt, FLAG-POT-FL; m, FLAG-POT1-S322L; v, vector control. (C) Quantification of overhang signals in (B). Native signals were normalized against denatured signals in the corresponding lanes and plotted as a ratio compared to the signal in the WT sample for each cell line, labeled as *ref*. Values represent means of two independent experiments, and error bars show SEMs.

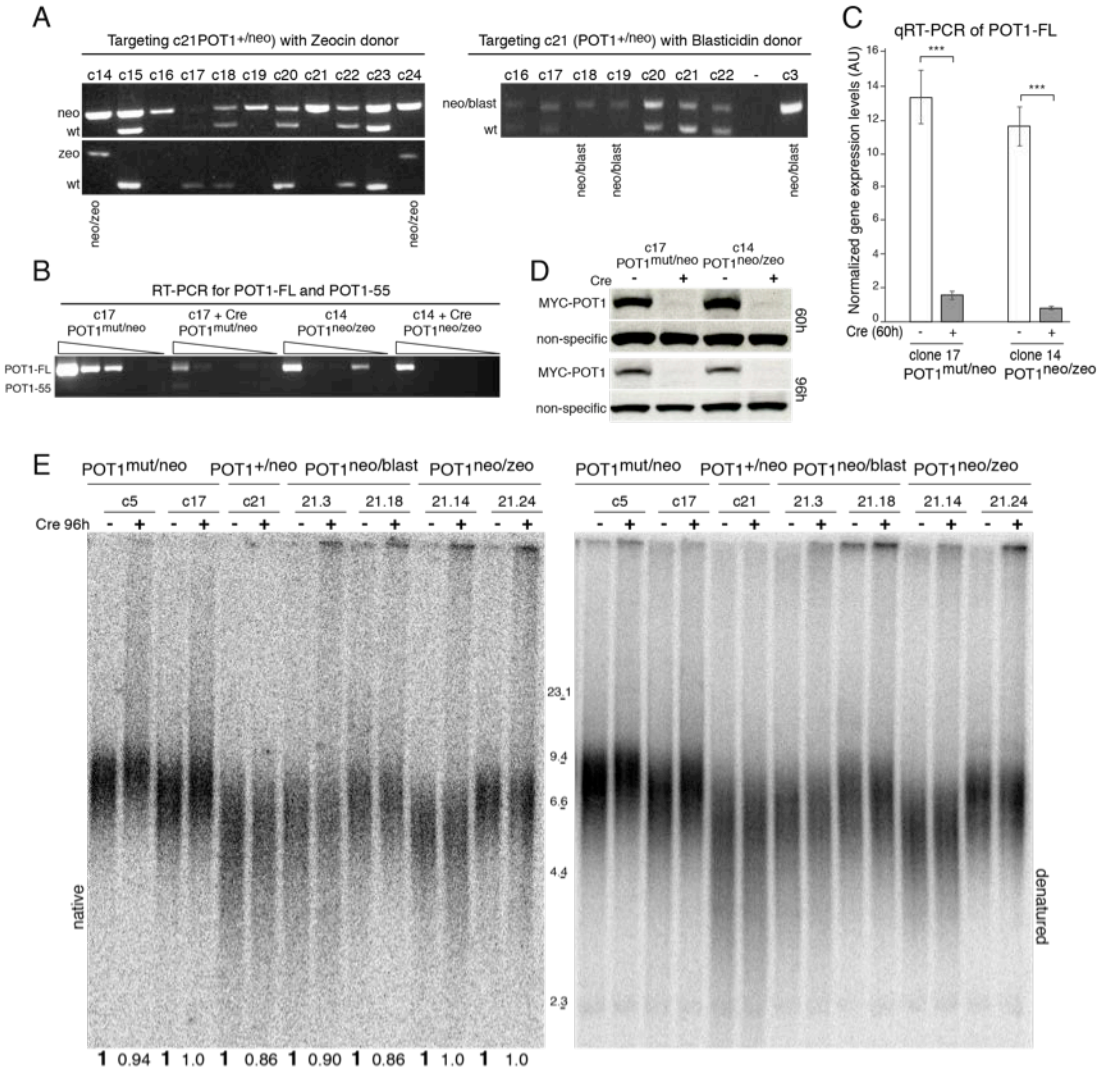

Figure 5.7 No change in 3' telomere overhangs upon deletion of both POT1 isoforms.
(A) Genotyping PCR of zeocin (left) and blasticidin (right) resistant clones. Top, PCR with primers F1, R1, and R2-PGK. Loss of WT allele indicates successful targeting. Bottom, PCR with primers F1, R1 and R4-Zeo. Appearance of top band and disappearance of bottom band confirms successful targeting. Genotypes of successfully targeted clones indicated below. (B) RT-PCR detecting POT1-FL and POT-55. 4-fold serial dilutions of reverse transcribed cDNA were used for PCR reactions. (C) qRT-PCR of POT1-FL in two clones before and 60 hours after expression of Cre. (D) Immunoblot showing deletion of POT1-FL in two clones at 60 or 96 hours after Cre expression. Genotypes as indicated. Non-specific band serves as loading control. (E) Gel for overhang analysis of clones lacking POT1-FL or both POT1-FL and POT1-55. Genotypes and cre treatment as indicated. Quantification of the gel shown below where overhang signals were normalized to total telomeric signals in each lane and listed as a ratio compared to the WT overhang signal of the corresponding cell line. WT overhang signals set to 1 are in bold with a larger font.

5.3 Summary of findings

Human POT1-FL, consistent with prior data [148], is required to inhibit ATR-dependent DNA damage signaling at telomeres. Whether POT1-55 functions as a dominant-negative allele exacerbating the occurrence of TIFs remains to be determined, as does the cell cycle dependence of TIF formation in POT1-FL knockout cells. Deprotected telomeres in POT1-FL-deficient cells were not vulnerable to NHEJ, as deduced by the lack of telomere fusions observed in these cells. However, an induction of telomere sister associations was noted in cells lacking POT1, but the molecular basis of these associations is not known.

Surprisingly, unlike mouse POT1a/b-deficiency [31], human cells lacking POT1 did not show a change in overhang status. The underlying cause of this discrepancy is not clear, and many options remain to be tested (discussed further in Chapter 6). Briefly, it is possible that POT1 is required to promote both resection, and CST-mediated fill-in synthesis, thereby resulting in no overall change in overhang signal when POT1 is deleted. Alternatively, removal of POT1 could allow telomerase to extend the overhang, and CST could be recruited to perform fill-in synthesis independently of POT1, leaving no net change in overhang lengths. Finally, although it seems unlikely, it is possible that steps upstream of ATR signaling, such as RPA loading on ssDNA play a role in overhang regulation.

The conditional knockout system we have generated in human cells will be of great use, not only to understand the functions of human POT1, but also as a

means to mechanistically evaluate numerous mutations recently identified in POT1 in various cancers [250-253] (see Chapter 6). One caveat of our system is the incomplete Cre-mediated deletion. One possible solution is to use a retroviral Cre that confers puromycin resistance and select for Cre-expressing cells. An option for future targeting strategies is to flank both the exogenously expressed cDNA and the hygromycin cassette with LoxP sites, such that cells are rendered sensitive to hyrgomycin upon treatment with Cre, and hygromycin selection can be retained to select for other constructs of interest.

Lastly, the POT1-55 knockout cell lines described in this chapter may be used to gain insight into the purpose of POT1-55. While the delineation of functions that mouse POT1a and –b perform is evident, it remains unclear why the POT1-55 isoform of human POT1 exists. It is difficult to hypothesize about potential roles of POT1-55 in the maintenance of telomere integrity, as it resembles a dominant negative mutant, is weakly expressed and removal of POT1-55 displays no apparent phenotype.

Chapter 6: Discussion

6.1 The role of mammalian Rap1

Analysis of mouse knockouts and TALEN-mediated human knockouts of Rap1 reveal that, unlike its yeast counterparts, mammalian Rap1 is not required for cellular and organismal viability, does not play a major role in telomere length regulation, and is largely dispensable for telomere protection. Loss of Rap1 does not affect the other components of shelterin, the modification of telomeric histones, the synthesis of TERRA, or the maintenance of the 3' telomeric overhang. Telomeres lacking Rap1 do not show consistent changes in their length, do not activate the DNA damage response, or become processed by NHEJ. However, we did find that mouse Rap1 is required to repress HDR at telomeres redundantly with Ku70/80, a function we were unable to test in human cells due to lethality ensuing deletion of Ku70 or -80. Remarkably, we observed that human Rap1, like its mouse and unicellular orthologs, affects gene expression. Therefore, we propose that the conservation of Rap1 reflects its role in transcriptional regulation, rather than a function at telomeres.

The dispensability of Rap1 in telomere end-protection was especially surprising with regard to previous reports implicating mammalian Rap1 as a repressor of NHEJ [213] [160]. An *in vitro* end-joining reaction with linear telomeric substrates could be repressed by addition of the Rap1/TRF2 complex, but not Rap1 or TRF2 alone [213]. Perhaps the better binding affinity of TRF2/Rap1 to duplex telomere substrates, than that of TRF2 (Chapter 3 and [235]), allowed for more efficient inhibition of NHEJ. An *in vivo* study shows Rap1 can be tethered to

HeLa telomeres by being fused to the DNA binding domain of a *S. pombe* protein that preferentially binds TTAGGG repeats (TebDB) [160]. Removal of endogenous Rap1/TRF2 by a dominant negative mutant results in fusions, which can be repressed by Rap1ΔCT-TebDB. Repression of NHEJ is not conferred by TebDB itself, however, it is possible that Rap1ΔCT-TebDB acts as a neomorph. The DNA-binding affinity of Rap1ΔCT-TebDB or its placement at telomeres may physically occlude access of DNA repair factors. Alternatively, it is possible that Rap1 plays a redundant role in the repression of telomere fusions in the absence of TRF2, however our preliminary data does not support this hypothesis. In addition, this setting of Rap1 at telomeres lacking TRF2 is highly unlikely to naturally occur, due to the requisite binding of Rap1 to TRF2 for maintenance of Rap1 protein levels and telomeric localization.

6.1.1 *Rap1 – a conserved telomeric protein with non-telomeric functions*

Several lines of evidence indicate that *Rap1* is a highly conserved component of mammalian shelterin. The human gene encoding Rap1 has diverged little from its chimpanzee counterpart (1 base change/100 codons; 0.25 amino acid (aa) changes/100 aa), whereas the genes for other shelterin components show much greater divergence (e.g., 3.6, 2.4, and 1.7 base changes/100 codons and 2.2, 1.1, and 0.65 aa changes/100 aa for TRF2, TRF1, and TIN2, respectively). Human and chimpanzee sequence was compared as

these sequences align most closely and allow for more accurate comparison of changes in nucleotide and amino acid sequence between shelterin proteins.

Data from the Exome Variant Server (NHLBI GO Exome Sequencing Project, Seattle, WA (URL: http://evs.gs.washington.edu/EVS/) [as of 02/2015]) identifies only 14 potentially deleterious (splice, nonsense, frame-shift or missense) mutations in *Rap1* in ~13,000 alleles sequenced. Compared to *Rap1*, a larger number of potentially deleterious mutations have been identified in all other shelterin components (19, 22, 50, 49 and 24 for TRF2, TRF1, TIN2, TPP1 and POT1, respectively).

Assessment of a gene damage index (GDI) derived from the 1000 Genomes Project [255], which reports on the cumulative mutational damage in a given human coding gene, places *Rap1* in the top 20% of human genes with regard to tolerance to mutation intolerance (Y. Itan, pers. comm.). In addition, *Rap1* ranks among the top 10% of coding human genes in terms of 'functional indispensability', a characteristic that incorporates gene centrality (based on interaction data pooled from various biological systems), structural information, and evolutionary constraints [256]. In this regard, only TIN2 scores higher than Rap1, as expected based on its multiple interaction interfaces in shelterin. The aforementioned estimates of gene conservation do not necessarily highlight essential genes, instead they aim to identify genes in which mutations may lead to disease phenotypes. Furthermore, it is possible that Rap1 may serve an important function in a specific tissue or cell type that we did not test, which may explain the selective pressure placed upon Rap1.

The level of conservation of Rap1 raises the question: what functional aspect of Rap1 is under selective pressure? The repression of HDR is unlikely to explain the conservation of Rap1, since the HDR phenotype only manifests itself when Ku70/80 are absent. It is also unlikely that Rap1 has a tissue specific role at telomeres, given that mice lacking Rap1 are alive and largely normal, and our demonstration that Rap1 deletion from human cell lines originating from different tissues show no overt telomere phenotype. The conservation of Rap1 is also not explained by a role in meiosis since the Rap1 knockout mice are fertile and, unlike yeast lacking Rap1, form a normal meiotic bouquet [19,36,217,218,257,258]. It is not excluded that Rap1 has (as yet unknown) multiple interactions within shelterin or with shelterin-associated factors that explain its conservation, or alternatively, that its role at telomeres is redundant. We favor the idea that the conservation of Rap1 is due to its role in transcriptional regulation [220-223,259] where it may have multiple distinct interaction partners that constrain its evolution.

Given that mammalian Rap1 is unlikely to bind directly to DNA [20,193], and that the majority of the chromosome-internal Rap1-associated loci are devoid of telomeric sequence [220,223], it is expected that interacting factors recruit Rap1 to these sites. In fact, complementation of Rap1-deficient MEFs with the Rap1 I312R allele (deficient in TRF2-binding), restores transcriptional regulation of ~85% of genes [221], consistent with the idea that Rap1 has binding partners that target Rap1 to these loci in a TRF2-independent manner. Identification of these factors could potentially illuminate (as yet undefined) telomere functions of Rap1.

Rap1 potentially evades being targeted for degradation by binding to TRF2 (Chapter 3), which is puzzling when trying to understand how Rap1 regulates transcription independently of TRF2. One possibility is that other binding partners are able to protect Rap1 from degradation. However, the nearly undetectable levels of Rap1 in TRF2-depleted cells [19,22,24], suggest that very low amounts of Rap1 would be bound to and protected by other factors. It would therefore be of interest to determine whether this residual non-telomeric Rap1 is sufficient for transcriptional regulation.

6.1.2 *Rationale for retention of Rap1 at telomeres*

If Rap is conserved due to its role in transcriptional regulation, this begs the question why its interaction with TRF2 and localization to telomeres is retained. One possibility is that TRF2 is required for Rap1 to localize to some of the chromosomal loci that it transcriptionally regulates. The aforementioned study[221] shows that ~15% of transcriptional regulation by Rap1 is dependent on its interaction with TRF2. In addition, ~15% of loci associated with human Rap1 also contain the consensus sequence for TRF2-binding [223].

Another possibility is that telomere length influences the transcriptional control performed by Rap1. Telomere shortening may result in displaced Rap1/TRF2 complexes, which can then bind to additional chromosome-internal sites. Several studies in human cells show that telomere shortening, prior to the induction of DNA damage signaling (as detected by TIF assays), can affect

expression of genes located both proximal [260,261] and distal [262] to telomeres. Hi-C (chromosome capture followed by high throughput sequencing) reveals that chromosome looping can place telomeres adjacent to genes located up to 10 Mb away [262], which could potentially be another mode of Rap1 recruitment to loci that it regulates. Moreover, both up- and down-regulation of transcripts are observed following telomere shortening [262], suggesting that gene expression does not seem to be inhibited by proximity to heterochromatic telomeric chromatin. Instead, it is more likely to be modulated by a transcription factor, similar to our observations of Rap1 function in both up- and down-regulation of gene expression.

It is unclear why telomere length should play a role in the control of gene expression. One possibility is that telomere shortening may initiate a transcriptional program that promotes entry into senescence. In *S. cerevisiae*, when critical telomere shortening is induced by deletion of telomerase (*tlc1Δ*), Rap1 relocalizes to hundreds of new target genes [263]. Redistribution of Rap1 in yeast during the onset of senescence is dependent on Mec1 (the ATR homolog), suggesting DNA damage also plays a role in Rap1 relocalization. DNA damage signaling is not reported to accompany the gene expression changes observed upon telomere shortening in human cells, which may suggest that other signals promote senescence in mammalian cells. Alternatively, the TIF assay is not the most sensitive method to evaluate DNA damage signaling and may miss low frequency events that are responsible for triggering this change in cell state. It will

be interesting to see if mammalian Rap1 is required to initiate a transcriptional program based on changes in telomere length.

6.1.3 *No Rap1 ortholog in Drosophila*

Drosophila telomeres, while serving the universal function of maintaining chromosomal integrity, lack many hallmarks of eukaryotic telomere structure and maintenance. For instance, *Drosophila* species lack telomerase, maintaining their telomeres by specialized retrotransposons instead, and they also have variable telomere repeats and sequence at their termini (reviewed in [285]). Furthermore, standard BLAST (*B*asic *L*ocal *A*lignment *S*earch *T*ool) searches have revealed no homologs of the shelterin components in *Drosophila* [286], while most non-telomeric human proteins have *Drosophila* homologs. In consideration of the non-telomeric role of Rap1, the selective pressure Rap1 appears to be under, and the advances in annotated sequence databases, we reexamined whether Rap1 could be identified in flies. Due to the low sequence conservation of Rap1, we used PSI-BLAST (*P*osition-*S*pecific *I*terative), which derives a position-specific scoring matrix that allows for detection of distant relationships between proteins. Consistent with previous reports, PSI-BLAST of the conserved BRCT and MYB domains of Rap1 revealed no related homologs in the Diptera order, suggesting that other proteins may have evolved to become functional analogs of Rap1 in flies.

6.2 The mechanism of HDR repression at telomeres

How mouse Rap1 represses HDR at telomeres when Ku70 is absent remains to be determined. The data in Chapter 3, showing that Rap1 when tethered to TRF1 fails to repress HDR, while negative, would suggest a requirement for Rap1/TRF2 complex formation in the inhibition of HDR. One possibility is that the complex might interact with a factor that represses HDR that Rap1 alone or TRF2 alone do not interact with. Two-hybrid and mass spectrometry have identified numerous protein complexes bound to Rap1 and/or TRF2 [21,78,225,264-266], but have not pinpointed a factor that could inhibit HDR. However, these experiments were not carried out in a setting where HDR is unleashed. Pull-down of TRF2/Rap1-associated proteins in $Rap1^{F/F}Ku70^{-/-}$ MEFs (where HDR is repressed), followed by elimination of factors that remain associated to TRF2 in a pull-down after Cre treatment (where HDR is induced), might nominate candidates for such HDR repressing factors.

Alternatively, experiments described in Chapter 3 and aforementioned studies [235,236] show that Rap1 can alter the DNA-binding activity of TRF2, but it is unclear whether this is relevant to HDR inhibition (see below, section 6.2.1). In addition, it is possible that Rap1, TRF2, and POT1a/b act together to repress HDR (see below, section 6.2.2).

6.2.1 *The effect of Rap1 on the DNA-binding activity of TRF2*

Our initial hypothesis was that Rap1 might promote binding of TRF2 to specific telomere structures that are reminiscent of substrates for HDR, such as the ds-ss transition at the telomere terminus. Doing so would presumably prevent loading of HDR factors, such as BRCA2 and Rad51, which are required for repair. Arat and Griffith [235] observed that Rap1/TRF2 binds better to a ds-ss telomere junction than a duplex telomere template. However, we, and Januskova et al. did not observe this difference. The conflicting results may be due to methods of protein purification and/or use of different substrates for the gel-shift assays. Preliminary gel-filtration chromatography revealed various oligomerization states within our purified proteins, which could affect their efficiency of DNA-binding. Therefore, careful characterization of DNA binding activities of TRF2 and Rap1/TRF2 to various telomere substrates needs to be conducted with homogenous protein populations. Additionally, these DNA-binding studies also need to be performed in the context of the entire shelterin complex, as POT1 binding to ssDNA may affect the binding affinity of Rap1/TRF2 to the ds-ss junction.

Insight into the mechanism of HDR repression by Rap1/TRF2 could also be acquired by performing a *d*isplacement *loop* (D-loop) assay. Here, in the presence of ATP (and Rad54 to stabilize filament formation and D-loops [267]), Rad51 polymerizes on a radiolabeled ssDNA probe, which contains complementary sequence to one strand of unlabeled supercoiled duplex DNA.

Strand invasion events where the ssDNA probe displaces one strand of duplex DNA can be detected by a shift in the migration of the ssDNA probe on an agarose gel [268]. To determine whether Rap1/TRF2 inhibits HDR by preventing strand invasion, the d-loop assay could be modified to use telomere-repeat sequences and compare the ability of TRF2 and Rap1/TRF2 to inhibit strand invasion.

6.2.2 *Rap1, TRF2 and POT1 may work together to repress HDR*

Data shown in Chapter 3 suggests that mouse Rap1/TRF2 and POT1a or –b may act together to inhibit HDR at telomeres. POT1a and -b were removed from telomeres in $Rap1^{F/F}Ku70^{-/-}$ MEFs by treatment with an shRNA targeting TPP1 (shTPP1). 10% of T-SCEs were observed on average when both POT1a/b were removed by shTPP1, or when Rap1 was deleted with Cre. No additive incidence of T-SCEs was detected when all three shelterin components (Rap1, POT1a and POT1b) were removed, suggesting they were epistatic in their repression of HDR. In contrast to these results, deletion of mouse TPP1, which phenocopies POT1a/b-deficiency, did not lead to induction of T-SCEs in a Ku70-deficient background (T. Kibe, unpubl.). Furthermore, deletion of TIN2, which also largely phenocopies POT1a/b-deletion, did not lead to induction of T-SCEs in the context of Ku70-deficiency (K. Takai, unpubl.).

One explanation to reconcile the results described above could be the time it takes for these MEFs to become immortalized. As discussed in Chapter 3,

$Ku70^{-/-}$ MEFs rapidly downregulate HDR at telomeres through an undefined mechanism. MEFs isolated from Ku-deficient embryos tend to have difficulty proliferating and immortalization times can vary significantly. Therefore, it is possible HDR was assessed too late in the TPP1/Ku70- and TIN2/Ku70-deficient MEFs. Isolation and immortalization of $Rap1^{F/F}Ku70^{-/-}$ and $TPP1^{F/F}Ku70^{-/-}$ MEFs in parallel would allow for a more accurate analysis of T-SCE frequencies. Alternatively, the TPP1sh could have off-target effects leading to the appearance of T-SCEs, which could easily be tested by treating $TPP1^{F/F}Ku70^{-/-}$ MEFs with the TPP1sh and assessing induction of T-SCEs.

The lack of T-SCEs in TPP1/Ku70- and TIN2/Ku70-deficient MEFs does not necessarily argue against the idea that POT1a/b may still act together with Rap1/TRF2 to repress T-SCEs. As discussed previously, POT1 can interact with TRF2 [21,152,185,234] and repression of HDR by POT1 may therefore be independent of its TIN2/TPP1-mediated recruitment to telomeres.

6.2.3 *What is the telomeric substrate for HDR?*

Detection of T-SCEs serve as our readout for HDR taking place at telomeres, however this assay does not report on the source of HDR initiation. Most of our studies have focused on the ds-ss telomere terminus as a structure vulnerable to HDR. Another source of telomeric HDR substrates could arise from replication errors. For instance, HDR is involved in restarting collapsed replication forks or bypassing a lesion encountered during replication (reviewed in [269]). Our

preliminary analysis of MEFs lacking TRF1 (required to facilitate telomere replication) and Ku80 showed an induction of T-SCEs, suggesting that telomeres are also vulnerable to HDR during DNA synthesis. Therefore numerous telomere configurations are likely to be vulnerable to HDR and further investigation into the mechanism of HDR, especially biochemical approaches, will need to take this into account.

6.2.4 *Ku70/80-deficient cells adapt to recover repression of HDR*

The downregulation of HDR at telomeres in late-passage $Ku70^{-/-}$ MEFs was an intriguing finding, supporting the notion that HDR is stringently regulated (reviewed in [270]), and warrants further investigation. First, it will be of interest to determine whether this down-regulation of HDR is global or telomere-specific. Assessment of global HDR using the DR-GFP assay designed in the Jasin lab [171,271] proved to be difficult due to the low rate of targeted genomic integrations in MEFs, as well as variable transfection efficiencies and cell survival post transfection. The DR-GFP reporter construct contains one copy of GFP that has been rendered dysfunctional (due to the insertion of an I-SceI site), and a donor partial GFP sequence. Induction of a DSB by transfection of the I-SceI endonuclease, and repair by HDR using the donor GFP template restores GFP expression. Optimal use of this assay involves integration of a single copy of the reporter into the *HPRT* locus to remove confounding effects from location of and multiple copy integration. Recent developments in genome editing using

CRISPR-Cas9 based technologies might now allow for efficient targeting of the DR-GFP construct into MEFs and determine global recombination levels in late-passage Ku70 deficient MEFs.

Secondly, identification of factors that perform this inhibition of HDR will be interesting as they may illuminate aspects of HDR regulation that are as yet unknown. A preliminary microarray to assess gene expression changes in early- and late-passage Ku70-deficient MEFs yielded a list of 64 significantly deregulated genes. Additional microarrays using multiple Ku70-deficient cell lines need to be performed to see if the same hits are generated. In addition, analysis of gene expression changes in early- and late-passage Ku-proficient cells will assist in eliminating candidate genes that are artifacts due to long-term tissue culture.

Lastly, the finding that Ku70-deficient MEFs down-regulate HDR in culture, raises the question of whether other processes adapting to Ku70-deficiency occur during embryogenesis. A notable difference between mouse and human Ku70/80 is that acute deletion of Ku70 or Ku80 in human somatic HCT116 cells results in lethality and massive telomere recombination [240,241,272], while mice lacking Ku70 or Ku80 are alive and fertile, albeit smaller and showing defects in DNA repair [113,273]. Development of conditional mouse knockouts of Ku components should be informative to investigate whether acute deletion of Ku from mouse somatic cells has similar effects as those reported in human cells.

6.3 Investigating the role(s) of human POT1

We describe the generation of conditional TALEN-mediated human knockouts of POT1-FL and double knockouts of POT1-FL/POT1-55. Due to a small percentage of cells that consistently escape Cre-mediated deletion of POT1-FL, the potential cellular lethality of human POT1 knockouts cannot be conclusively determined. Our current system provides a timeframe of 3-6 days within which to assess telomere phenotypes of POT1-deficiency, comparable to the approach undertaken for investigation of mouse POT1 proteins.

6.3.1 *Functions of POT1 in telomere end-protection*

Deletion of full-length human POT1 induces an ATR-dependent TIF response (~65%), similar to mouse cells lacking POT1a/b (~75%) [31,148]. Incomplete knockdown of human POT1 with shRNAs may explain the intermediate TIF response (~40%) observed in a previous study [184]. Alternatively, it is possible that the presence of POT1-55 in cells lacking POT1-FL contributes to the additional induction of TIFs. The rationale for this explanation is derived from phenotypes of the dominant-negative alleles of POT1a and –b that lack their first OB fold, akin to human POT1-55. Overexpression of POT1aΔOB or POT1bΔOB results in a moderate induction of TIFs (~25%), presumably by displacing endogenous POT1a/b [246]. No dominant-negative phenotype is observed prior to deletion of POT1-FL, likely due to the 10-fold lower expression of POT1-55 [184], placing it at a disadvantage to compete with POT1-FL for binding

to TPP1 and telomeric recruitment. Analysis of TIFs in the double knockout POT1-FL/POT1-55 will reveal whether POT1-55 acts as a dominant-negative in the absence of POT1-FL. It is not clear why telomeres are most vulnerable to DNA damage signaling during G1, when POT1 is depleted by shRNAs [184]. Given that 65% of cells lacking POT1-FL are TIF-positive, it is likely that TIFs persist through most of the cell cycle. However, cell-cycle analysis needs to be performed to confirm normal phase distribution.

Despite the telomere deprotection induced upon loss of POT1-FL, telomeres do not appear to succumb to NHEJ. NHEJ is also largely repressed at telomeres depleted for POT1 with siRNA or shRNA, which show a very low incidence of telomere fusions (~0.1%) [184,185]. However, 2% of chromosome fusions are detected in POT1a and –b knockout MEFs [31]. Taking into account the low frequency of chromosome fusions and the few experimental replicates analyzed, additional assessment is required to determine whether this difference is significant.

Deletion of human POT1-FL and mouse POT1 proteins leads to induction of telomere sister associations, where 8% and 1.4% [31] of telomeres engage in sister associations, respectively. The frequency of these events seem to vary between cell lines [159], as basal levels of telomere sister associations in the human and mouse cell lines prior to Cre infection are 4% and 0% [31], respectively. The telomere sister associations are not a result of NHEJ [156]. Instead, low frequencies of telomere sister associations occur in settings where ATR is

activated [159], and robust induction of this phenotype is observed when telomeres encounter replication problems [156]. Based on the low induction (2-fold) of telomere sister associations in cells lacking POT1-FL, we do not expect to observe a fragile telomere phenotype, but this remains to be confirmed. Telomere sister associations are likely due to non-covalent interactions, such as strand invasion, but the exact molecular basis of these events and their consequences for telomere integrity remain unknown.

6.3.2 *Telomere length regulation by POT1-55*

An interesting observation shown in Chapter 5 is the slight increase of telomere length in cells lacking POT1-FL, which is not detected upon loss of POT1-FL/POT1-55. A mutant allele of human POT1 that lacks its first OB fold (POT1ΔOB) [79] induces extreme telomere lengthening when overexpressed in HTC75 cells, presumably through a similar mechanism as described before, involving displacement of endogenous POT1 and loss of telomerase inhibition. Similar to POT1ΔOB, POT1-55 may be responsible for the lengthening of telomeres observed upon deletion of POT1-FL. However, depletion of POT1 with siRNA also resulted in telomere elongation [29], therefore it is unclear why a setting lacking both isoforms of human POT1 would not show telomere lengthening. Since the experiment has only been conducted once, it is possible that subsequent repetitions will show a telomere elongation phenotype. Additionally, if treatment of cells lacking POT1-FL or POT1-FL/POT1-55 with a telomerase

inhibitor abolishes the observed increase in telomere length, this would confirm that loss of POT1 allows telomerase access to telomeres.

The raison d'être of POT1-55 remains unclear. Low levels of POT1-55 protein suggest POT1-FL will most likely outcompete it for binding to TPP1 and residency at telomeres, although this has not been formally shown with endogenous proteins. Furthermore, the potential dominant negative action of POT1-55 in exposing telomeres to DNA damage signaling must be repressed. Conversely, POT1-55 may function to facilitate telomere elongation, which could be important in cell types that proliferate extensively, but it must also be carefully regulated such that it does not confer immortal properties to an oncogenic transformed cell.

6.3.3 *Generation of telomeric overhangs*

In stark contrast to the extended overhangs observed in POT1a/b double knockout MEFs, and the reduction in overhangs after partial knockdown of human POT1, no change in overhang length was observed upon deletion of POT1-FL or POT1-FL/POT1-55. In light of the role of mouse POT1a and –b in overhang protection [152,153] and maintenance [31,32,52,177], and the existence of an overhang phenotype in human POT1 knockdown studies [184,185], it is highly improbable that POT1-FL is not involved in telomere 3' overhang regulation. Instead, we favor the hypothesis that POT1 has a more complex, dual role in overhang generation, mediating both resection and fill-in synthesis.

The CST complex is required to generate telomeric 3' overhangs [51-53], is proposed to inhibit telomerase activity, and interacts with human POT1 [247,248]. It is tempting to speculate that human POT1, similar to mouse POT1b, recruits CST to telomeres to generate overhangs of appropriate length by fill-in synthesis. If POT1 is required for CST recruitment to telomeres, depleting CST components with shRNAs should have no effect on overhang length in cells lacking POT1-FL. However, if CST associates with telomeres in the absence of POT1, depletion of CST may result in increased overhangs, allowing us to distinguish between the two possibilities.

Telomere 3' overhang signal increases transiently in S/G2 [177,181] due to extensive resection by Exo1 [52]. While there is no evidence that POT1 and Exo1 interact, it would be of interest to determine the changes in overhang signal after shRNA depletion of Exo1 in POT-FL knockout cells. No change in overhang signal would suggest Exo1 recruitment or activity is promoted by POT1. If POT1 does not play a role in facilitating Exo1 action, we would expect to see a reduction in overhang signal. An alternate experiment to determine whether POT1 regulates Exo1 is to assess the transient increase in overhang length in S/G2, with the expectation of not detecting an increase if POT1 mediates Exo1 recruitment.

Based on studies in yeast [274,275], mammalian Exo1 is presumed to be recruited to DSBs after initial processing by the MRN complex, whereafter Exo1, in parallel with the BLM helicase, can extensively resect DSBs [125] [124]. Therefore,

it is possible that POT1 regulates a nuclease other than Exo1, or binds to as of yet undefined factors. However, the aforementioned experiments are likely to yield insights into the mechanism of overhang regulation by human POT1. Our observation of unchanged telomere overhangs upon loss of POT1 does not replicate the 30% decrease in overhang signal detected following treatment with an shRNA for POT1. A potential explanation of this discrepancy is that low levels of residual POT1 may be sufficient to recruit CST, but higher levels of POT1 are required to stimulate resection.

Other hypotheses, albeit less likely, include overhang extension by TERT, and RPA-mediated regulation. Loss of POT1 may allow telomerase to extend 3' overhangs, and fill-in synthesis could be mediated by CST, which can localize to telomeres independently of POT1 [51]. Steps upstream of ATR signaling may be involved in DNA overhang regulation. For instance, similar to its role in DNA repair, when POT1 is removed, perhaps RPA directs the 5' to 3' resection [276] at the telomere terminus and recruits Polα Primase [277] to perform the fill-in reaction.

6.3.4 *POT1 mutations - a compelling link between telomere dysfunction and disease*

Genomic sequencing studies in the past two years have identified 29 heterozygous POT1 mutations (and counting) in cases of Chronic Lymphocytic Leukemia and Familial Melanoma [250-253]. Majority of the mutations occur in the N-terminal regions of POT1, within the DNA-binding OB folds, and are predicted to

act as dominant-negative alleles. There are also several C-terminal mutations that may prove interesting to investigate, as they may illuminate as yet unknown functions or binding partners of POT1. Additionally, the C-terminus of POT1 contains the proposed interacting domains for CST and TPP1. Analysis of C-terminal patient mutations may reveal separation-of-function mutants that are defective in single aspects of POT1 function. Several N-terminal mutations in POT1 have been characterized. Aside from observations of chromosomal abnormalities, fragile telomeres, and telomere lengthening, exact mechanisms of pathogenesis remain to be elucidated. The TALEN-mediated conditional knockouts of human POT1 will provide a useful resource to identify the dysfunctional phenotypes encoded by these mutations.

Chapter 7: Materials and Methods

7.1 General procedures

7.1.1 *Mammalian cell culture*

MEFs were isolated from E13.5 embryos and maintained in DMEM supplemented with 1 mM sodium-pyruvate, 100 U/mL penicillin, 0.1 μg of streptomycin per ml, 0.2 mM L-glutamine, 0.1 mM nonessential amino acids, and 15% fetal bovine serum (FBS). Primary MEFs were immortalized by retroviral infection with pBabeSV40-LT (gift from Greg Hannon).

HCT116, HT1080, ARPE-19, and HeLa1.3 cells were grown in Dulbecco modified Eagle medium (DMEM) supplemented with L-glutamine, penicillin-streptomycin, nonessential amino acids and 15% bovine calf serum (BCS, HyClone). SV40-large T transformed (neo resistant) BJ fibroblasts were cultured in complete DMEM containing 199 medium (4:1) and 10% BCS.

7.1.2 *Retroviral gene delivery*

For infection of mouse cells, 24 h prior to transfection, $5x10^6$ Phoenix ecotropic packaging cells were plated in 10 cm dishes. Phoenix cells were transfected with 20 μg of the appropriate plasmid by calcium phosphate precipitation. Media was changed 6-8 h after transfection. 36 h after transfection, media containing virus was collected, and filtered through 0.45 μM filter. Polybrene was added to a final concentration of 4 μg/mL. MEFs that had been plated 12-24 h earlier in 10 cm dishes and were ~40% confluent were infected. 3

infections were performed at 12 h intervals. Time zero was set at 12h after first infection. Infected cells were then selected for with the appropriate antibiotic (puromycin 2μg/mL, hygromycin 90μg/mL). Selection was deemed complete when uninfected control cells all died in the presence of antibiotic.

For human cells, the above protocol was used with the following modifications. Phoenix amphotropic packaging cells were used to produce virus. Human cells were infected 3 times at 4 h intervals. Time zero was set at 12 h after first infection. Puromycin was used at 750 ng/mL, hygormycin was used at 135 μg/mL.

For infection with Cre recombinase, a Sloan Kettering facility produced virus from retroviruses pMMP Hit&Run Cre and pWZL Cre. The viruses were used to infect cells as described above. Selection with hygromycin followed infection with pWZL Cre. No selection was performed after treatment with Hit&Run Cre.

For the tamoxifen-inducible Cre-ERT2 system, 500nM of 4-OHT was added to cells. Media was changed 6 h later and that was deemed time zero.

7.1.3 *Growth curves*

Growth curves were presented as population doublings over time and were calculated by the following formula: original PD + (ln(# cells counted/# cells seeded)/ln(2)).

7.1.4 *Immunoblotting (IB)*

Immunoblotting was performed as previously described [22]. Briefly, cells were harvested by trypsinization, resuspended in Laemmli buffer (100mM Tris-HCl pH 6.8, 200 mM DTT, 3% SDS, 20% glycerol, 0.05% bromophenol blue) at 10,000 cells per μl, denatured for 5 min at 95°C, sheared with an insulin needle, and resolved on SDS/PAGE gels using 100,000 cells per lane. Blots were blocked in 5% non-fat dry milk/PBS + 0.1% Tween20.

7.1.5 *Coimmunoprecipitation (Co-IP) from transfected 293T cells*

2 x 10^6 293T cells were plated 24 h before co-transfection with calcium phosphate co-precipitation using 10 μg each of FLAG-tagged and MYC-tagged constructs. Cells were harvested at 36 h after transfection, washed once with PBS, and lysed on ice for 10 min in a high salt buffer (50 mM Tris-HCl pH 7.2, 400 mM NaCl, 1% Triton X-100, 0.1% SDS, 1 mM EDTA, 1 mM DTT, 1 mM PMSF and cocktail of protease inhibitors). Salt concentration was brought down to 200 mM by addition of ice-cold water (drop-wise while mixing) and lysates were spun at 4°C at 14,000 rpm for 10 min. Supernatants were used in immunoprecipitations. 5% of the supernatant was saved as 'input' for western blot analysis and the remaining supernatant was pre-cleared with preblocked (10% BSA in PBS overnight) protein G-Sepharose beads for 1 h at 4°C. Lysates were incubated overnight at 4°C with a 40 μl slurry of Sepharose beads conjugated to 9E10-Myc or M2-FLAG mouse monoclonal antibody. Beads were

washed 5 times with ice-cold PBS. Proteins were eluted by boiling for 5 min in Laemmli buffer and analyzed by SDS-PAGE and immunoblotting.

7.1.6 *Immunofluorescence-fluorescence in situ hybridization (IF-FISH)*

IF-FISH was conducted as previously described [278]. Briefly, cells grown on coverslips were fixed for 10 min in 2% paraformaldehyde/3% sucrose at room temperature, followed by three 5 min PBS washes. Coverslips were incubated in blocking solution (1 mg/ml BSA, 3% goat serum, 0.1% TritonX-100, 1 mM EDTA in PBS) for 30 min, followed by incubation with primary antibodies diluted in blocking solution for 1 h at rt. Cells were washed three times for 5 min with PBS and then incubated with secondary antibodies diluted in blocking solution for 30 min at rt. Antibodies used were as listed at the end of this chapter. Coverslips were dehydrated with 70%, 95% and 100% ethanol and allowed to dry. Hybridizing solution (70% formamide, 0.5% blocking reagent from Roche, 10 mM Tris-HCl pH 7.2 and FITC-OO-(CCCTAA)3 or TAMRA-OO-$[TTAGGG]_3$ PNA probe from Applied Biosystems) was added to each coverslip and denatured at 80ºC for 5 min, followed by a 2 h incubation at rt. Two 15-min washes in 70% formamide/10 mM Tris-HCl pH 7.2 and three 5-min washes with PBS were performed. DNA was stained with DAPI in the PBS washes and coverslips were mounted using antifade reagent ProLong Gold from Life Technologies. Images were captured using a Zeiss AxioPlan II microscope with a Hamamatsu C4742-

95 camera using Volocity software from Perkin Elmer. For distance of telomeres from nuclear membrane, calculations were made using Image J software.

7.1.7 *Telomeric FISH and chromosome orientation-FISH (CO-FISH)*

Telomeric FISH and CO-FISH were conducted as previously described [119,154]. Briefly, colcemid was added to cells 2 hours prior to harvest. Cells were collected by trypsinization, swollen in 0.075 M KCl and fixed overnight at 4ºC in methanol:acetic acid (3:1). Metaphase spreads were dropped on glass slides and aged overnight. Slides were hybridized with FITC-OO-$[CCCTAA]_3$ or TAMRA-OO-$[TTAGGG]_3$ PNA probe in hybridizing solution, denatured at 80ºC for 5 min and incubated for 2 h at rt. Two 15-min washes in 70% formamide/10 mM Tris-HCl pH 7.2 and three 5 min washes with 0.1 M Tris-HCl pH 7.2/0.15 M NaCl/0.08% Tween20 were performed. DAPI was added to last wash for DNA stain. Slides were dehydrated in 70%, 95%, and 100% ethanol and mounted using ProLong Gold antifade from Life Technologies. Images were captured using a Zeiss AxioPlan II microscope with a Hamamatsu C4742-95 camera using Volocity software from Perkin Elmer. For CO-FISH, BrdU:BrdC (3:1) was added 14 h prior to harvest. Harvesting and metaphase conditions were as described for FISH. Slides were treated with 0.5 mg/ml RNase A diluted in PBS, stained with 0.5 μg/ml Hoechst 33258, exposed to 5400J/m^2 of UV light and subsequently digested with 800 U of Exonuclease III from Promega for 10 min at room temperature. Slides were rinsed with PBS, dehydrated with 70%, 95% and 100%

ethanol and sequentially hybridized with TAMRA-OO-$[TTAGGG]_3$ and FITC-OO-$[CCCTAA]_3$ for 2 h each at rt, without denaturation. Washing, mounting and capture conditions were as described for FISH.

7.1.8 *Chromatin immunoprecipitation (ChIP)*

ChIP was performed as previously described [79]. Briefly, cells were fixed 1% paraformaldehyde/culture medium for 45 min at room temperature. Glycine was added to 0.2 M to stop the cross-linking. Cells were pelleted by centrifugation and washed with ice-cold PBS, followed by a final wash in PBS/1 mM PMSF. The cells were resuspended in cell lysis buffer (5 mM PIPES (pH 8.0), 85 mM KCl, 0.5% Nonidet P-40, 1 mM PMSF, protease inhibitor cocktail from Roche), incubated on ice for 15 min and sonicated for 10 min (30 sec on/30 sec off) in a water-bath sonicator. Supernatants of lysates were incubated with the appropriate antibody at 4 °C overnight and then for 45 min with ChIP-grade protein G magnetic beads (Dynal, Invitrogen). Immunoprecipitated DNA was washed, eluted from the beads, and precipitated with ethanol after reversal of the cross-links and Proteinase K treatment. The DNA samples were dissolved in water, boiled and loaded on dot blots, and hybridized with an 800-bp probe labeled with Klenow and a primer for the C-rich telomeric repeat strand. Signal intensity measured by ImageQuant software was normalized to the signals of the input DNA on the same blot.

7.1.9 *Genomic blotting, telomere length and telomere overhang analysis*

Cells were harvested by trypsinization, washed with PBS, and either pelleted and frozen at -80ºC (for telomere length analysis) or processed immediately (for genotyping and telomere overhang analysis) for genomic DNA collection. Genomic DNA was extracted as previously described [4]. DNA for genotyping was digested with appropriate enzymes, quantitated by fluorometry using Hoechst 33258 and 10 μg was loaded on a 0.7% agarose gel run in 0.5X TBE. DNA for telomere overhang and length analysis was digested with *Mbo*I and *Alu*I, quantified using Hoechst, and 1 μg was run on 0.7% agarose gels in 0.5X TBE.

For genomic blots used for genotyping and telomere length analysis, the gels were depurinated with 0.5N HCl, denatured and neutralized using standard Southern blotting procedures and transferred as previously described [4]. For genotyping, probes (indicated in figures) were Klenow-labeled using random primers and α-^{32}P-dCTP. For telomere length analysis, a Sty11 probe with ~800 bp of telomeric repeats [279] was Klenow-labeled with the TelC [CCCTAA]4 oligo and α-^{32}P-dCTP. Membranes were exposed to PhosphorImager screens and quantified with ImageQuant software.

For telomere overhang analysis, gels were dried and probed with a [CCCTAA]4 end-labeled with Polynucleotide kinase and γ-^{32}P-ATP as previously described [280]. The gel was washed at 55°C three times for 30 min each in 4xSSC, once for 30 min in 4x SSC/0.1% SDS, and exposed to a PhosphoImager

screen overnight. After the image was captured, the gel was denatured in 0.5 M NaOH, 1.5 M NaCl for 30 min, neutralized with two 15 min washes in 0.5 M Tris-HCl pH 7.5, 3 M NaCl, and hybridized overnight with the same probe at 55°C. The gel was washed and exposed as above. The ss G-rich overhang signal in the native gel was quantified with ImageQuant software and normalized to the total telomeric DNA quantified after the gel had been denatured and rehybridized with the telomeric probe.

For telomere overhang analysis of mouse genomic DNA, $1x10^6$ cells were resuspended in PBS and mixed 1:1 (v/v) with 2% agarose (SeaKem) in PBS and set in plug molds (BioRad). Plugs were digested overnight with Proteinase K buffer (10mM Tris-HCl pH 8.0, 250mM EDTA, 0.2% sodium deoxycholate, 1% sodium lauryl sarcosine), washed four times for 1 hr each with TE, with 1 mM PMSF in the last wash. Plugs were washed once more with H2O and digestion buffer. Plugs were incubated overnight at 37°C with 60 U MboI. The following day, the plugs were washed once in TE, and once in 0.5xTBE, and loaded onto a 1% agarose/0.5xTBE gel. Samples were run for 24 hours on a CHEF-DRII PFGE apparatus (BioRad) in 0.5xTBE. The settings were as follows: initial pulse, 5 s; final pulse, 5 s; 6 V/cm; 14°C. Gels were dried and the same protocol outlined above was followed for hybridization, detection of signal, and quantification.

7.1.10 *Northern analysis for TERRA*

Total RNA was prepared using RNeasy Mini Spin columns (QIAGEN) according to the manufacturer's instructions and northern blot analysis was performed as previously described [281]. Briefly, 20μg of RNA was loaded onto 1.2% formaldehyde agarose gels and separated by gel electrophoresis. RNA was transferred to a Hybond-N+ membrane and crosslinked in a UV Stratalinker. The blot was prehybridized in Church mix at 55°C for 1 hour, followed by overnight hybridization with a Sty11 probe [279]. The blot was washed 3 times for 15 minutes at 55°C with Church wash and then exposed to a Phosphorimager screen for 5 days. Screens were scanned using ImageQuant software and quantified in Image J using the ethidium bromide stained 18S RNA as a loading control for normalization.

7.1.11 *Microarray analysis*

Total RNA was isolated from cell lines using RNeasy Mini spin columns (QIAGEN) with DNase digestion, according to the manufacturer's instructions. Microarray hybridization and scanning were performed at the Genomics core facility at Rockefeller University, using Whole Human Genome DNA microarrays (Illumina HumanHT-12 v4). The data was analyzed using GeneSpring v12.6. Normalization was performed using quantiles and data was filtered to remove absent genes using flag calls.

Experiments for HT1080 and HCT116 cell lines were performed in replicate, using two independent isolations of RNA. Differentially expressed genes were identified after performing moderated T-Tests and applying the Benjamini-Hochberg False Discovery Rate method. A further fold change of 3 or 2.75 was applied to the HT1080 and HCT116 clones respectively to identify genes that were highly transcriptionally deregulated due to the absence of Rap1. Microarrays for ARPE-19 were not performed in replicate and therefore an extremely stringent fold change threshold was applied to remove false negatives and identify differentially expressed genes, which were subsequently validated by qRT-PCR.

7.1.12 *Quantitative reverse transcription-polymerase chain reaction (qRT-PCR)*

For qRT-PCR, cDNA was prepared from 1μg of total RNA by using Thermoscript Reverse Transcriptase (Invitrogen). Quantitative PCR reactions were performed using Life Technologies SYBR Green Master Mix on an Applied Biosystems 7900HT Sequence Detection System. Differences between samples calculated using QuantStudio software (Applied Biosystems) using the ΔCT method and were normalized to GAPDH.

For human Rap1, two independent isolations of RNA and reverse transcriptase reactions were conducted and the experiment was repeated six times for clones 23, 25, 30 and the parental cell line. The experiment for clone 26 was conducted in triplicate. For human POT1, qRT-PCR was conducted in

triplicate. Data was pooled to derive the mean averages and standard deviations. Significance was calculated using a two-tailed unpaired T-Test. Primers used are listed at the end of this chapter.

7.1.13 *Nickel-affinity purification of His-tagged proteins*

Human shelterin proteins were produced in baculovirus prior to this work[20]. Sf9 insect cells were infected with baculovirus expressing shelterin components for two days and purified as previously described [22]. Briefly, infected cells were harvested and lysed in 5 ml of cold lysis buffer (50 mM Tris, pH 7.4, 150 mM NaCl, 1% Triton X-100, 5 mM β-mercaptoethanol supplemented with Roche Applied Science protease inhibitor mixture) per 100 ml of cell culture. All subsequent steps were done at 4 °C. After incubation on ice for 10 min, the mixture was sonicated and cleared by centrifugation at 13,200 rpm for 20 min. His tagged proteins were isolated using chelating Sepharose fast flow (GE Healthcare) nickel resin. Proteins were bound to the resin, washed and eluted with 1 M Imidazole. Protein yield and purity was quantified on SDS-PAGE gels against a BSA standard.

7.1.14 *Electrophoretic Mobility Shift Assays (EMSA)*

Binding reactions were conducted as previously described [20]. Briefly, of EMSAs were conducted in in 4% Glycerol, 0.5 μg*E. Coli* DNA, 20 mM Glycine-KOH [pH 9.0], 10 mM DTT, and 50 ng β-casein per 20 μl. Reaction with probe

and protein were incubated at 4° C for 30 min and run on a 0.6% agarose gel in 0.1 × TBE at 4° C. Gels were dried onto DE81 paper and analyzed by autoradiography or by exposure on a Phosphorimager. DNA probes were prepared as described previously [11]. In brief, the HindIII/Asp718 fragment containing $(TTAGGG)_{12}$ repeats was purified from pTH12 [11] and filled in with [α-^{32}P]dCTP and Klenow enzyme. Other probes used in this study were generated by annealing oligos (sequence is section 7.2), digesting with Asp718 and filling in with [α-^{32}P]dCTP and Klenow. Dissociation constants were calculated using SigmaPlot by graphing % of bound probe against protein concentration.

7.1.15 *Genotyping and sequencing*

PCR was performed in 25 μl containing 50 ng of DNA, 0.2 μM of each primer, 0.1 μM dNTPs, 1.5 mM $MgCl_2$, 50 mM KCl, 10 mM Tris-HCl pH 8.0, and 0.5 U of TaKaRa Taq polymerase. Conditions were as follows: 95°C for 4 min, 25 cycles of 95°C for 30 sec, 60°C for 30 sec, 72°C for 45 sec and final extension at 72°C for 5 min.

Sequencing of heterozygous clones to identify mutations was conducted by PCR-amplifying the remaining 'WT' allele. PCR products were eluted from agarose gels and sequenced. For sequencing of homozygous 'WT' clones, eluted PCR products were cloned by TA cloning (Life Technologies). A minimum of 8 resulting TA clones per cell line were sequenced to identify mutations in both alleles.

7.1.16 *Gene targeting and cell cloning*

All cell lines were transfected in 10 cm dishes at a density of $3x10^6$ cells using Lipofectamine 2000 (Life Technologies) with 4 μg of each TALEN construct and 20 μg of the appropriate donor construct. 48 hours after transfection, all cell lines, except for HeLa1.3, were plated in selection medium in 10 cm plates at varying densities ranging from 3,900 to 500,000 cells (using two-fold dilutions). HeLa1.3 cells were plated in 10 cm dishes using two-fold dilutions starting from 8000 cells down to 75 cells. G418 was used at 1 mg/ml to select neomycin-resistant HCT116 cells, at 900 μg/ml for HT1080 cells, and at 800 μg/ml for ARPE-19 cells. Blasticidin was used at 5 μg/ml for HT1080 and HeLa1.3 selection, and at 2.5 μg/ml for SV40LT BJ selection. Zeocin was used at 100μg/ml for HT1080 cells.

For Rap1 targeting, clones emerged at a frequency of approximately 1 clone per 500 plated HCT116 cells, 1 clone per 2,600 plated HT1080 cells, 1 clone per 7,800 plated ARPE-19 cells, 1 clone per 125 plated HeLa1.3 cells, and 1 clone per 62,500 plated SV40LT BJ cells. The media was not changed after initial plating.

For POT1 targeting, clones emerged at a frequency of approximately 1 clone per 3000 plated HT1080 cells in neomycin selection, 1 clone per 4000 plated HT1080 cells in zeocin selection, and 1 clone per 15 plated HT1080 cells in blasticidin selection. 75% of HT1080 clones picked after blasticidin selection died after continuous culturing in blasticidin.

Clones were picked 12 days later for all cell lines except the SV40LT BJ clones, which were picked 3 weeks after plating. Approximately 60-70 clones were picked for each cell line using cloning cylinders from plates that contained well-spaced clones and the cells were transferred into 24 well plates. After reaching confluence, half of the cells in each well were harvested to extract genomic DNA, while the remaining cells were expanded into 6 well plates. Approximately 30-40 clones were screened per cell line.

7.2 Mouse and human TERF2IP targeting

7.2.1 *Mouse TERF2IP targeting (by Agnel Sfeir)*

The *Rap1* targeting vector was generated by cloning restriction fragments from a BAC clone into the pSL301 vector (Invitrogen). A neomycin cassette flanked by 2 FRT sites and containing a LoxP site was inserted into a *CspC*I site in the first intron. A second LoxP site, together with an *Nde*I site was introduced by inserting an oligonucleotide into a *BsmB*I site within the second intron. The vector was linearized with *Not*I and gene targeting of C57BL/6J ES cells was performed using standard techniques. ES cell clones with the correct integration were identified by southern blots of *Nde*I digested DNA using a 350-bp probe downstream of exon 3 outside the targeting vector. A correctly targeted ES clone was injected into C57BL/6J blastocyst to generate chimeric male founders. Crossing the chimeras to albino C57BL/6J females delivered offspring with the

Rap1$^{F/+}$ genotype. Rap1 targeted mice were maintained in a C57BL/6J background. The neomycin cassette was deleted by crossing the mice to the FLPe-deleter mouse strain (Jackson Labs). The Rap1$^{\Delta ex2}$ allele was generated by crossing the Rap1$^{F/+}$ to the E2a-Cre deleter strain (Jackson Labs). Rap1$^{F/F}$ mice were crossed with Ku70$^{-/+}$ mice (obtained from F. Alt, Harvard Medical School, Boston MA).

7.2.2 *TALENs and the TERF2IP targeting construct*

The heterodimeric TALEN pair for *TERF2IP* targeting was constructed using the following RVD sequences. LEFT2: 5'-HD-NG-NN-NG-NN-HD-NG-NN-NG-NG-HD-NG-NG-HD-NG-HD-NG, RIGHT1: 5'-HD-NG-NN-NN-NI-NN-NG-NG-HD-NG-HD-NG-NG-NI-NG-NG-3'. TALENs were constructed by Dirk Hockemeyer. The PGK Neomycin cassette from the PL451 vector (NCI) was liberated using restriction enzymes *Nhe*I (5') and *Bst*BI (3') and ligated into *Nhe*I- and *Bst*BI- digested pSL301 (cloning vector from Invitrogen). The pEF Blasticidin cassette from plasmid pEF/Bsd (Life Technologies) was released using *Nhe*I (5') and *Eco*RI (3') and ligated into *Nhe*I- and *Eco*RI- digested pSL301. The 5' and 3' homology arms were PCR-amplified with restriction site overhangs from genomic SV40LT BJ fibroblast DNA. Primers for PCR of the 5' arm were as follows: 5'-ATGCGGTACCTTGCCCAAACTCCTGTCTTCTTAGGGC-3' and 5'-GCATGCTAGCAGAGAAGAACAGCACAGATTAGCAATAGCC-3'. Primers for PCR of the 3' arm were 5'-

ATGCTTCGAACTAGATTTACTCATTATTTTTTTCCCTACC-3' and 5'-GCATTTCGAACCTGTAATCCCAGCACTTTGGGAG-3'. The resulting 600 bp 5' homology arm ends 7 bp from the intron 1/exon 2 junction and has *Kpn*I and *Nhe*I sites on the 5' and 3' ends, respectively. The resulting 578 bp 3' homology arm starts 32 bp from the exon 2/intron 2 junction and has *Bst*BI restriction sites at both ends. The homology arms were cloned into the relevant restriction sites in pSL301 containing either the PGK Neomycin or pEF Blasticidin. The 3' homology arm insertion was screened for orientation and the donor constructs were sequenced using the following primers: T7, T3, 5'-GCTCGCGTCGTGCAGGACGT-3' (PGK internal primer), and 5'-GCTGTGCTCGACGTTGTCAC-3' (Neomycin internal primer).

7.3 POT1 gene targeting

7.3.1 *TALENs and the POT1 targeting construct*

The heterodimeric TALEN pair for *POT1* targeting was constructed using the following RVD sequences. LEFT: 5'-NI-NI-NI-NI-NG-NI-NG-NG-NN-NI-NI-NI-NN-NG-HD-NI-NN-3', RIGHT: 5'-NN-NI-NN-HD-NI-NI-NG-NI-NI-NG-HD-NG-NN-NN-NI-3'. TALENs were constructed by Siobhan Gregg, Supawat Thongtip and Shaheen Kabir using the FLASH assembly system **(REYON REF)**. The PGK Neomycin cassette from the PL451 vector (NCI) was liberated using restriction enzymes *Nhe*I (5') and *Bam*HI (3') and ligated into *Nhe*I- and *Bam*HI- digested

pSL301 (cloning vector from Invitrogen). The SV40 Zeocin cassette from pSV40/Zeo2 (Invitrogen) was liberated using restriction enzymes *Nhe*I (5') and *Bam*HI (3') and ligated into *Nhe*I- and *Bam*HI- digested pSL301. The pEF Blasticidin cassette from plasmid pEF/Bsd (Life Technologies) was released using *Nhe*I (5') and *Bam*HI (3') was liberated using restriction enzymes *Nhe*I (5') and *Bam*HI (3') and ligated into *Nhe*I- and *Bam*HI- digested pSL301. The pEF promoter of the blasticidin cassette was replaced with a PGK promoter by cloning it out of PL451 by NheI/XbaI digest and cloning it into NheI-digested pEF blasticidin. The STOP cassette was digested out of Lox-Stop-Lox TOPO (available from Addgene, Tyler Jacks lab) with BamHI and EcoRI and cloned into the relevant sites of the neomycin, blasticidin and zeocin donor constructs. The 5' and 3' homology arms were PCR-amplified with restriction site overhangs from genomic HT1080 DNA. Primers for PCR of the 5' arm were as follows: 5'-CTACCACCAGTGTTTGAAGTTATCG-3' and 5'-AATATTTTACCTGACTTTCAATATTTTAAAGC-3'. Primers for PCR of the 3' arm were 5'- CTCTGTATTGTTCACTGAAACTAGTTAGCAC-3' and 5'-CCAGAAGTGCATTGAACAAAAAAGCTC-3'. The resulting 647 bp 5' homology arm ends 14 bp from the intron 2/exon 3 junction and has *Xho*I and *Nhe*I sites on the 5' and 3' ends, respectively. The resulting 649 bp 3' homology arm starts 43 bp from the exon 3/intron 3 junction and has *EcoR*I restriction 5' and a blunt 3' end. The homology arms were cloned into the relevant restriction sites in pSL301 containing either the PGK Neomycin or pGK Blasticidin or pSV40 Zeocin.

7.4 List of primers

7.4.1 *Genotyping*

Mouse Rap1 primers:

F1: 5'-CATGCACTTGTACACATACAA-3';

F2: 5'-GCTTCTTCCACCAAAACTGC-3';

R: 5'-TTTGACAGTTGATAGGAAATGAAC-3'

Human Rap1 primers:

F1: 5'- GTGGATTGTGGTACGT GGCCCAGATCTGCC-3';

R1: 5'-TAACATACCACAACCTCCTCAAACTCCCGG-3';

POT1 primers:

F1: 5'-GTGTACTTCAGAACCATGTATAGCACACC-3'

R1: 5'-GGGCTTCATAGTTTCCACTAAAGAGCAGGC-3'

PGK internal primer:

R2: 5'-CATCTGCACGAGACTAGTGAGACGTGCTAC-3'

Zeocin internal primer:

R4: 5’-GAGCACCGGAACGGCACTGGTCAACT-3’

7.4.2 *RT-PCR*

Human GAPDH (published in [282])

5’-TGCACCACCAACTGCTTAGC-3’

5’-GGCATGGACTGTGGTCATGAG-3’

Human CDO1

5’-CGCCAAGTTCGACCAGTACAGG-3’

5’-GGTATGATCATGAATACTGCTGCC-3’

Human LHX2

5’-GGACGGTAGCATCTACTGCAAGG-3’

5’-CCAAGTCCCGAGCGCGCATCACC-3’

Human LRRC17

5’-CAAGCCTGAGGTGGACTCAACT-3’

5’-CTGGAGGGATGTTGTTTGGCAC-3’

POT1 coding exon 2 (anneals to both isoforms)

5’-CACCCCTGAATCAACTTAAGGGTGG-3’

POT1 coding exon 3 (anneals only to POT1-FL)

5’-CTGGTCCACAATAGTTACAACTGAGC-3’

POT1 coding exon 2-4 junction (anneals only to POT1-55)

5’-TATACTTGAATCAGTTCCTTTGC-3’

POT1 coding exon 4 (anneals to both isoforms)

5’-GCTCCGTCCACTTCTGCTTTGCCCA-3’

POT1 coding exon 9 (anneals to both isoforms)

5’-CAGACTGAAATAGTCTTCTGGGC-3’

POT1 coding exon 13 (anneals to both isoforms)

5’-CCATGAGATAGGCTTCTAGTACTCC-3’

POT1 coding exon 15 (anneals to both isoforms)

5’-CATCTTCTGCAACTGTGGTGTC-3’

7.4.3 *EMSA probes*

Junction probe

5’-ATGCGGTACCGGATGTCACTCAGCAGACGGTTAGGGTTAGGGTTAGGG
CACTAGTTAGGGTTAG-3’

5’-CTAGTGCCCTAACCCTAACCCTAACCGTCTGCTGAGTGACATCCGGTACC
GCAT-3’

[TTAGGG]3-repeat probe

5’-ATGCGGTACCGGATGTCACTCAGCAGACGGTTAGGGTTAGGGTTAG-3’

5’-CTAACCCTAACCCTAACCGTCTGCTGAGTGACATCCGGTACCGCAT-3’

7.5 List of shRNAs

Mouse TPP1:

Target sequence 5’-GGACACATGGGCTGACGGA-3’

Mouse Rap1:

sh1 target sequence 5’- ACAGGCAATGCCTTGTGGAAA -3’

sh2 target sequence 5’-CTTCATCTCCA CGCAGTACAT-3’

7.6 List of antibodies

Antigen	ID	Source	Uses
hRap1	765	de Lange lab	ChIP, IB
hTRF2	647	de Lange lab	ChIP
hTRF1	371	de Lange lab	ChIP
hTIN2	864	de Lange lab	ChIP
POT1	ab124784	Abcam	IB, ChIP
hTPP1	1151	de Lange lab	ChIP
mRap1	1252	de Lange lab	IB, IF, ChIP
mTRF2	1254	de Lange lab	IB, ChIP
mTRF1	1449	de Lange lab	IB, ChIP
mTIN2	1447	de Lange lab	IF, ChIP
POT1a	1221	de Lange lab	IB, ChIP
POT1b	1223	de Lange lab	IB, ChIP
MYC	9E10	Calbiochem	IB, IP
MYC	9B11	Cell signaling	IF, ChIP
FLAG	M2	Sigma	IB, IP, IF
53BP1	100-304	Novus	IF

Lamin A	L1293	Sigma	IF
Alpha-tubulin	T9026	Sigma	IB
Chk2	611570	BD Transduction	IB
Chk1-P	Ser345	Cell Signaling	IB
Chk1	Sc-8408	Santa Cruz	IB
H3K9me1	ab9045	Abcam	ChIP
H3K9me2	ab1220	Abcam	ChIP
H3K9me3	ab8898	Abcam	ChIP
HP1alpha	ab77256	Abcam	ChIP
HP1beta	ab10478	Abcam	ChIP
HP1gamma	ab10480	Abcam	ChIP
Acetyl Histone H4	06-598	Millipore	ChIP

7.7 List of cell lines

Cell Line	Organism, Organ	Notes
TRF2$^{F/-}$ p53$^{-/-}$	Mouse, E13.5 MEFs	[24]
TRF2$^{F/F}$ Ku70$^{-/-}$	Mouse, E13.5 MEFs	[154]
Rap1$^{F/F}$	Mouse, E13.5 MEFs	This work
Rap1$^{\Delta ex2/\ \Delta ex2}$	Mouse, E13.5 MEFs	This work, Agnel Sfeir
Rap1$^{F/F}$ Ku70$^{-/-}$	Mouse, E13.5 MEFs	This work
Rap1$^{F/F}$ Ku70$^{+/-}$	Mouse, E13.5 MEFs	This work
Rap1$^{F/\Delta ex2}$ Ku70$^{-/-}$	Mouse, E13.5 MEFs	This work
TRF1$^{F/F}$ Cre-ERT2	Mouse, E13.5 MEFs	Agnel Sfeir
HT1080	Human, Fibrosarcoma	ATCC
HCT116	Human, Colorectal carcinoma	ATCC
ARPE-19	Human, Retinal pigment epithelial	ATCC
BJ	Human, foreskin	ATCC
HeLa1.3	Human, Cervical adeoncarcinoma	[22]
Phoenix ecotropic	Human, Epithelial	
Phoenix amphotropic	Human, Epithelial	
293T	Human, Kidney	

Chapter 8: References

1. Muller, H. J. The remaking of chromosomes. *The Collecting Net, Woods Hole* **8**, 182-195 (1938).
2. McClintock, B. The stability of broken ends of chromosomes in Zea mays. *Genetics* **26**, 234-282 (1941).
3. Shampay, J., Szostak, J. W. & Blackburn, E. H. DNA sequences of telomeres maintained in yeast. *Nature* **310**, 154-157 (1984).
4. de Lange, T. et al. Structure and variability of human chromosome ends. *Mol Cell Biol* **10**, 518-527 (1990).
5. Lejnine, S., Makarov, V. L. & Langmore, J. P. Conserved nucleoprotein structure at the ends of vertebrate and invertebrate chromosomes. *Proc Natl Acad Sci USA* **92**, 2393-2397 (1995).
6. Gomes, N. M. et al. Comparative biology of mammalian telomeres: hypotheses on ancestral states and the roles of telomeres in longevity determination. *Aging Cell* **10**, 761-768 (2011).
7. Moyzis, R. K. et al. A highly conserved repetitive DNA sequence, (TTAGGG)n, present at the telomeres of human chromosomes. *Proc Natl Acad Sci USA* **85**, 6622-6626 (1988).
8. Brown, W. R. Molecular cloning of human telomeres in yeast. *Nature* **338**, 774-776 (1989).
9. Cross, S. H., Allshire, R. C., McKay, S. J., McGill, N. I. & Cooke, H. J. Cloning of human telomeres by complementation in yeast. *Nature* **338**, 771-774 (1989).
10. Palm, W. & de Lange, T. How shelterin protects mammalian telomeres. *Annu Rev Genet* **42**, 301-334 (2008).
11. Zhong, Z., Shiue, L., Kaplan, S. & de Lange, T. A mammalian factor that binds telomeric TTAGGG repeats in vitro. *Mol Cell Biol* **12**, 4834-4843 (1992).
12. Chong, L. et al. A human telomeric protein. *Science* **270**, 1663-1667 (1995).
13. Bilaud, T. et al. Telomeric localization of TRF2, a novel human telobox protein. *Nat Genet* **17**, 236-239 (1997).

14. Broccoli, D. et al. Comparison of the human and mouse genes encoding the telomeric protein, TRF1: chromosomal localization, expression and conserved protein domains. *Hum Mol Genet* **6**, 69-76 (1997).
15. Bianchi, A., Smith, S., Chong, L., Elias, P. & de Lange, T. TRF1 is a dimer and bends telomeric DNA. *Embo J* **16**, 1785-1794 (1997).
16. Broccoli, D., Smogorzewska, A., Chong, L. & de Lange, T. Human telomeres contain two distinct Myb-related proteins, TRF1 and TRF2. *Nat Genet* **17**, 231-235 (1997).
17. Bianchi, A. et al. TRF1 binds a bipartite telomeric site with extreme spatial flexibility. *Embo J* **18**, 5735-5744 (1999).
18. Chen, Y. et al. A conserved motif within RAP1 has diversified roles in telomere protection and regulation in different organisms. *Nat Struct Mol Biol* **18**, 213-221 (2011).
19. Sfeir, A., Kabir, S., van Overbeek, M., Celli, G. B. & de Lange, T. Loss of Rap1 induces telomere recombination in the absence of NHEJ or a DNA damage signal. *Science* **327**, 1657-1661 (2010).
20. Li, B., Oestreich, S. & de Lange, T. Identification of human Rap1: implications for telomere evolution. *Cell* **101**, 471-483 (2000).
21. Ye, J. Z. et al. TIN2 binds TRF1 and TRF2 simultaneously and stabilizes the TRF2 complex on telomeres. *J Biol Chem* **279**, 47264-47271 (2004).
22. Takai, K. K., Hooper, S., Blackwood, S., Gandhi, R. & de Lange, T. In vivo stoichiometry of shelterin components. *J Biol Chem* **285**, 1457-1467 (2010).
23. Li, B. & de Lange, T. Rap1 affects the length and heterogeneity of human telomeres. *Mol Biol Cell* **14**, 5060-5068 (2003).
24. Celli, G. B. & de Lange, T. DNA processing is not required for ATM-mediated telomere damage response after TRF2 deletion. *Nat Cell Biol* **7**, 712-718 (2005).
25. Kim, S. H., Kaminker, P. & Campisi, J. TIN2, a new regulator of telomere length in human cells. *Nat Genet* **23**, 405-412 (1999).

26. Houghtaling, B. R., Cuttonaro, L., Chang, W. & Smith, S. A dynamic molecular link between the telomere length regulator TRF1 and the chromosome end protector TRF2. *Curr Biol* **14**, 1621-1631 (2004).
27. Chen, Y. et al. A shared docking motif in TRF1 and TRF2 used for differential recruitment of telomeric proteins. *Science* **319**, 1092-1096 (2008).
28. Liu, D. et al. PTOP interacts with POT1 and regulates its localization to telomeres. *Nat Cell Biol* **6**, 673-680 (2004).
29. Ye, J. Z. et al. POT1-interacting protein PIP1: a telomere length regulator that recruits POT1 to the TIN2/TRF1 complex. *Genes Dev* **18**, 1649-1654 (2004).
30. Baumann, P. & Cech, T. R. Pot1, the putative telomere end-binding protein in fission yeast and humans. *Science* **292**, 1171-115. (2001).
31. Hockemeyer, D., Daniels, J. P., Takai, H. & de Lange, T. Recent expansion of the telomeric complex in rodents: Two distinct POT1 proteins protect mouse telomeres. *Cell* **126**, 63-77 (2006).
32. Wu, L. et al. Pot1 deficiency initiates DNA damage checkpoint activation and aberrant homologous recombination at telomeres. *Cell* **126**, 49-62 (2006).
33. Lei, M., Podell, E. R. & Cech, T. R. Structure of human POT1 bound to telomeric single-stranded DNA provides a model for chromosome end-protection. *Nat Struct Mol Biol* **11**, 1223-1229 (2004).
34. Loayza, D., Parsons, H., Donigian, J., Hoke, K. & de Lange, T. DNA binding features of human POT1: A nonamer 5'-TAGGGTTAG-3' minimal binding site, sequence specificity, and internal binding to multimeric sites. *J Biol Chem* **279**, 13241-13248 (2004).
35. Cooper, J. P., Nimmo, E. R., Allshire, R. C. & Cech, T. R. Regulation of telomere length and function by a Myb-domain protein in fission yeast. *Nature* **385**, 744-747 (1997).

36. Kanoh, J. & Ishikawa, F. spRap1 and spRif1, recruited to telomeres by Taz1, are essential for telomere function in fission yeast. *Curr Biol* **11**, 1624-1630 (2001).
37. Miyoshi, T., Kanoh, J., Saito, M. & Ishikawa, F. Fission yeast Pot1-Tpp1 protects telomeres and regulates telomere length. *Science* **320**, 1341-1344 (2008).
38. Li, B., Espinal, A. & Cross, G. A. Trypanosome telomeres are protected by a homologue of mammalian TRF2. *Mol Cell Biol* **25**, 5011-5021 (2005).
39. Yang, X., Figueiredo, L. M., Espinal, A., Okubo, E. & Li, B. RAP1 is essential for silencing telomeric variant surface glycoprotein genes in Trypanosoma brucei. *Cell* **137**, 99-109 (2009).
40. Buchman, A. R., Kimmerly, W. J., Rine, J. & Kornberg, R. D. Two DNA-binding factors recognize specific sequences at silencers, upstream activating sequences, autonomously replicating sequences, and telomeres in Saccharomyces cerevisiae. *Mol Cell Biol* **8**, 210-225 (1988).
41. Longtine, M. S., Wilson, N. M., Petracek, M. E. & Berman, J. A yeast telomere binding activity binds to two related telomere sequence motifs and is indistinguishable from RAP1. *Curr Genet* **16**, 225-239 (1989).
42. Conrad, M. N., Wright, J. H., Wolf, A. J. & Zakian, V. A. RAP1 protein interacts with yeast telomeres in vivo: overproduction alters telomere structure and decreases chromosome stability. *Cell* **63**, 739-750 (1990).
43. Lin, J. J. & Zakian, V. A. The Saccharomyces CDC13 protein is a single-strand TG1-3 telomeric DNA- binding protein in vitro that affects telomere behavior in vivo. *Proc Natl Acad Sci USA* **93**, 13760-13765 (1996).
44. Nugent, C. I., Hughes, T. R., Lue, N. F. & Lundblad, V. Cdc13p: a single-strand telomeric DNA-binding protein with a dual role in yeast telomere maintenance. *Science* **274**, 249-252 (1996).
45. Grandin, N., Reed, S. I. & Charbonneau, M. Stn1, a new Saccharomyces cerevisiae protein, is implicated in telomere size regulation in association with Cdc13. *Genes Dev* **11**, 512-27. (1997).

46. Grandin, N., Damon, C. & Charbonneau, M. Cdc13 prevents telomere uncapping and Rad50-dependent homologous recombination. *Embo J* **20**, 6127-6139 (2001).
47. Chandra, A., Hughes, T. R., Nugent, C. I. & Lundblad, V. Cdc13 both positively and negatively regulates telomere replication. *Genes Dev* **15**, 404-14. (2001).
48. Martin, V., Du, L. L., Rozenzhak, S. & Russell, P. Protection of telomeres by a conserved Stn1-Ten1 complex. *Proc Natl Acad Sci U S A* **104**, 14038-14043 (2007).
49. Goulian, M., Heard, C. J. & Grimm, S. L. Purification and properties of an accessory protein for DNA polymerase alpha/primase. *J Biol Chem* **265**, 13221-13230 (1990).
50. Casteel, D. E. et al. A DNA polymerase-{alpha}{middle dot}primase cofactor with homology to replication protein A-32 regulates DNA replication in mammalian cells. *J Biol Chem* **284**, 5807-5818 (2009).
51. Miyake, Y. et al. RPA-like mammalian Ctc1-Stn1-Ten1 complex binds to single-stranded DNA and protects telomeres independently of the Pot1 pathway. *Mol Cell* **36**, 193-206 (2009).
52. Wu, P., Takai, H. & de Lange, T. Telomeric 3' Overhangs Derive from Resection by Exo1 and Apollo and Fill-In by POT1b-Associated CST. *Cell* **150**, 39-52 (2012).
53. Surovtseva, Y. V. et al. Conserved telomere maintenance component 1 interacts with STN1 and maintains chromosome ends in higher eukaryotes. *Mol Cell* **36**, 207-218 (2009).
54. Wan, M., Qin, J., Songyang, Z. & Liu, D. OB fold-containing protein 1 (OBFC1), a human homolog of yeast Stn1, associates with TPP1 and is implicated in telomere length regulation. *J Biol Chem* **284**, 26725-26731 (2009).
55. Watson, J. D. Origin of concatemeric T7 DNA. *Nat New Biol* **239**, 197-201 (1972).

56. Olovnikov, A. M. A theory of marginotomy. The incomplete copying of template margin in enzymic synthesis of polynucleotides and biological significance of the phenomenon. *J Theor Biol* **41**, 181-190 (1973).
57. Hayflick, L. The limited in vitro lifetime of human diploid cell strains. *Exp Cell Res* **37**, 614-636 (1965).
58. de Lange, T. How telomeres solve the end-protection problem. *Science* **326**, 948-952 (2009).
59. Waga, S. & Stillman, B. The DNA replication fork in eukaryotic cells. *Annu Rev Biochem* **67**, 721-751 (1998).
60. Ohki, R., Tsurimoto, T. & Ishikawa, F. In vitro reconstitution of the end replication problem. *Mol Cell Biol* **21**, 5753-5766 (2001).
61. Bodnar, A. G. et al. Extension of life-span by introduction of telomerase into normal human cells. *Science* **279**, 349-352 (1998).
62. Harley, C. B. et al. Telomerase, cell immortality, and cancer. *Cold Spring Harb Symp Quant Biol* **59**, 307-315 (1994).
63. Szostak, J. W. & Blackburn, E. H. Cloning yeast telomeres on linear plasmid vectors. *Cell* **29**, 245-255 (1982).
64. Greider, C. W. & Blackburn, E. H. The telomere terminal transferase of Tetrahymena is a ribonucleoprotein enzyme with two kinds of primer specificity. *Cell* **51**, 887-898 (1987).
65. Lundblad, V. & Szostak, J. W. A mutant with a defect in telomere elongation leads to senescence in yeast. *Cell* **57**, 633-643 (1989).
66. Lendvay, T. S., Morris, D. K., Sah, J., Balasubramanian, B. & Lundblad, V. Senescence mutants of Saccharomyces cerevisiae with a defect in telomere replication identify three additional EST genes. *Genetics* **144**, 1399-1412 (1996).
67. Lingner, J. et al. Reverse transcriptase motifs in the catalytic subunit of telomerase. *Science* **276**, 561-567 (1997).
68. Nakamura, T. M. et al. Telomerase catalytic subunit homologs from fission yeast and human. *Science* **277**, 955-959 (1997).

69. Meyerson, M. et al. hEST2, the putative human telomerase catalytic subunit gene, is up- regulated in tumor cells and during immortalization. *Cell* **90**, 785-95. (1997).
70. Feng, J. et al. The RNA component of human telomerase. *Science* **269**, 1236-1241 (1995).
71. Blasco, M. A. et al. Telomere shortening and tumor formation by mouse cells lacking telomerase RNA. *Cell* **91**, 25-34. (1997).
72. Shay, J. W. & Bacchetti, S. A survey of telomerase activity in human cancer. *Eur J Cancer* **33**, 787-791 (1997).
73. Counter, C. M. et al. Telomere shortening associated with chromosome instability is arrested in immortal cells which express telomerase activity. *Embo J* **11**, 1921-1929 (1992).
74. Kim, N. W. et al. Specific association of human telomerase activity with immortal cells and cancer. *Science* **266**, 2011-205. (1994).
75. Marcand, S., Gilson, E. & Shore, D. A protein-counting mechanism for telomere length regulation in yeast. *Science* **275**, 986-990 (1997).
76. van Steensel, B. & de Lange, T. Control of telomere length by the human telomeric protein TRF1. *Nature* **385**, 740-743 (1997).
77. Smogorzewska, A. et al. Control of human telomere length by TRF1 and TRF2. *Mol Cell Biol* **20**, 1659-1668 (2000).
78. O'Connor, M. S., Safari, A., Liu, D., Qin, J. & Songyang, Z. The human Rap1 protein complex and modulation of telomere length. *J Biol Chem* **279**, 28585-28591 (2004).
79. Loayza, D. & de Lange, T. POT1 as a terminal transducer of TRF1 telomere length control. *Nature* **424**, 1013-1018 (2003).
80. Ye, J. Z. & de Lange, T. TIN2 is a tankyrase 1 PARP modulator in the TRF1 telomere length control complex. *Nat Genet* **36**, 618-623 (2004).
81. Xin, H. et al. TPP1 is a homologue of ciliate TEBP-beta and interacts with POT1 to recruit telomerase. *Nature* **445**, 559-562 (2007).

82. Latrick, C. M. & Cech, T. R. POT1-TPP1 enhances telomerase processivity by slowing primer dissociation and aiding translocation. *EMBO J* **29**, 924-933 (2010).
83. Tejera, A. M. et al. TPP1 is required for TERT recruitment, telomere elongation during nuclear reprogramming, and normal skin development in mice. *Dev Cell* **18**, 775-789 (2010).
84. Abreu, E. et al. TIN2-tethered TPP1 recruits human telomerase to telomeres in vivo. *Mol Cell Biol* **30**, 2971-2982 (2010).
85. Zhong, F. L. et al. TPP1 OB-fold domain controls telomere maintenance by recruiting telomerase to chromosome ends. *Cell* **150**, 481-494 (2012).
86. Nandakumar, J. et al. The TEL patch of telomere protein TPP1 mediates telomerase recruitment and processivity. *Nature* **492**, 285-289 (2012).
87. Sexton, A. N. et al. Genetic and molecular identification of three human TPP1 functions in telomerase action: recruitment, activation, and homeostasis set point regulation. *Genes Dev* **28**, 1885-1899 (2014).
88. Sancar, A., Lindsey-Boltz, L. A., Unsal-Kacmaz, K. & Linn, S. Molecular mechanisms of mammalian DNA repair and the DNA damage checkpoints. *Annu Rev Biochem* **73**, 39-85 (2004).
89. Matsuoka, S., Huang, M. & Elledge, S. J. Linkage of ATM to cell cycle regulation by the Chk2 protein kinase. *Science* **282**, 1893-1897 (1998).
90. Chaturvedi, P. et al. Mammalian Chk2 is a downstream effector of the ATM-dependent DNA damage checkpoint pathway. *Oncogene* **18**, 4047-4054 (1999).
91. Matsuoka, S. et al. Ataxia telangiectasia-mutated phosphorylates Chk2 in vivo and in vitro. *Proc Natl Acad Sci U S A* **97**, 10389-10394 (2000).
92. Sanchez, Y. et al. Conservation of the Chk1 checkpoint pathway in mammals: linkage of DNA damage to Cdk regulation through Cdc25. *Science* **277**, 1497-1501 (1997).

93. Liu, Q. et al. Chk1 is an essential kinase that is regulated by Atr and required for the G(2)/M DNA damage checkpoint. *Genes Dev* **14**, 1448-1459 (2000).
94. Mailand, N. et al. Rapid destruction of human Cdc25A in response to DNA damage. *Science* **288**, 1425-149. (2000).
95. Costanzo, V. et al. Reconstitution of an ATM-dependent checkpoint that inhibits chromosomal DNA replication following DNA damage. *Mol Cell* **6**, 649-659 (2000).
96. Xiao, Z. et al. Chk1 mediates S and G2 arrests through Cdc25A degradation in response to DNA-damaging agents. *J Biol Chem* **278**, 21767-21773 (2003).
97. Tibbetts, R. S. et al. A role for ATR in the DNA damage-induced phosphorylation of p53. *Genes Dev* **13**, 152-17. (1999).
98. Lakin, N. D., Hann, B. C. & Jackson, S. P. The ataxia-telangiectasia related protein ATR mediates DNA-dependent phosphorylation of p53. *Oncogene* **18**, 3989-395. (1999).
99. Shieh, S. Y., Ahn, J., Tamai, K., Taya, Y. & Prives, C. The human homologs of checkpoint kinases Chk1 and Cds1 (Chk2) phosphorylate p53 at multiple DNA damage-inducible sites. *Genes Dev* **14**, 289-300 (2000).
100. Hirao, A. et al. DNA damage-induced activation of p53 by the checkpoint kinase Chk2. *Science* **287**, 1824-1827 (2000).
101. Burma, S., Chen, B. P., Murphy, M., Kurimasa, A. & Chen, D. J. ATM phosphorylates histone H2AX in response to DNA double-strand breaks. *J Biol Chem* **276**, 42462-42467 (2001).
102. Ward, I. M. & Chen, J. Histone H2AX is phosphorylated in an ATR-dependent manner in response to replicational stress. *J Biol Chem* **276**, 47759-47762 (2001).
103. Lou, Z., Minter-Dykhouse, K., Wu, X. & Chen, J. MDC1 is coupled to activated CHK2 in mammalian DNA damage response pathways. *Nature* **421**, 957-961 (2003).

104. Stewart, G. S., Wang, B., Bignell, C. R., Taylor, A. M. & Elledge, S. J. MDC1 is a mediator of the mammalian DNA damage checkpoint. *Nature* **421**, 961-966 (2003).
105. Goldberg, M. et al. MDC1 is required for the intra-S-phase DNA damage checkpoint. *Nature* **421**, 952-956 (2003).
106. Mattiroli, F. et al. RNF168 ubiquitinates K13-15 on H2A/H2AX to drive DNA damage signaling. *Cell* **150**, 1182-1195 (2012).
107. Fradet-Turcotte, A. et al. 53BP1 is a reader of the DNA-damage-induced H2A Lys 15 ubiquitin mark. *Nature* **499**, 50-54 (2013).
108. Takai, H., Smogorzewska, A. & de Lange, T. DNA damage foci at dysfunctional telomeres. *Curr Biol* **13**, 1549-1556 (2003).
109. d'Adda di Fagagna, F. et al. A DNA damage checkpoint response in telomere-initiated senescence. *Nature* **426**, 194-198 (2003).
110. Yan, C. T. et al. IgH class switching and translocations use a robust non-classical end-joining pathway. *Nature* **449**, 478-482 (2007).
111. Corneo, B. et al. Rag mutations reveal robust alternative end joining. *Nature* **449**, 483-486 (2007).
112. Baumann, P. & West, S. C. DNA end-joining catalyzed by human cell-free extracts. *Proc Natl Acad Sci U S A* **95**, 14066-14070 (1998).
113. Gu, Y. et al. Growth retardation and leaky SCID phenotype of Ku70-deficient mice. *Immunity* **7**, 653-665 (1997).
114. Zhu, C., Bogue, M. A., Lim, D. S., Hasty, P. & Roth, D. B. Ku86-deficient mice exhibit severe combined immunodeficiency and defective processing of V(D)J recombination intermediates. *Cell* **86**, 379-389 (1996).
115. Frank, K. M. et al. Late embryonic lethality and impaired V(D)J recombination in mice lacking DNA ligase IV. *Nature* **396**, 173-17. (1998).
116. Audebert, M., Salles, B., Weinfeld, M. & Calsou, P. Involvement of polynucleotide kinase in a poly(ADP-ribose) polymerase-1-dependent DNA double-strand breaks rejoining pathway. *J Mol Biol* **356**, 257-265 (2006).

117. Simsek, D. et al. DNA ligase III promotes alternative nonhomologous end-joining during chromosomal translocation formation. *PLoS Genet* **7**, e1002080 (2011).
118. Wang, M. et al. PARP-1 and Ku compete for repair of DNA double strand breaks by distinct NHEJ pathways. *Nucleic Acids Res* **34**, 6170-6182 (2006).
119. van Steensel, B., Smogorzewska, A. & de Lange, T. TRF2 protects human telomeres from end-to-end fusions. *Cell* **92**, 401-413 (1998).
120. Sfeir, A. & de Lange, T. Removal of shelterin reveals the telomere end-protection problem. *Science* **336**, 593-597 (2012).
121. Mateos-Gomez, P. A. et al. Mammalian polymerase theta promotes alternative NHEJ and suppresses recombination. *Nature* (2015).
122. Sartori, A. A. et al. Human CtIP promotes DNA end resection. *Nature* **450**, 509-514 (2007).
123. Moynahan, M. E., Chiu, J. W., Koller, B. H. & Jasin, M. Brca1 controls homology-directed DNA repair. *Mol Cell* **4**, 511-518 (1999).
124. Nimonkar, A. V., Ozsoy, A. Z., Genschel, J., Modrich, P. & Kowalczykowski, S. C. Human exonuclease 1 and BLM helicase interact to resect DNA and initiate DNA repair. *Proc Natl Acad Sci U S A* **105**, 16906-16911 (2008).
125. Gravel, S., Chapman, J. R., Magill, C. & Jackson, S. P. DNA helicases Sgs1 and BLM promote DNA double-strand break resection. *Genes Dev* **22**, 2767-2772 (2008).
126. Sugiyama, T., Zaitseva, E. M. & Kowalczykowski, S. C. A single-stranded DNA-binding protein is needed for efficient presynaptic complex formation by the Saccharomyces cerevisiae Rad51 protein. *J Biol Chem* **272**, 7940-7945 (1997).
127. Wang, X. & Haber, J. E. Role of Saccharomyces single-stranded DNA-binding protein RPA in the strand invasion step of double-strand break repair. *PLoS Biol* **2**, E21 (2004).

128. Raderschall, E., Golub, E. I. & Haaf, T. Nuclear foci of mammalian recombination proteins are located at single-stranded DNA regions formed after DNA damage. *Proc Natl Acad Sci U S A* **96**, 1921-1926 (1999).
129. Xia, F. et al. Deficiency of human BRCA2 leads to impaired homologous recombination but maintains normal nonhomologous end joining. *Proc Natl Acad Sci U S A* **98**, 8644-8649 (2001).
130. Baumann, P., Benson, F. E. & West, S. C. Human Rad51 protein promotes ATP-dependent homologous pairing and strand transfer reactions in vitro. *Cell* **87**, 757-766 (1996).
131. Davies, A. A. et al. Role of BRCA2 in control of the RAD51 recombination and DNA repair protein. *Mol Cell* **7**, 273-282 (2001).
132. Wu, L. & Hickson, I. D. The Bloom's syndrome helicase suppresses crossing over during homologous recombination. *Nature* **426**, 870-874 (2003).
133. Chen, X. B. et al. Human Mus81-associated endonuclease cleaves Holliday junctions in vitro. *Mol Cell* **8**, 1117-1127 (2001).
134. Ciccia, A., Constantinou, A. & West, S. C. Identification and characterization of the human mus81-eme1 endonuclease. *J Biol Chem* **278**, 25172-25178 (2003).
135. Ip, S. C. et al. Identification of Holliday junction resolvases from humans and yeast. *Nature* **456**, 357-361 (2008).
136. Bailey, S. M., Goodwin, E. H. & Cornforth, M. N. Strand-specific fluorescence in situ hybridization: the CO-FISH family. *Cytogenet Genome Res* **107**, 14-17 (2004).
137. Cesare, A. J. & Reddel, R. R. Alternative lengthening of telomeres: models, mechanisms and implications. *Nat Rev Genet* **11**, 319-330 (2010).
138. Londono-Vallejo, J. A., Der-Sarkissian, H., Cazes, L., Bacchetti, S. & Reddel, R. R. Alternative lengthening of telomeres is characterized by high rates of telomeric exchange. *Cancer Res* **64**, 2324-2327 (2004).

139. Bechter, O. E., Shay, J. W. & Wright, W. E. The Frequency of Homologous Recombination in Human ALT Cells. *Cell Cycle* **3**, 547-549 (2004).
140. Bosco, G. & Haber, J. E. Chromosome break-induced DNA replication leads to nonreciprocal translocations and telomere capture. *Genetics* **150**, 1037-1047 (1998).
141. Morrow, D. M., Connelly, C. & Hieter, P. “Break copy” duplication: a model for chromosome fragment formation in Saccharomyces cerevisiae. *Genetics* **147**, 371-382 (1997).
142. Saini, N. et al. Migrating bubble during break-induced replication drives conservative DNA synthesis. *Nature* **502**, 389-392 (2013).
143. Wilson, M. A. et al. Pif1 helicase and Poldelta promote recombination-coupled DNA synthesis via bubble migration. *Nature* **502**, 393-396 (2013).
144. Le, S., Moore, J. K., Haber, J. E. & Greider, C. W. RAD50 and RAD51 define two pathways that collaborate to maintain telomeres in the absence of telomerase. *Genetics* **152**, 143-152 (1999).
145. Lingner, J., Cooper, J. P. & Cech, T. R. Telomerase and DNA end replication: no longer a lagging strand problem? *Science* **269**, 1533-1534 (1995).
146. Griffith, J. D. et al. Mammalian telomeres end in a large duplex loop. *Cell* **97**, 503-14. (1999).
147. Stansel, R. M., de Lange, T. & Griffith, J. D. T-loop assembly in vitro involves binding of TRF2 near the 3’ telomeric overhang. *EMBO J* **20**, 5532-5540 (2001).
148. Denchi, E. L. & de Lange, T. Protection of telomeres through independent control of ATM and ATR by TRF2 and POT1. *Nature* **448**, 1068-1071 (2007).
149. Takai, K. K., Kibe, T., Donigian, J. R., Frescas, D. & de Lange, T. Telomere protection by TPP1/POT1 requires tethering to TIN2. *Mol Cell* **44**, 647-659 (2011).

150. Kibe, T., Osawa, G. A., Keegan, C. E. & de Lange, T. Telomere Protection by TPP1 Is Mediated by POT1a and POT1b. *Mol Cell Biol* **30**, 1059-1066 (2010).
151. Guo, X. et al. Dysfunctional telomeres activate an ATM-ATR-dependent DNA damage response to suppress tumorigenesis. *EMBO J* **26**, 4709-4719 (2007).
152. Barrientos, K. S. et al. Distinct functions of POT1 at telomeres. *Mol Cell Biol* **28**, 5251-5264 (2008).
153. Gong, Y. & de Lange, T. A Shld1-controlled POT1a provides support for repression of ATR signaling at telomeres through RPA exclusion. *Mol Cell* **40**, 377-387 (2010).
154. Celli, G. B., Lazzerini Denchi, E. & de Lange, T. Ku70 stimulates fusion of dysfunctional telomeres yet protects chromosome ends from homologous recombination. *Nat Cell Biol* **8**, 885-890 (2006).
155. Palm, W., Hockemeyer, D., Kibe, T. & de Lange, T. Functional dissection of human and mouse POT1 proteins. *Mol Cell Biol* **29**, 471-482 (2009).
156. Sfeir, A. et al. Mammalian telomeres resemble fragile sites and require TRF1 for efficient replication. *Cell* **138**, 90-103 (2009).
157. Martinez, P. et al. Increased telomere fragility and fusions resulting from TRF1 deficiency lead to degenerative pathologies and increased cancer in mice. *Genes Dev* **23**, 2060-2075 (2009).
158. Vannier, J. B., Pavicic-Kaltenbrunner, V., Petalcorin, M. I., Ding, H. & Boulton, S. J. RTEL1 Dismantles T Loops and Counteracts Telomeric G4-DNA to Maintain Telomere Integrity. *Cell* **149**, 795-806 (2012).
159. Zimmermann, M., Kibe, T., Kabir, S. & de Lange, T. TRF1 negotiates TTAGGG repeat-associated replication problems by recruiting the BLM helicase and the TPP1/POT1 repressor of ATR signaling. *Genes Dev* **28**, 2477-2491 (2014).
160. Sarthy, J., Bae, N. S., Scrafford, J. & Baumann, P. Human RAP1 inhibits non-homologous end joining at telomeres. *EMBO J* **28**, 3390-3399 (2009).

161. Karlseder, J., Broccoli, D., Dai, Y., Hardy, S. & de Lange, T. p53- and ATM-dependent apoptosis induced by telomeres lacking TRF2. *Science* **283**, 1321-1325 (1999).
162. Konishi, A. & de Lange, T. Cell cycle control of telomere protection and NHEJ revealed by a ts mutation in the DNA-binding domain of TRF2. *Genes Dev* **22**, 1221-1230 (2008).
163. Dimitrova, N., Chen, Y. C., Spector, D. L. & de Lange, T. 53BP1 promotes non-homologous end joining of telomeres by increasing chromatin mobility. *Nature* **456**, 524-528 (2008).
164. Lottersberger, F., Bothmer, A., Robbiani, D. F., Nussenzweig, M. C. & de Lange, T. Role of 53BP1 oligomerization in regulating double-strand break repair. *Proc Natl Acad Sci U S A* **110**, 2146-2151 (2013).
165. Zimmermann, M., Lottersberger, F., Buonomo, S. B., Sfeir, A. & de Lange, T. 53BP1 regulates DSB repair using Rif1 to control 5' end resection. *Science* **339**, 700-704 (2013).
166. Dimitrova, N. & de Lange, T. Cell cycle dependent role of MRN at dysfunctional telomeres: ATM signaling-dependent induction of NHEJ in G1 and resection-mediated inhibition of NHEJ in G2. *Mol Cell Biol* **29**, 5552-5563 (2009).
167. Attwooll, C. L., Akpinar, M. & Petrini, J. H. The mre11 complex and the response to dysfunctional telomeres. *Mol Cell Biol* **29**, 5540-5551 (2009).
168. Deng, Y., Guo, X., Ferguson, D. O. & Chang, S. Multiple roles for MRE11 at uncapped telomeres. *Nature* **460**, 914-918 (2009).
169. Doksani, Y., Wu, J. Y., de Lange, T. & Zhuang, X. Super-resolution fluorescence imaging of telomeres reveals TRF2-dependent T-loop formation. *Cell* **155**, 345-356 (2013).
170. Okamoto, K. et al. A two-step mechanism for TRF2-mediated chromosome-end protection. *Nature* **494**, 502-505 (2013).

171. Pierce, A. J., Johnson, R. D., Thompson, L. H. & Jasin, M. XRCC3 promotes homology-directed repair of DNA damage in mammalian cells. *Genes Dev* **13**, 2633-2638 (1999).
172. Wang, R. C., Smogorzewska, A. & de Lange, T. Homologous recombination generates T-loop-sized deletions at human telomeres. *Cell* **119**, 355-368 (2004).
173. Fouche, N. et al. The basic domain of TRF2 directs binding to DNA junctions irrespective of the presence of TTAGGG repeats. *J Biol Chem* **281**, 37486-37495 (2006).
174. Poulet, A. et al. TRF2 promotes, remodels and protects telomeric Holliday junctions. *EMBO J* **28**, 641-651 (2009).
175. Saint-Leger, A. et al. The basic N-terminal domain of TRF2 limits recombination endonuclease action at human telomeres. *Cell Cycle* **13**, (2014).
176. Choi, K. H., Farrell, A. S., Lakamp, A. S. & Ouellette, M. M. Characterization of the DNA binding specificity of Shelterin complexes. *Nucleic Acids Res* **39**, 9206-9223 (2011).
177. Wu, P., van Overbeek, M., Rooney, S. & de Lange, T. Apollo Contributes to G Overhang Maintenance and Protects Leading-End Telomeres. *Mol Cell* **39**, 1-12 (2010).
178. Lam, Y. C. et al. SNMIB/Apollo protects leading-strand telomeres against NHEJ-mediated repair. *EMBO J* **29**, 2230-2241 (2010).
179. van Overbeek, M. & de Lange, T. Apollo, an Artemis-related nuclease, interacts with TRF2 and protects human telomeres in S phase. *Curr Biol* **16**, 1295-1302 (2006).
180. Lenain, C. et al. The Apollo 5' exonuclease functions together with TRF2 to protect telomeres from DNA repair. *Curr Biol* **16**, 1303-1310 (2006).
181. Dai, X. et al. Molecular steps of G-overhang generation at human telomeres and its function in chromosome end protection. *EMBO J* **29**, 2788-2801 (2010).

182. He, H. et al. POT1b protects telomeres from end-to-end chromosomal fusions and aberrant homologous recombination. *Embo J* **25**, 5180-5190 (2006).
183. Davoli, T., Denchi, E. L. & de Lange, T. Persistent telomere damage induces bypass of mitosis and tetraploidy. *Cell* **141**, 81-93 (2010).
184. Hockemeyer, D., Sfeir, A. J., Shay, J. W., Wright, W. E. & de Lange, T. POT1 protects telomeres from a transient DNA damage response and determines how human chromosomes end. *EMBO J.* **24**, 2667-2678 (2005).
185. Yang, Q., Zheng, Y. L. & Harris, C. C. POT1 and TRF2 cooperate to maintain telomeric integrity. *Mol Cell Biol* **25**, 1070-1080 (2005).
186. Sfeir, A. J., Chai, W., Shay, J. W. & Wright, W. E. Telomere-end processing the terminal nucleotides of human chromosomes. *Mol Cell* **18**, 131-138 (2005).
187. Shore, D. & Nasmyth, K. Purification and cloning of a DNA binding protein from yeast that binds to both silencer and activator elements. *Cell* **51**, 721-732 (1987).
188. Hardy, C. F., Balderes, D. & Shore, D. Dissection of a carboxy-terminal region of the yeast regulatory protein RAP1 with effects on both transcriptional activation and silencing. *Mol Cell Biol* **12**, 1209-1217 (1992).
189. Cockell, M. et al. The carboxy termini of Sir4 and Rap1 affect Sir3 localization: evidence for a multicomponent complex required for yeast telomeric silencing. *J Cell Biol* **129**, 909-924 (1995).
190. Liu, C. & Lustig, A. J. Genetic analysis of Rap1p/Sir3p interactions in telomeric and HML silencing in Saccharomyces cerevisiae. *Genetics* **143**, 81-93 (1996).
191. Pardo, B. & Marcand, S. Rap1 prevents telomere fusions by nonhomologous end joining. *EMBO J* **24**, 3117-3127 (2005).
192. Konig, P., Giraldo, R., Chapman, L. & Rhodes, D. The crystal structure of the DNA-binding domain of yeast RAP1 in complex with telomeric DNA. *Cell* **85**, 125-136 (1996).

193. Hanaoka, S. et al. NMR structure of the hRap1 Myb motif reveals a canonical three-helix bundle lacking the positive surface charge typical of Myb DNA-binding domains. *J Mol Biol* **312**, 167-175 (2001).
194. Yu, X., Chini, C. C., He, M., Mer, G. & Chen, J. The BRCT domain is a phospho-protein binding domain. *Science* **302**, 639-642 (2003).
195. Hardy, C. F., Sussel, L. & Shore, D. A RAP1-interacting protein involved in transcriptional silencing and telomere length regulation. *Genes Dev* **6**, 801-814 (1992).
196. Wotton, D. & Shore, D. A novel Rap1p-interacting factor, Rif2p, cooperates with Rif1p to regulate telomere length in Saccharomyces cerevisiae. *Genes Dev* **11**, 748-760 (1997).
197. Hirano, Y. & Sugimoto, K. Cdc13 telomere capping decreases Mec1 association but does not affect Tel1 association with DNA ends. *Mol Biol Cell* **18**, 2026-2036 (2007).
198. Viscardi, V., Bonetti, D., Cartagena-Lirola, H., Lucchini, G. & Longhese, M. P. MRX-dependent DNA damage response to short telomeres. *Mol Biol Cell* **18**, 3047-3058 (2007).
199. Bianchi, A. & Shore, D. Increased association of telomerase with short telomeres in yeast. *Genes Dev* **21**, 1726-1730 (2007).
200. Sabourin, M., Tuzon, C. T. & Zakian, V. A. Telomerase and Tel1p preferentially associate with short telomeres in S. cerevisiae. *Mol Cell* **27**, 550-561 (2007).
201. Hector, R. E. et al. Tel1p preferentially associates with short telomeres to stimulate their elongation. *Mol Cell* **27**, 851-858 (2007).
202. Hirano, Y., Fukunaga, K. & Sugimoto, K. Rif1 and rif2 inhibit localization of tel1 to DNA ends. *Mol Cell* **33**, 312-322 (2009).
203. Silverman, J., Takai, H., Buonomo, S. B., Eisenhaber, F. & de Lange, T. Human Rif1, ortholog of a yeast telomeric protein, is regulated by ATM and 53BP1 and functions in the S-phase checkpoint. *Genes Dev* **18**, 2108-2119 (2004).

204. Di Virgilio, M. et al. Rif1 prevents resection of DNA breaks and promotes immunoglobulin class switching. *Science* **339**, 711-715 (2013).
205. Escribano-Diaz, C. et al. A cell cycle-dependent regulatory circuit composed of 53BP1-RIF1 and BRCA1-CtIP controls DNA repair pathway choice. *Mol Cell* **49**, 872-883 (2013).
206. Feng, L., Fong, K. W., Wang, J., Wang, W. & Chen, J. RIF1 Counteracts BRCA1-mediated End Resection during DNA Repair. *J Biol Chem* **288**, 11135-11143 (2013).
207. Chapman, J. R. et al. RIF1 is essential for 53BP1-dependent nonhomologous end joining and suppression of DNA double-strand break resection. *Mol Cell* **49**, 858-871 (2013).
208. Buonomo, S., Wu, Y., Ferguson, D. & de Lange, T. Mammalian Rif1 contributes to replication stress survival and homology-directed repair. *J Cell Biol* **187**, 385-398 (2009).
209. Cornacchia, D. et al. Mouse Rif1 is a key regulator of the replication-timing programme in mammalian cells. *EMBO J* **31**, 3678-3690 (2012).
210. Yamazaki, S. et al. Rif1 regulates the replication timing domains on the human genome. *EMBO J* **31**, 3667-3677 (2012).
211. Miller, K. M., Ferreira, M. G. & Cooper, J. P. Taz1, Rap1 and Rif1 act both interdependently and independently to maintain telomeres. *EMBO J* **24**, 3128-3135 (2005).
212. Marcand, S., Pardo, B., Gratias, A., Cahun, S. & Callebaut, I. Multiple pathways inhibit NHEJ at telomeres. *Genes Dev* **22**, 1153-1158 (2008).
213. Bae, N. S. & Baumann, P. A RAP1/TRF2 complex inhibits nonhomologous end-joining at human telomeric DNA ends. *Mol Cell* **26**, 323-334 (2007).
214. Cesare, A. J., Groff-Vindman, C., Compton, S. A., McEachern, M. J. & Griffith, J. D. Telomere loops and homologous recombination-dependent telomeric circles in a Kluyveromyces lactis telomere mutant strain. *Mol Cell Biol* **28**, 20-29 (2008).

215. Yu, E. Y., Yen, W. F., Steinberg-Neifach, O. & Lue, N. F. Rap1 in Candida albicans: an unusual structural organization and a critical function in suppressing telomere recombination. *Mol Cell Biol* **30**, 1254-1268 (2010).
216. Scherthan, H. in *Telomeres* (eds de Lange, T., Lundblad, V. & Blackburn, E.) 225-260 (Cold Spring Harbor Laboratory Press, Cold Spring Harbor, New York, 2005).
217. Chikashige, Y. & Hiraoka, Y. Telomere binding of the Rap1 protein is required for meiosis in fission yeast. *Curr Biol* **11**, 1618-1623 (2001).
218. Chikashige, Y. et al. Meiotic proteins bqt1 and bqt2 tether telomeres to form the bouquet arrangement of chromosomes. *Cell* **125**, 59-69 (2006).
219. Crabbe, L., Cesare, A. J., Kasuboski, J. M., Fitzpatrick, J. A. & Karlseder, J. Human telomeres are tethered to the nuclear envelope during postmitotic nuclear assembly. *Cell Rep* **2**, 1521-1529 (2012).
220. Martinez, P. et al. Mammalian Rap1 controls telomere function and gene expression through binding to telomeric and extratelomeric sites. *Nat Cell Biol* **12**, 768-780 (2010).
221. Yeung, F. et al. Nontelomeric role for Rap1 in regulating metabolism and protecting against obesity. *Cell Rep* **3**, 1847-1856 (2013).
222. Martinez, P. et al. RAP1 protects from obesity through its extratelomeric role regulating gene expression. *Cell Rep* **3**, 2059-2074 (2013).
223. Yang, D. et al. Human telomeric proteins occupy selective interstitial sites. *Cell Res* **21**, 1013-1027 (2011).
224. Teo, H. et al. Telomere-independent Rap1 is an IKK adaptor and regulates NF-kappaB-dependent gene expression. *Nat Cell Biol* **12**, 758-767 (2010).
225. Svendsen, J. M. et al. Mammalian BTBD12/SLX4 assembles a Holliday junction resolvase and is required for DNA repair. *Cell* **138**, 63-77 (2009).
226. Lee, O. H. et al. Genome-wide YFP fluorescence complementation screen identifies new regulators for telomere signaling in human cells. *Mol Cell Proteomics* **10**, M110.001628 (2011).

227. Kabir, S., Sfeir, A. & de Lange, T. Taking apart Rap1: An adaptor protein with telomeric and non-telomeric functions. *Cell Cycle* **9**, 4061-4067 (2010).
228. Blasco, M. A. The epigenetic regulation of mammalian telomeres. *Nat Rev Genet* **8**, 299-309 (2007).
229. Feuerhahn, S., Iglesias, N., Panza, A., Porro, A. & Lingner, J. TERRA biogenesis, turnover and implications for function. *FEBS Lett* **584**, 3812-3818 (2010).
230. Tsai, Y. L., Tseng, S. F., Chang, S. H., Lin, C. C. & Teng, S. C. Involvement of replicative polymerases, tel1p, mec1p, cdc13p, and the ku complex in telomere-telomere recombination. *Mol Cell Biol* **22**, 5679-5687 (2002).
231. Hecht, A., Laroche, T., Strahl-Bolsinger, S., Gasser, S. M. & Grunstein, M. Histone H3 and H4 N-termini interact with SIR3 and SIR4 proteins: a molecular model for the formation of heterochromatin in yeast. *Cell* **80**, 583-592 (1995).
232. Hecht, A., Strahl-Bolsinger, S. & Grunstein, M. Spreading of transcriptional repressor SIR3 from telomeric heterochromatin. *Nature* **383**, 92-96 (1996).
233. Moretti, P. & Shore, D. Multiple interactions in sir protein recruitment by rap1p at silencers and telomeres in yeast. *Mol Cell Biol* **21**, 8082-8094 (2001).
234. Liu, D., O'Connor, M. S., Qin, J. & Songyang, Z. Telosome, a mammalian telomere-associated complex formed by multiple telomeric proteins. *J Biol Chem* **279**, 51338-51342 (2004).
235. Arat, N. O. & Griffith, J. D. Human Rap1 interacts directly with telomeric DNA and regulates TRF2 localization at the telomere. *J Biol Chem* **287**, 41583-41594 (2012).
236. Janouskova, E. et al. Human Rap1 modulates TRF2 attraction to telomeric DNA. *Nucleic Acids Res* (2015).
237. Chen, F. et al. High-frequency genome editing using ssDNA oligonucleotides with zinc-finger nucleases. *Nat Methods* **8**, 753-755 (2011).

238. Urnov, F. D., Rebar, E. J., Holmes, M. C., Zhang, H. S. & Gregory, P. D. Genome editing with engineered zinc finger nucleases. *Nat Rev Genet* **11**, 636-646 (2010).
239. Sedivy, J., Vogelstein, B., Liber, H., Hendrickson, E. A. & Rosmarin, A. Gene Trageting in Human Cells Without Isogenic DNA. *Science* **283**, 9- 9a (1999).
240. Li, G., Nelsen, C. & Hendrickson, E. A. Ku86 is essential in human somatic cells. *Proc Natl Acad Sci USA* **99**, 832-837 (2002).
241. Wang, Y., Ghosh, G. & Hendrickson, E. A. Ku86 represses lethal telomere deletion events in human somatic cells. *Proc Natl Acad Sci U S A* **106**, 12430-12435 (2009).
242. Jackson, E. L. et al. Analysis of lung tumor initiation and progression using conditional expression of oncogenic K-ras. *Genes Dev* **15**, 3243-3248 (2001).
243. Lakso, M. et al. Targeted oncogene activation by site-specific recombination in transgenic mice. *Proc Natl Acad Sci U S A* **89**, 6232-6236 (1992).
244. Mao, X., Fujiwara, Y. & Orkin, S. H. Improved reporter strain for monitoring Cre recombinase-mediated DNA excisions in mice. *Proc Natl Acad Sci U S A* **96**, 5037-5042 (1999).
245. Janbandhu, V. C., Moik, D. & Fassler, R. Cre recombinase induces DNA damage and tetraploidy in the absence of loxP sites. *Cell Cycle* **13**, 462-470 (2014).
246. Hockemeyer, D. et al. Telomere protection by mammalian POT1 requires interaction with TPP1. *Nat Struct Mol Biol* **14**, 754-761 (2007).
247. Chen, L. Y., Redon, S. & Lingner, J. The human CST complex is a terminator of telomerase activity. *Nature* **488**, 540-544 (2012).
248. Diotti, R., Kalan, S., Matveyenko, A. & Loayza, D. DNA-directed Polymerase Subunits Play a Vital Role in Human Telomeric Overhang Processing. *Mol Cancer Res* (2014).

249. Kelleher, C., Kurth, I. & Lingner, J. Human protection of telomeres 1 (POT1) is a negative regulator of telomerase activity in vitro. *Mol Cell Biol* **25**, 808-818 (2005).
250. Ramsay, A. J. et al. POT1 mutations cause telomere dysfunction in chronic lymphocytic leukemia. *Nat Genet* **45**, 526-530 (2013).
251. Robles-Espinoza, C. D. et al. POT1 loss-of-function variants predispose to familial melanoma. *Nat Genet* **46**, 478-481 (2014).
252. Shi, J. et al. Rare missense variants in POT1 predispose to familial cutaneous malignant melanoma. *Nat Genet* **46**, 482-486 (2014).
253. Fabbri, G. et al. Genetic lesions associated with chronic lymphocytic leukemia transformation to Richter syndrome. *J Exp Med* **210**, 2273-2288 (2013).
254. Toledo, L. I. et al. A cell-based screen identifies ATR inhibitors with synthetic lethal properties for cancer-associated mutations. *Nat Struct Mol Biol* **18**, 721-727 (2011).
255. Abecasis, G. R. et al. An integrated map of genetic variation from 1,092 human genomes. *Nature* **491**, 56-65 (2012).
256. Khurana, E., Fu, Y., Chen, J. & Gerstein, M. Interpretation of genomic variants using a unified biological network approach. *PLoS Comput Biol* **9**, e1002886 (2013).
257. Scherthan, H., Sfeir, A. & de Lange, T. Rap1-independent telomere attachment and bouquet formation in mammalian meiosis. *Chromosoma* **120**, 151-157 (2011).
258. Shibuya, H., Ishiguro, K. & Watanabe, Y. The TRF1-binding protein TERB1 promotes chromosome movement and telomere rigidity in meiosis. *Nat Cell Biol* **16**, 145-156 (2014).
259. Kabir, S., Hockemeyer, D. & de Lange, T. TALEN Gene Knockouts Reveal No Requirement for the Conserved Human Shelterin Protein Rap1 in Telomere Protection and Length Regulation. *Cell Rep* **9**, 1273-1280 (2014).

260. Lou, Z. et al. Telomere length regulates ISG15 expression in human cells. *Aging (Albany NY)* **1**, 608-621 (2009).
261. Stadler, G. et al. Telomere position effect regulates DUX4 in human facioscapulohumeral muscular dystrophy. *Nat Struct Mol Biol* **20**, 671-678 (2013).
262. Robin, J. D. et al. Telomere position effect: regulation of gene expression with progressive telomere shortening over long distances. *Genes Dev* **28**, 2464-2476 (2014).
263. Platt, J. M. et al. Rap1 relocalization contributes to the chromatin-mediated gene expression profile and pace of cell senescence. *Genes Dev* **27**, 1406-1420 (2013).
264. Zhu, X. D., Kuster, B., Mann, M., Petrini, J. H. & de Lange, T. Cell-cycle-regulated association of RAD50/MRE11/NBS1 with TRF2 and human telomeres. *Nat Genet* **25**, 347-352 (2000).
265. Song, K., Jung, D., Jung, Y., Lee, S. G. & Lee, I. Interaction of human Ku70 with TRF2. *FEBS Lett* **481**, 81-5. (2000).
266. Zhu, X. D. et al. ERCC1/XPF Removes the 3' Overhang from Uncapped Telomeres and Represses Formation of Telomeric DNA-Containing Double Minute Chromosomes. *Mol Cell* **12**, 1489-1498 (2003).
267. Mazin, A. V., Alexeev, A. A. & Kowalczykowski, S. C. A novel function of Rad54 protein. Stabilization of the Rad51 nucleoprotein filament. *J Biol Chem* **278**, 14029-14036 (2003).
268. Raynard, S. & Sung, P. Assay for human Rad51-mediated DNA displacement loop formation. *Cold Spring Harb Protoc* **2009**, pdb.prot5120 (2009).
269. Li, X. & Heyer, W. D. Homologous recombination in DNA repair and DNA damage tolerance. *Cell Res* **18**, 99-113 (2008).
270. Heyer, W. D., Ehmsen, K. T. & Liu, J. Regulation of homologous recombination in eukaryotes. *Annu Rev Genet* **44**, 113-139 (2010).

271. Pierce, A. J., Hu, P., Han, M., Ellis, N. & Jasin, M. Ku DNA end-binding protein modulates homologous repair of double-strand breaks in mammalian cells. *Genes Dev* **15**, 3237-3242 (2001).
272. Fattah, F. J., Lichter, N. F., Fattah, K. R., Oh, S. & Hendrickson, E. A. Ku70, an essential gene, modulates the frequency of rAAV-mediated gene targeting in human somatic cells. *Proc Natl Acad Sci U S A* **105**, 8703-8708 (2008).
273. Nussenzweig, A. et al. Requirement for Ku80 in growth and immunoglobulin V(D)J recombination. *Nature* **382**, 551-555 (1996).
274. Mimitou, E. P. & Symington, L. S. Sae2, Exo1 and Sgs1 collaborate in DNA double-strand break processing. *Nature* **455**, 770-774 (2008).
275. Zhu, Z., Chung, W. H., Shim, E. Y., Lee, S. E. & Ira, G. Sgs1 helicase and two nucleases Dna2 and Exo1 resect DNA double-strand break ends. *Cell* **134**, 981-994 (2008).
276. Nimonkar, A. V. et al. BLM-DNA2-RPA-MRN and EXO1-BLM-RPA-MRN constitute two DNA end resection machineries for human DNA break repair. *Genes Dev* **25**, 350-362 (2011).
277. Dornreiter, I. et al. Interaction of DNA polymerase alpha-primase with cellular replication protein A and SV40 T antigen. *EMBO J* **11**, 769-776 (1992).
278. Dimitrova, N. & de Lange, T. MDC1 accelerates nonhomologous end-joining of dysfunctional telomeres. *Genes Dev* **20**, 3238-3243 (2006).
279. de Lange, T. Human telomeres are attached to the nuclear matrix. *Embo J* **11**, 717-724 (1992).
280. Karlseder, J., Smogorzewska, A. & de Lange, T. Senescence induced by altered telomere state, not telomere loss. *Science* **295**, 2446-2449 (2002).
281. Azzalin, C. M., Reichenbach, P., Khoriauli, L., Giulotto, E. & Lingner, J. Telomeric repeat containing RNA and RNA surveillance factors at mammalian chromosome ends. *Science* **318**, 798-801 (2007).

282. Vandesompele, J., De Preter, K., Pattyn, F., Poppe, B., Van Roy, N., De Paepe, A., Speleman, F. Accurate normalization of real-time quantitative RT-PCR data by geometric averaging of multiple internal control genes. *Genome Biol* **3(7)**, (2002).

283. Hsu, H., Gilley, D., Galande, SA., Hande, MP., Allen, B., Kim, S., Li, GC., Campisi, J., Kohwi-Shigematsu, T., Chen, DJ. Ku acts in a unique way at the mammalian telomere to prevent end joining. *Genes Dev* **14(22),** (2000).

284. Bianchi, A., de Lange, T. Ku binds telomeric DNA in vitro. *J Biol Chem* **274(30)**, (1999).

285. Rong, YS. Telomere capping in Drosophila: dealing with chromosome ends that most resemble DNA breaks. *Chromosoma* **117,** (2008).

286. Cenci, G., Ciapponi, L., Gatti, M. The mechanism of telomere protection: a comparison between Drosophila and humans. *Chromosoma* ***114,*** (2005).